Politecnico di Torino

ScuDo
Scuola di Dottorato ~ Doctoral School
WHAT YOU ARE, TAKES YOU FAR

Doctoral Dissertation
Doctoral Program in Electrical, Electronics and Communications Engineering
(34^{th}cycle)

Investigation of Molecular FCN for Beyond-CMOS

Technology, design, and modeling for nanocomputing

By

Yuri Ardesi

******

Supervisor(s):
Prof. Gianluca Piccinini, Supervisor, Politecnico di Torino

Doctoral Examination Committee:
Prof. Maciej Krzywiecki, Referee, Silesian University of Technology
Prof. Rosaria Rinaldi, Referee, Università del Salento

Politecnico di Torino
2022

Declaration

I hereby declare that, the contents and organization of this dissertation constitute my own original work and does not compromise in any way the rights of third parties, including those relating to the security of personal data.

Yuri Ardesi
2022

* This dissertation is presented in partial fulfillment of the requirements for **Ph.D. degree** in the Graduate School of Politecnico di Torino (ScuDo).

To those who fight
alone, silently.

Acknowledgements

I would like to thank **Prof. Gianluca Piccinini** - dept. of Electronics and Telecommunications, Politecnico di Torino[1] - for his incredible guidance as PhD supervisor and mentor, helping me to understand the meaning of academic research and supporting me in every choice. At the same level, I would like to thank **Prof. Mariagrazia Graziano** - dept. of Applied Science and Technology, Politecnico di Torino - *de facto* co-supervisor, for her precious support and incredible humanity and empathy.

Secondly, I would like to thank my PhD colleagues who worked on molecular technologies in the VLSILAB[2] - dept. of Electronics and Telecommunications, Politecnico di Torino. In alphabetical order: **Giuliana Beretta**, **Fabrizio Mo**, **Chiara Elfi Spano**. I want to recognize their precious help in collaborating on the project as teammates, supporting and motivating me every day, and helping me discovering and understanding my potentials and limitations, strengths and weaknesses. Many thanks also go to **Dr. Ruiyu Wang**, who followed me during my master thesis and started the SCERPA development, and **Dr. Azzurra Pulimeno**, who started the development of MoSQuiTo.

Much works were also possible thanks to master thesis students who worked with me on molecular Field-Coupled Nanocomputing. Following the alphabetic order: **Giorgio Alemanno**, **Dario Castagneri**, **Roberta Claudino**, **Christian Fabiano**, **Alessandro Gaeta Erik Lo Grasso**, **Luciano Macrì**, **Sara Puglia**, **Federico Ravera**, **Giovanni Sanclemente**, **Mattia Siviero**, **Duc Tan Tran**, and **Daniele Volpintesta**.

I also want to acknowledge the help from the CoMeTa research group[3] - dept. of Applied Science and Technology, Politecnico di Torino - for their support in

[1] Politecnico di Torino, official website - Accessed on 18 August 2022
[2] VLSILAB Politecnico di Torino, official website - Accessed on 18 August 2022
[3] CoMeTa Politecnico di Torino, DISAT webpage- Accessed on 18 August 2022

setting up the first attempts in realizing molecular devices experimentally and for their theoretical support regarding physical chemistry: **Prof. Sabrina Grassini**, **Dr. Alessio Gullino**, and **Amina Vietti**.

Finally, my PhD studies were possible also thanks to the people I met in the **VLSILAB**, in particular, I would like to thank some of the colleagues who supported me daily and were for me colleagues, friends, mentors, and sometimes role models. Some of them would deserve a chapter of the dissertation for the importance they had during my last three years.

Furthermore, I would like to acknowledge also the IEEE Student Branch of Politecnico di Torino[4], that I had the pleasure to serve as a volunteer for two consecutive years.

At the same level, I would like to express my gratitude to my lifelong friends, who were part of the journey. They supported me in the worst moments, and partied with me in the best ones.

Finally, to those who believed me from the beginning. I would like to acknowledge them in the lowest paragraph of this section, reminding you that a good house is hardly ever judged by foundations. Yet foundations support the house, and no attractive superficial thing, which generally lets houses be bought by customers, would ever make sense on a house with bad foundations. These are **my parents**: the foundations of this work.

[4]Politecnico di Torino IEEE Student Branch, official website - Accessed on 18 August 2022

Contents

List of Figures

List of Tables

List of Acronyms

AC Aggregated Charge

AIMD Ab Initio Molecular Dynamics

BOA Born-Oppenheimer Approximation

BOMD Bohr-Oppenheimer Molecular Dynamics

CAD Computer-Aided Design

CHELPG CHarges from ELectrostatic Potentials using a Grid-based method

CMOS Complementary Metal-Oxide Semiconductor

DFT Density Functional Theory

EDA Electronic Design Automation

FCN Field-Coupled Nanocomputing

FEM Finite Element Modelling

FFT Fast Fourier Transform

GTO Gaussian Type Orbital

HDL Hydrogen Depassivation Lithography

HF Hartree-Fock

HOMO Highest Occupied Molecular Orbital

IDE Integrated Development Environment

IR Interaction Radius

LB Langmuir-Blodgett

LUMO Lowest Unoccupied Molecular Orbital

MD Molecular Dynamics

MEMS Micro-Electro-Mechanical System

MEP Molecular Electrostatic Potential

MO Molecular Orbital

MOSFET Metal-Oxide-Semiconductor Field-Effect Transistor

MoSQuiTo Molecular Simulator Quantum-dot cellular automata Torino

MSOA Molecular Safe-Operating Area

MUT Molecule Under Test

NML Nano-Magnetic Logic

OMBD Organic Molecular Beam Deposition

OMBE Organic Molecular Beam Epitaxy

PES Potential Energy Surface

QCA Quantum-dot Cellular Automata

QM Quantum Mechanics

RT-TDDFT Real-Time Time-Dependent Density Functional Theory

SAM Self-Assembled Monolayer

SCERPA Self-Consistent ElectRostatic Potential Algorithm

SCF Self-Consistent Field

SET Single-Electron Transistor

SiQAD Silicon Quantum Atomic Designer

STM Scanning Tunnelling Microscopy

STO Slater Type Orbital

ToPoliNano TOrino POLItecnico NANOtechnology

TSA Two-State Approximation

TSOA Technological Safe-Operating Area

UHV Ultra-High Vacuum

VACT Vin-Aggregated Charge Transcharacteristics

VHDL VHSIC (Very High Speed Integrated Circuits) Hardware Description Language

VVT Vin-Vout Transcharacteristics

Preface

Among the technologies proposed to overextend the CMOS era, the molecular Field-Coupled Nanocomputing (FCN) is one of the most attractive technologies for future digital electronics. It encodes the information in nanometric molecules, following the Quantum-dot Cellular Automata (QCA) paradigm, permitting the realization of tiny and very dense digital devices working at ambient temperature. Furthermore, it propagates and elaborates the information through intermolecular electrostatic interaction at a very high speed. No current flow is involved in the information transport, thus minimizing the power dissipation.

Notwithstanding the increased interest for molecular FCN, fueled by outstanding simulative and theoretical results, a working prototype has not yet been realized, unlike other FCN technologies such as the Nano Magnetic Logic (NML) or the Metallic QCA. Indeed, the difficulties correlated to the need for very high resolution for the nanofabrication of devices and for measuring molecule charges make the realization and the measurement of a working prototype challenging. Besides, the molecular FCN literature investigates the information encoding in molecules from a theoretical perspective and simultaneously employs the two-state approximation typical of the general QCA paradigm to study complex digital architectures. However, few attempts have been made to link the molecular characteristics to the two-state approximation models. Consequently, general QCA simulation tools scarcely consider the effective physics of the molecular interaction, preventing the assessment of molecular FCN technology as a possible candidate for future digital electronics. The literature proposes a vast amount of digital architectures which are supposed to be implemented with molecules, despite a real connection between circuits and molecular nature is still the chain missing link.

This work demonstrates a methodological procedure to fill the gap between the physical molecular perspective and the circuit level. First, it analyses molecules with

ab initio calculation, considering the effective molecular physics, demonstrating the encoding of the information in the static and dynamic regimes at different temperatures by considering the effect of molecular vibrations. Then, it models the molecule as an electronics device and develops the Self-Consistent Electrostatic Potential Algorithm (SCERPA): an optimized tool that permits the fast simulation of molecular FCN circuits by maintaining a solid link with molecular physics and providing results based on *ab initio* characterization of molecules. The tool is therefore used to analyze molecular FCN circuits and establish the physical-aware design of digital devices by considering the effective physics of the molecules. First, obtained results quantitatively describe the functioning, the stability, the crosstalk, and possible memory effects of molecular FCN devices. Secondly, results give feedback to technologists for the eventual realization of a working prototype, conceiving and demonstrating multi-lines clocked molecular devices, which favors the stability of information encoding and reduces the constraints on the resolution for the nanopatterning.

This work fulfills the aim of filling the gap between the physical molecular perspective and the circuit level. It addresses and motivates the necessity of considering the molecular physics in the design of molecular circuits, intensely motivating the use of a physical-aware design tool and circumscribing the use of the general QCA tools for the design of molecular FCN circuits. Furthermore, this thesis work motivates further research on developing and validating a CAD-integrated physical-aware simulator able to provide reliable analyses of molecular devices and circuits and addresses the essential aspects of molecular FCN technology, making it promising as a candidate for future digital electronics.

The following paragraphs report the organization of the document:

Chapter 1 (Introduction and Background) discusses the state-of-the-art of the molecular Field-Coupled Nanocomputing (FCN): the Quantum-dot Cellular Automata (QCA), the essential devices, and the clocking mechanism. It describes literature molecules and the realization of write-in, clocking, and readout systems. It also presents experimental techniques promising for fabricating molecular devices. Finally, the chapter introduces the methods and tools used in this thesis to analyze molecular FCN circuits.

Chapter 2 (Theoretical Background) discusses time-dependent/independent computational chemistry theories to analyze molecular problems. Also, it describes the molecular properties fundamental for understanding analyses and models of

molecular FCN devices, such as molecular vibrations and polarizability. Finally, it briefly describes the two-state approximation theory to link with the QCA literature.

Chapter 3 (Modelling the molecules and the molecular interaction) models and analyzes molecules proposed for molecular FCN through *ab initio* calculation. It analyses and models monostable and bistable molecules, detailing the effect of electric fields generated by molecules or external electrodes in the static and dynamic regime. This chapter also discusses and validates a model for evaluating molecule ground state energy.

Chapter 4 (Modelling the molecular interaction in FCN circuits: SCERPA) describes the mathematics of the Self-Consistent Electrostatic Potential Algorithm (SCERPA) and discusses the iterative procedure convergence and computational cost. Then, it introduces and assesses approximation techniques for speeding up the calculation, eventually favoring the integration of SCERPA in current CAD tools, and describes the organization and the features of the MATLAB implementation.

Chapter 5 (Molecular FCN circuits) analyses the functioning, the stability, the crosstalk, and possible memory effects of molecular FCN devices. First, the inverters and majority voters are analyzed by addressing the dependencies between molecular nature and circuit-level functioning. Then, this chapter demonstrates a physical-aware design on digital devices by considering the effective physics of the molecules.

Chapter 6 (Conclusion) discusses the thesis outcomes by highlighting the open points which should be investigated to ensure molecular FCN is a possible candidate for future digital electronics, thus providing feedback for the fabrication of a molecular FCN prototype. Also, the future developments of the SCERPA algorithm are discussed, motivating further research on developing a physical-aware simulator able to provide reliable analyses of molecular devices and circuits.

Chapter 1

Introduction and Background

The first chapter of this thesis introduces and discusses the state-of-the-art of the molecular Field-Coupled Nanocomputing (FCN) intended as a possible candidate for future digital electronics. In particular, this chapter introduces the Quantum-dot Cellular Automata (QCA) paradigm and its possible implementations, eventually describing the key aspects of molecular technology. The essential devices used to propagate and elaborate the logic information and the clocking mechanism that will be deeply discussed in this thesis are also introduced. From a technological perspective, this chapter describes the molecules available in the literature, the realization of the input, output, and clocking structures for the integration of FCN with standard Complementary Metal-Oxide Semiconductor (CMOS) technology and the experimental techniques which are promising for the realization of molecular devices, with particular interest regarded the Self-Assembled Monolayer (SAM). Finally, the current models and tools used to analyze molecular FCN devices and circuits are discussed. With a particular interest in the Molecular Simulator Quantum-dot cellular automata Torino (MoSQuiTo) methodology, which will be extendedly used in this work.

1.1 Digital electronics state-of-the-art

The scaling of CMOS permitted the increase of performance and complexity of digital electronics in the last decades thanks to the realization of devices with broad applications [1]. Furthermore, the development of applications requiring wireless

connections on mobile devices, e.g., the Internet of Things, profoundly changed the evolution of electronic technology, which is now more focused on low-power devices. Indeed, most mobile devices are supplied with batteries, which provide a limited amount of energy, thus motivating digital electronics researchers to pursue low-power and high-speed computing devices. In CMOS, the power consumption of circuits may be well-described by the expression:

$$P = fV_{DD}^2$$

Where f and V_{DD} are the operating frequency and supply voltage, respectively. For this reason, in the last few decades, a decrease in the power supply has been used to minimize power consumption. However, reducing power supply required technologists to decrease transistor saturation current, with the consequential decrease of the maximum switching speed, thus limiting maximum computing capabilities. Consequently, a trade-off between power consumption and computational speed is currently necessary.

The immediate approach followed in the last decades to increase performance is device scaling. Indeed, a significant density in terms of Metal-Oxide-Semiconductor Field-Effect Transistor (MOSFET) per chip is achievable, and distances (i.e., interconnection delays) are reduced, eventually reducing power dissipation.

However, with a small transistor size, many quantum effects impinge on the behavior and performance of the transistors and force device models to become more complex, making the analysis and the design of electronic circuits more difficult. In addition, scaling creates problems with power dissipation due to an increase in leakage currents (i.e., a vast dark silicon area).

The very famous Moore's law has guided the CMOS scaling for years. However, from the 80s, many publications claimed the end of the law, and every 5-10 years, researchers wonder when Moore's law will not be followed anymore [2].

"Moore's Law is dead, long live Moore's Law"

Although the pessimistic predictions, Moore's law has continued uninterrupted thanks to the introduction of new alternative devices and technologies. Nevertheless, CMOS technology is approaching the fundamental limit since current technological

nodes are very close to the atomic dimension. Therefore, it will be practically impossible to satisfy Moore's Law by reducing transistor size sooner or later.

For this purpose, several devices based on novel physical devices and architectures are being explored to permit performance improvement of digital electronics. In particular, three strands are currently being explored. First, the "More Moore" wants to increase electronics performance by forcing the scaling process to its limit, increasing the device density at the most industrial possibilities, and eventually exploiting possible technological tricks. The "More than Moore" enables digital devices to improve performance by exploiting heterogeneous integration and inserting novel electronics applications, eventually integrating non-computing elements such as Micro-Electro-Mechanical System (MEMS). Finally, the "Beyond CMOS" trend aims to increase performance by introducing new devices which may eventually be based on alternative physical behaviors.

This thesis focuses on Beyond-CMOS, where several technologies have been proposed for computing. Among the different technologies proposed in the Beyond-CMOS context, this thesis focuses on the molecular FCN. Indeed, the intrinsic nanometric size of molecules makes them favorable for high-device circuit density and high-speed operations. At the same time, Field-Coupled Nanocomputing does not require electron transport, thus electrical current, making it very promising for low-power electronics.

1.2 Field-Coupled Nanocomputing

Among the technologies proposed in the Beyond-CMOS scenario, FCN devices are one of the most promising to bypass CMOS. The basic idea of FCN is to exploit nanostructured elements which store the information in some physical quantity. Then, information can be transferred element-by-element using local field interaction.

The quantum-dot cellular automata

An example of the FCN paradigm is the so-called QCA, proposed by Lent et al. in 1993 [3]. Here, two charges are positioned in a system composed of four quantum dots arranged in a squared manner (the so-called QCA cell), see Fig. 1.1(a). Thanks to Coulomb repulsion, the two charges in the QCA occupy the antipodal quantum

dots in two possible configurations, depicted in Fig. 1.1(b). From a theoretical perspective, the four quantum dots are characterized by four normalized charges $Q_1, \cdots, Q_4$, and the so-called *QCA Logic Polarization* (P) is defined as:

$$P = \frac{(Q_2 + Q_3) - (Q_1 + Q_4)}{Q_1 + Q_2 + Q_3 + Q_4} \tag{1.1}$$

The two configurations used to encode logic information, as depicted in Fig. 1.1(b), are the ones such that:

- Logic 0: $Q_1 = Q_4 = 1$ and $Q_2 = Q_3 = 0$, thus $P = -1$
- Logic 1: $Q_1 = Q_4 = 0$ and $Q_2 = Q_3 = 1$, thus $P = +1$

The concept of the cellular automaton was introduced in the 1940s by Stanislaw Ulam and John von Neumann and is already used in different fields such as mathematics and computability theory. It generally consists of a grid of a finite number of cells that may be in an ON or OFF state. Each cell has several neighbor cells that can influence, or be influenced by, according to a certain predefined rule. Precisely, by aligning several QCA cells, the Coulomb repulsion enables the information to propagate cell-by-cell by copying the information logic on the line [4]. Fig. 1.1(c) shows two wires propagating logic '1' and logic '0'. The first cell of the wire is the driver cell, and its logic information is set externally to propagate specific logic information. By switching the driver logic state from '0' to '1', or vice versa, the information on the wire ideally changes to copy driver configuration, permitting the information propagation. Notice that no charge net transport is involved in propagating the information, thus no current flow, reducing the power dissipation and making this paradigm promising for low-power electronics.

Within the general QCA paradigm, two added quantum dots might be inserted to enable a third configuration, which can be externally forced and used to encode no information. For clarity, Fig. 1.1(d) shows the QCA cell made with six quantum dots with the three possible configurations. Logic states '0' and '1' are encoded with the two electrons on the antipodal quantum dots, whereas the NULL state is encoded when the two electrons occupy the central quantum dots. The NULL state does not encode logic information, yet it is necessary as an intermediate state to delete information and favor the switching between logic states [3].

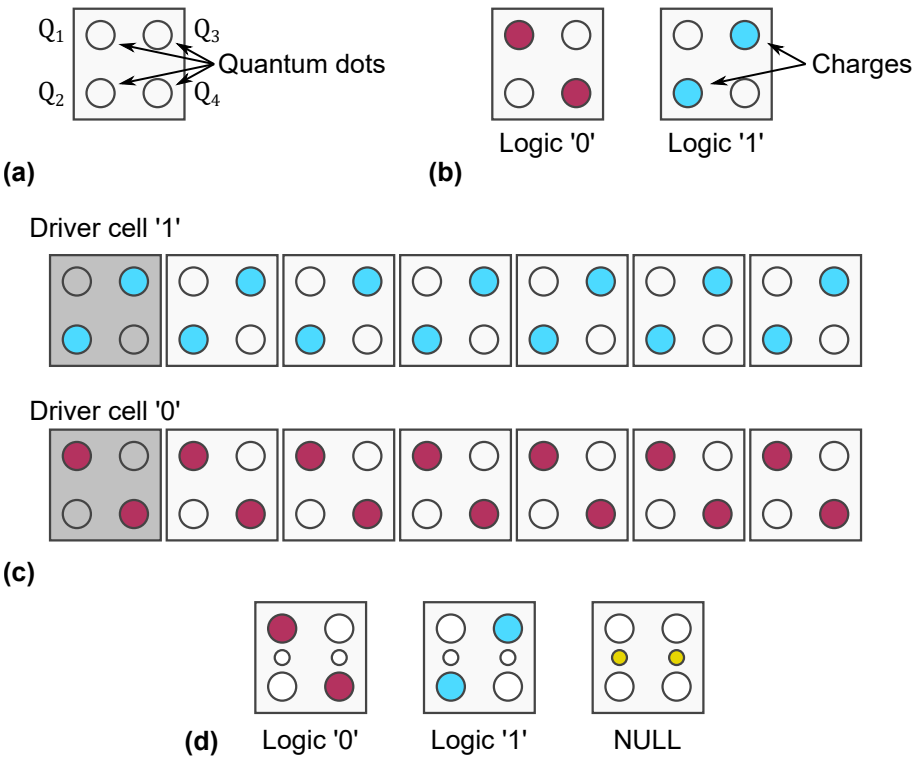

Fig. 1.1 Basics of QCA encoding: (a) Basic cell composed by four quantum dots. (b) QCA cell with two electrons located to encode logic values ‘0’ and ‘1’, respectively. (c) Basic cell composed by six quantum dots. (d) QCA cell with two electrons located to encode logic values ‘0’ and ‘1’ and NULL state, respectively.

Clocking system

As already seen in the previous paragraphs, the Coulomb repulsion can be used to define the information in a QCA cell and propagate the information in QCA wires. Nevertheless, if one wants to propagate the information on long wires, problems related to metastable conditions may happen, and the information propagation may be corrupted [5]. For this purpose, a clocking system is necessary to guide the information propagation. In the general QCA paradigm, the clock changes the potential barriers between cell quantum dots to favor or discourage tunneling, thus inhibiting or promoting the encoding and the consequent propagation of the logic state. For example, in a QCA cell composed of six quantum dots, the clock may be intended as an external stimulus that forces the charge to occupy the two added dots to encode the so-called NULL state.

Regarding QCA wires, they can be divided into the so-called clock zones. Fig. 1.2(a) shows a QCA wire subdivided into four clock zones. Each region can be activated or inhibited according to the clock field. In particular, applying the clock field along the wire makes it possible to guide the information propagation. According to the applied clock, four different phases are defined:

- **Switch phase**: potential barriers are slowly increased to favor the adiabatic switch of cells (equivalently, the charge is removed from the added dots), and cells are moved from the NULL state to one of the two logical states.
- **Hold phase**: potential barriers are kept high to preserve the information. Ideally, no switching of the cell between the logical states is possible; the clock forces the charges to occupy the logic dots.
- **Release phase**: potential barriers are slowly lowered to favor the adiabatic switch of cells towards the NULL state (equivalently, the charge is removed from the logic dots).
- **Relax phase**: potential barriers are kept low to maintain cells in the NULL state; the clock forces the charges to stay in the null dots.

The four phases assembled in a clock signal constitute the clock cycle, generally applied to a single clock region. Fig. 1.2(b) depicts a schematic representation of the clock cycle. In particular, if the device is subdivided into four clock regions

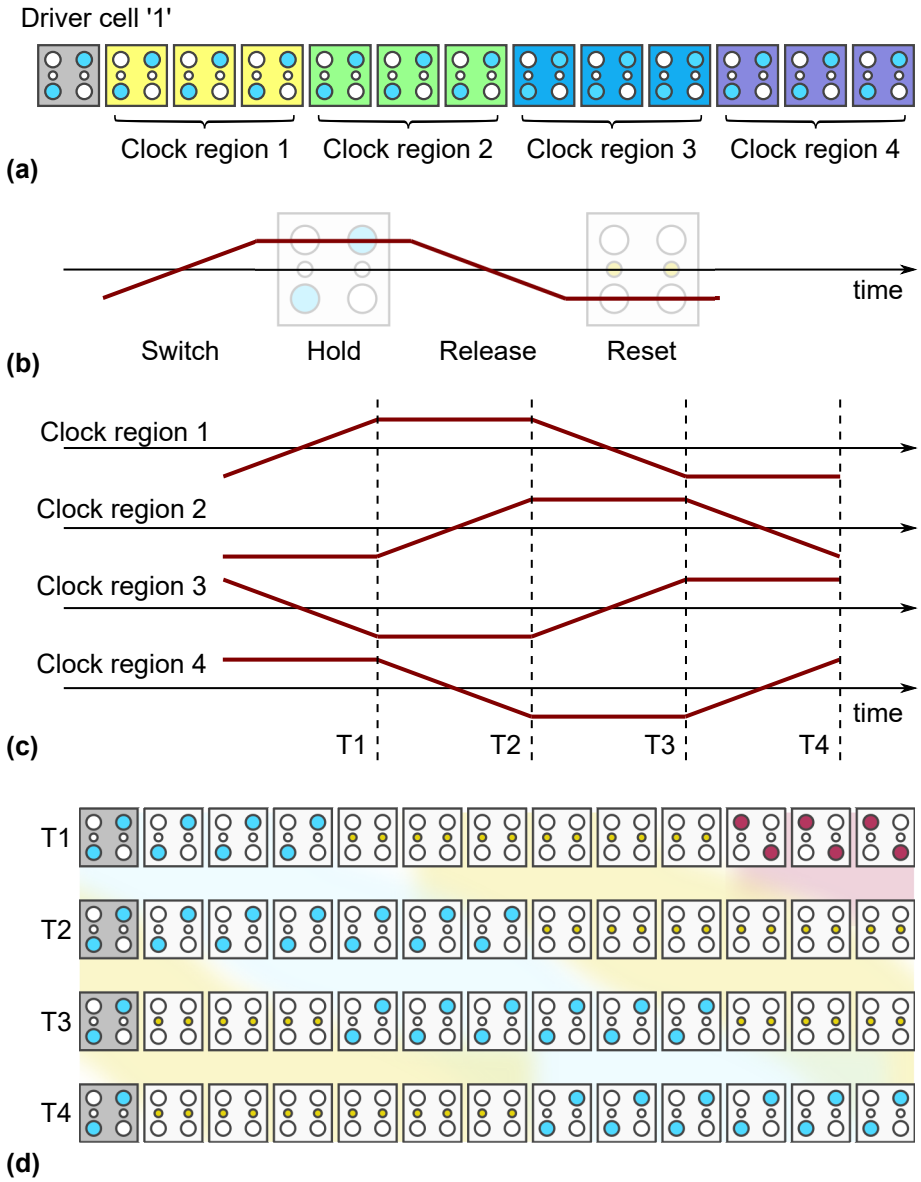

Fig. 1.2 Clocking of QCA cells: (a) Basic QCA wire subdivided into four clock regions. (b) The clock cycle comprises the four clock phases: switch, hold, release, and reset. (c) Four clock cycles shifted by a $\pi/2$ quantity intended to be applied on a four-clock region wire to propagate the information. (d) Propagation of the information on a clocked QCA wire.

which arrange periodically on the circuit, four clock cycles shifted by a quantity $\pi/2$ are applied to the circuit to allow the correct propagation and elaboration of the digital information, see Fig. 1.2(c). As a mean of example, Fig. 1.2(d) shows the propagation in a wire subdivided into four clock regions, each time step (T1, T2, T3, and T4) is associated with a precise timestep reported in Fig. 1.2(c). The shown wire previously encoded '0' (time T1) and propagated, at time T4, logic '1' after a clock cycle.

Indeed, the clocking mechanism permits the implementation of pipelining, eventually increasing the throughput of QCA devices. The clocking mechanism also allows controlling the switching of QCA cells well. In principle, the power dissipation can be reduced to an arbitrarily small amount by acting on the clock timing, thus making the propagation completely adiabatic [6]. The reduction of power dissipation is a direct consequence of the adiabatic theorem:

A physical system remains in its instantaneous eigenstate if a given perturbation is acting on it slowly enough and if there is a gap between the eigenvalue and the rest of the Hamiltonian spectrum.

Formally, the clock is never slow enough to guarantee the adiabatic switching, which means some energy is always dissipated in an actual case. For this reason, it is necessary to introduce the concept of quasi-adiabatic switching. To sum up, the clock introduces several advantages:

- It makes quasi-adiabatic propagation possible by avoiding rapid variations of the QCA cell state.
- It makes pipelining possible, thus increasing the throughput of digital devices.
- It avoids abrupt switching of cells, thus meta-stability problems in the circuits which may create aberrations in the propagation of the information [5].
- It enables true power gain [6]. The clock compensates for losses in intercell coupling.

Elaboration of the information in QCA technology

So far, we have described the information propagation in QCA wires. Moreover, by arranging different QCA cells in specific layouts, it is possible to exploit the

electrostatic interaction to implement digital devices such as the majority voters, inverters, routing devices, logic gates, adders, and even programmable elements [7, 8].

In particular, the inverter and the majority voter are the essential devices implemented in the QCA paradigm. Indeed, any logic function can be realized by exploiting inverters and majority voters, also providing area optimization [9, 10].

Fig. 1.3(a) shows the inverter in the two possible logic configurations: the electrostatic repulsion permits the inversion of the information. Indeed, input logic '1' is inverted to '0', whereas input logic '0' is inverted to '1'. Additionally, Fig. 1.3(b) shows the majority voter in all the eight possible configurations. In this case, the device has three inputs (i.e., three drivers), and the output encodes the majority of the input logic values. Table 1.1 shows the truth table of a majority voter with inputs A, B, and C, and output OUT. The truth table fits the configurations depicted in Fig. 1.3(b). It is interesting to notice that fixing one of the inputs makes it possible to encode essential logic gates. Indeed, by fixing $A = 0$ the logic function is $OUT = A \cdot B$, whereas with $A = 1$ the majority voter encodes the OR function $OUT = A + B$. Again, the majority voter implements OR and AND functions that, together with the inversion operation, permits any logic function implementation. For this purpose, QCA connections also become relevant to route the information among majority voters and inverters. Fig. 1.4(a) shows the most common planar interconnections used to move the information on the plane. The L-connection allows for rotating the information propagation by $\pi/2$. The T-connection splits the information into the two orthogonal directions. Finally, the fanout device allows replicating the information in the three possible directions. Many efforts have also been carried out to realize possible crosswire devices which allow the information to cross wires. The most trivial solution consists in the use of a multilayer crosswire which makes use of a second QCA plane to cross the wire physically [7], shown in Fig. 1.4(b). The crosswire can also be realized with 3D QCA paradigms [11]. These solutions efficiently achieve the information crossing, yet it is not easy to fabricate with all possible QCA-based technologies, for instance, with molecules. Other solutions have been therefore proposed to realize planar crosswires, shown in Fig. 1.4(c). The planar crosswire can be realized by engineering the QCA cells so that the diagonal interaction permits inversion of the information when the two inputs are opposite and copy when the two inputs are equal [12, 13], resulting in the realization of a planar crosswire.

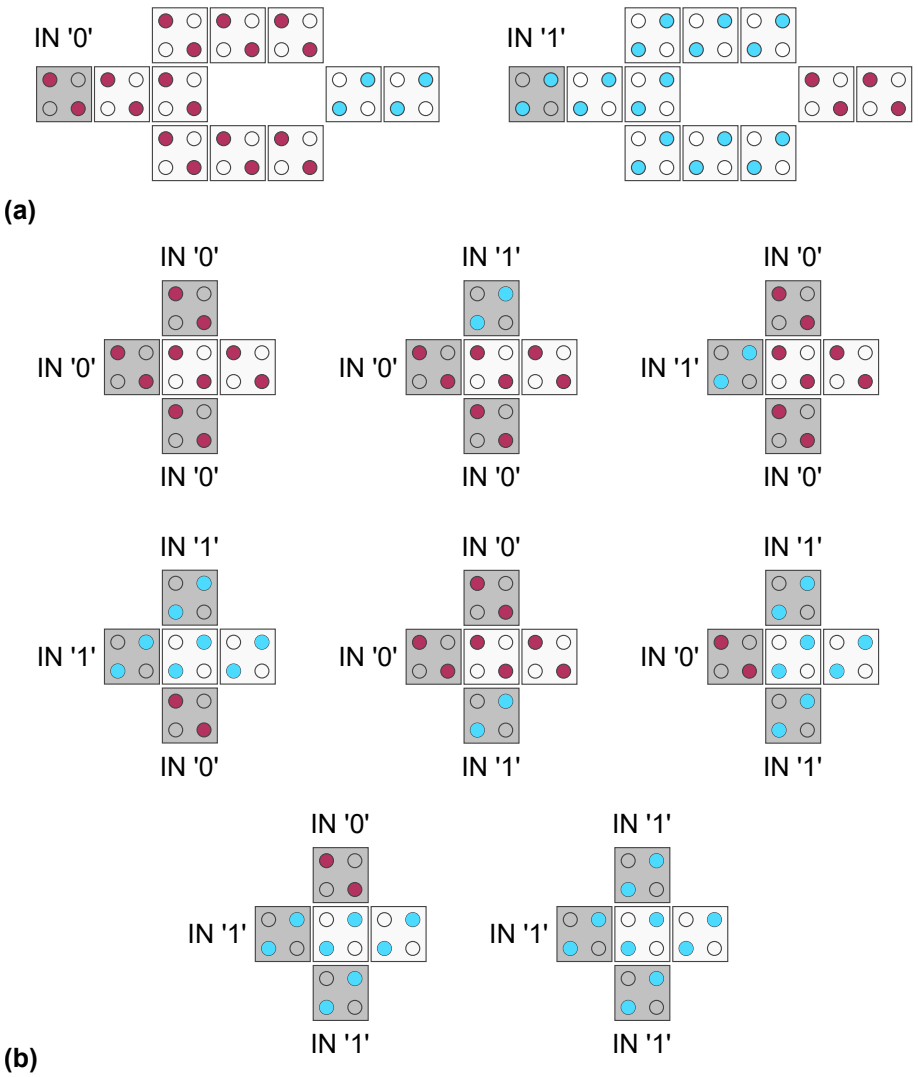

Fig. 1.3 Basic QCA devices: (a) The QCA inverter inverting either '0' and '1' logic values. (b) The QCA majority voter in all the eight possible input configurations.

Table 1.1 Majority Voter Truth table

A	B	C	OUT
0	0	0	0
0	0	1	0
0	1	0	0
0	1	1	1
1	0	0	0
1	0	1	1
1	1	0	1
1	1	1	1

A=0		
B	C	OUT
0	0	0
0	1	0
1	0	0
1	1	1

A=1		
B	C	OUT
0	0	0
0	1	1
1	0	1
1	1	1

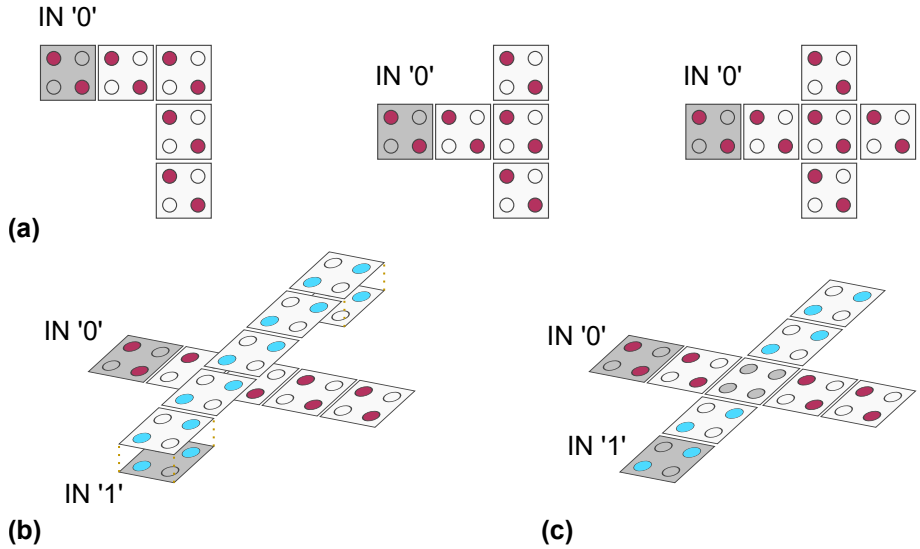

Fig. 1.4 Basic QCA routing connections: (a) Planar interconnections: L, T, and fanout. (b) Multilayer crosswire. (c) Coplanar crosswire.

Implementations of the field-coupled nanocomputing

Field-coupled Nanocomputing may be, in general, implemented by purely reconstructing the quantum-dot cellular automata, creating four quantum dots, and provoking two charge excess. An example is the quantum-dot cellular automata implemented with semiconductor or metal dots [14–16], schematically depicted in Fig. 1.5(a). Here, two solid quantum dots are connected squarely. The possible charge in the quantum dots may tunnel vertically thanks to ad-hoc deposited tunnel junctions, whereas it can influence horizontally adjacent quantum dots through coupling capacitors.

The QCA can also be implemented through molecules [17, 18]. In this case, the single charge is substituted by the charge distribution on the molecule, which polarizes according to the external electric stimuli generated by other molecules or external electrodes [19]. Fig. 1.5(b) shows two bis-ferrocene molecules [20, 21] encoding the three QCA states in the charge distribution of molecules, mimicking the behavior of an ideal QCA cell. The molecular implementation of the QCA is one of the most promising. Indeed, it permits the fabrication of uniformly sized devices with nanometric dimension [22], and it promises extremely low power consumption at ambient temperature and very high frequency [6].

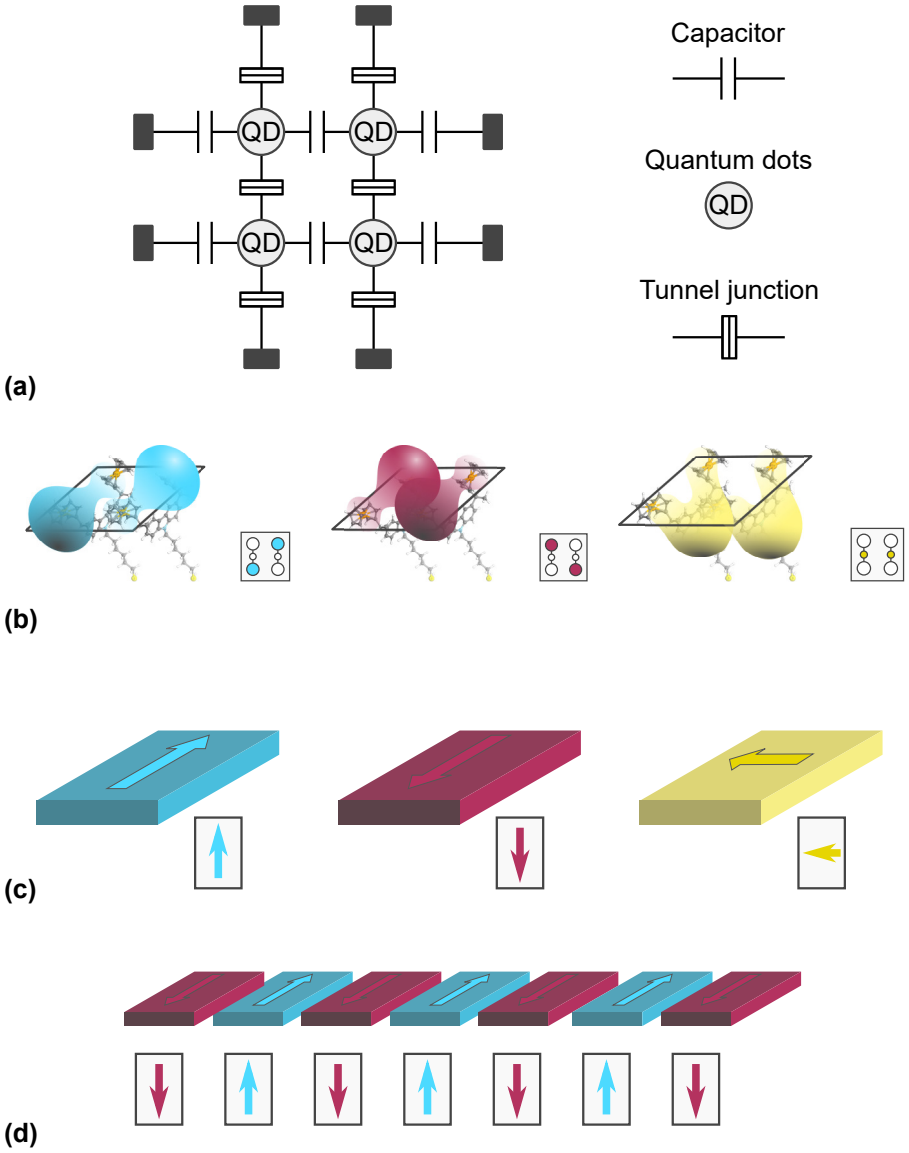

Fig. 1.5 Basics of QCA encoding: (a) Basic cell composed by four quantum dots. (b) QCA cell with two electrons located to encode logic values '0' and '1', respectively. (c) Basic cell composed by six quantum dots. (d) QCA cell with two electrons located to encode logic values '0' and '1' and NULL state, respectively.

The molecular QCA technology will be named in this work with the more general name molecular FCN. Indeed, there are specific characteristics of the technology which may differ from the standard and formal definition of the QCA [13]. The FCN can also be realized with devices that do not perfectly fit the QCA concept. For instance, in Nano-Magnetic Logic (NML), the information is encoded in the magnetization of micromagnets, see Fig. 1.5(c), that can communicate through local magnetic coupling among adjacent magnets, eventually permitting the information propagation, see Fig. 1.5(d).

1.3 Molecular Field-Coupled Nanocomputing

The Molecular FCN is a promising implementation of the QCA paradigm, which exploits molecular cells. Generally, the molecular cell is obtained by virtually encasing two molecules in a squared manner. Possible molecule redox centers act as quantum dots and enable the QCA paradigm, thus encoding the logic and NULL states. Considering molecules with three redox centers consist of the so-called molecular half-cell. Two juxtaposed half-cells create the molecular FCN cell, equivalent to the QCA cell. The two molecules are generally intended to be oxidized; therefore, one positive charge is present on each molecule, and the logic encoding is possible thanks to the localization of the electron cloud on redox centers. The total charge of the molecular FCN cell is 2 e. Notice that this holds only from the point of view of the QCA paradigm. Counterions are generally placed to make the charge of the entire cell neutral and avoid interference among cells [21]. When the two oxidation-relate charges occupy the logic dots, the molecular cell encodes logic ‘1 ’ or ‘0’, whereas the NULL state can be implemented by forcing the charge in the bottom groups of the molecule by using an external electric clock field [23, 24]. Similar to the general QCA paradigm, the clocking field guides information propagation and elaboration. It is essential to notice that the two oxidation charges should not leave the molecular cell. Otherwise, the QCA paradigm cannot be implemented since charge transport among cells would be present: molecules are used as charge containers. Notice that, in principle, molecules should also be reduced: the total charge of the molecular FCN cell would be -2 e or neutral [25]. The electrostatic nature of the molecule will be deeply discussed in this thesis.

Several reasons make molecular FCN promising. Indeed, all the molecules are intrinsically nanometric and have the same size, permitting the realization of uniformly sized and highly dense devices. Density on the order of 10^{11} – 10^{14} devices cm^{-2} can be achieved with molecular FCN [22]. Also, molecular FCN cells do not require cryogenic conditions and can be used at room temperature [26] enabling very low-power dissipation at very high speed, which is expected to reach 1 THz [6].

Notice that, from an experimental point of view, the chemistry world is often opposite to that requested by the molecular FCN technology. Indeed, the paradigm relies on the encoding and propagation of the information on single molecules. Yet, most laboratory chemists are generally able to observe the combined effects and properties of whole monolayers rather than single molecules whose isolation is still highly challenging, even though much research is ongoing in the analysis of single molecules [27–29] and will probably be even more available in the future. Computational chemistry, physical chemistry, and modelling techniques represent a set of essential tools for understanding and assessing molecular technologies in this context. Indeed single molecule behaviour phenomena, e.g. molecular vibrations, are well known from theory even though challenging to measure with an experimental set-up. Computational chemistry tools may instead evaluate single-molecule behaviour, which may then be combined with theoretical models to predict circuit-level effects.

1.3.1 Molecules for Molecular Field-Coupled Nanocomputing

Several molecules of several types have been proposed to implement molecular FCN. This work distinguishes the molecules in terms of stability and electrostatic behavior. For simplicity, we consider the molecules as a system composed of three charges, here named *dots*: Q_1, Q_2, and Q_3. In particular, we will refer to Q_1 and Q_2 as *active dots* since they are intended to provide logic capability in molecular FCN, whereas Q_3 is considered as the *NULL dot*, thus the DOT enabling the encoding of the NULL state. The molecular FCN cell is created by juxtaposing two molecules. The logic encoding is possible when the molecule charge is aggregated on Q_1 or Q_2. According to the stability of the molecule, we can have two types of molecules:

- Bistable molecule: the charge naturally aggregates on one of the two dots Q_1 and Q_2. At the thermal equilibrium, the molecule naturally shows a dipole

moment. Two stable configurations exist and are energetically equivalent. Some energy is necessary to switch the molecule between the two states.

- Monostable molecule: at the thermal equilibrium, the charge does not aggregate on Q_1 nor Q_2. Thus the molecule does not show a dipole in the switching direction. Energy should be applied to force the charge to move from one dot to another and to keep the charge aggregated on the dot.

Notice that the molecule stability can be generalized. Indeed the molecule can also show three stable states when the molecule is stable when the charge naturally aggregates on Q_3 also. In general, each molecule can show many states, all stable. Generally, we consider a bistable molecule to have two stable states with the same energy. In general, the energy of the stable states may be different. Each state is, in any case, a minimum in the Potential Energy Surface (PES) of the molecule (see Section 2 for theoretical details on the PES). Notice that molecular FCN was proposed with bistable molecules, whereas monostable molecules have been addressed recently as possible molecules to implement computation [30, 5, 31]. According to the molecule electrostatic nature, we can instead have four types of molecules:

- Neutral molecules: when encoding logic information, the sum of the charges constituting the active dots is null ($Q_1 + Q_2 = 0$), and the overall molecule charge is always null ($Q_1 + Q_2 + Q_3 = 0$).
- Oxidized molecules: when encoding logic information, the sum of the charges constituting the active dots is +1 ($Q_1 + Q_2 = 1$), and the overall molecule charge is always +1 ($Q_1 + Q_2 = +1$).
- Reduced molecules: when encoding logic information, the sum of the charges constituting the active dots is -1 ($Q_1 + Q_2 = -1$), and the overall molecule charge is always -1 ($Q_1 + Q_2 = -1$).
- Zwitterionic molecules: the sum of the charges constituting the logic dots is +1 ($Q_1 + Q_2 = 1$), whereas the overall molecule charge is always zero ($Q_1 + Q_2 + Q_3 = 0$) [32, 33]. This molecule is an intermediate situation between the neutral and the oxidized species [13].

Notice that oxidized (and reduced) molecules are often coupled with a counterion to ensure molecule neutrality. In this case, the molecule is electrostatically similar

to a zwitterionic compound. However, the counterion should be considered in the analysis of the molecule, especially when interfacing with other molecules, as it may be responsible for possible disturbances in the intermolecular interaction [13, 34, 35].

Several molecules have been proposed for implementing the molecular FCN paradigm in the last decades. However, the physical behavior of molecules is often assumed to be consistent with the QCA paradigm: a molecule can switch between two stable states via electron transfer.

Two important molecules from the modelling and historical perspectives are the diallyl-butane and the decatriene:

- The diallyl-butane, shown in Fig. 1.6(a), was proposed as a two-dot molecule, thus a possible molecular half cell. It consists of two allyl groups working as aggregation points, thus dots. This molecule has been deeply studied for molecular FCN application. In particular, it was one of the pioneer molecules used for modeling molecular devices. In the beginning, the molecule was proposed as a bistable molecule [17], even though recent works analyzed the molecule with specific computational methods demonstrating that the diallyl-butane is a monostable molecule [30].
- The decatriene molecule, Fig. 1.6(b), is composed of three ethylene groups. C=C bonds act as quantum dots. This molecule has been analyzed as cation as a reference molecule for 3-dot molecule modeling, demonstrating that the switching of a molecule composed of three dots can be approximated with a 3×3 Hamiltonian matrix [36].

The presented molecules have been used often for modeling purposes and are good candidates for explaining computation basics, yet they are not easy to synthesize and difficult to deposit. Indeed, a few others molecules have been lately proposed to favor the assessment of the technology, eventually demonstrating the deposition of a SAM. In this context, mixed-valence compounds are promising as possible candidates for computation.

The bis-ferrocene molecule, shown in Fig. 1.6(c), was synthesized ad-hoc for molecular FCN [20]. It is composed of two ferrocene units linked by a carbazole. The molecule has been successfully anchored on a gold substrate through the link with a hexanethiol [21]. This molecule has been deeply studied in the literature

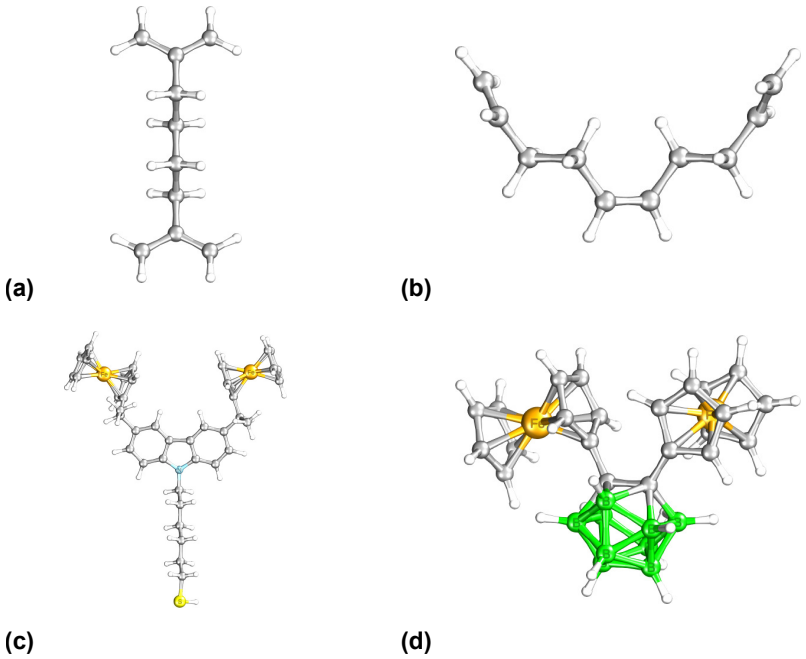

Fig. 1.6 Molecules proposed in the literature for Molecular FCN: (a) diallyl-butane. (b) Decatriene. (c) bis-ferrocene. (d) Dyferrocenyl Carborane.

and analyzed from an electrostatic point of view, demonstrating from a theoretical perspective the possibility of encoding logic information [18].

Finally, the dyferrocenyl carborane represents one of the last molecules synthesized ad-hoc for the implementation of the considered technology [37]. The molecule includes two ferrocene units and a carborane cage that acts as an internal counterion. In addition, the molecule is zwitterionic. Thus it is overall neutral.

Other molecules have also been proposed. For example, some researchers also proposed molecular computation using actin proteins [38, 39]. At the current state-of-the-art, researchers are still pursuing the perfect molecule providing encoding and switching capabilities, eventually considering also the easiness related to the synthesis and deposition of the molecule on the substrate [40].

1.3.2 Input and output of molecular FCN devices

The realization of a write-in and a readout system is necessary to guarantee the usability of the eventual device and the possible integrability of molecular FCN with CMOS technology. Concerning the realization of inputs, the single molecule may be

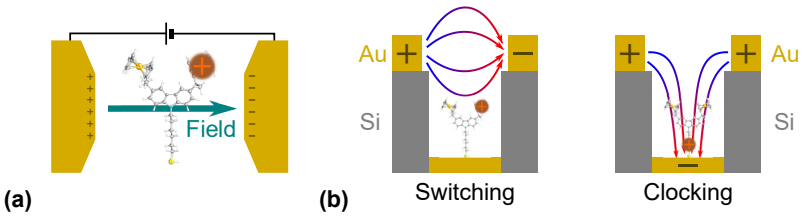

Fig. 1.7 Write-in and clocking structures: (a) Schematic representation of a write-in system; two electrodes generate an electric field that forces the bis-ferrocene molecule to polarize, thus the possible charge to aggregated on one of the two ferrocene units. (b) Possible structure realized to provide both write-in and clocking capabilities. In *Switching* configuration, only the top electrodes are connected to the external voltage, creating a field that polarizes the bis-ferrocene molecule and aggregates the charge on one of the two ferrocene groups. In *Clocking* configuration, the two top electrodes are connected to the same voltage, whereas the bottom electrode is connected to a different voltage. This configuration creates a field that forces the charge to aggregate on the bottom (or top) groups of the molecule, providing RESET or HOLD states.

positioned between two electrodes [19, 41], making possible the application of an electric field that forces the charge to distribute in a precise manner, see Fig. 1.7(a). Recent works [42] also proposed a three-electrode realization which also permits the clocking mechanism, shown in Fig. 1.7(b).

Concerning the readout system, authors in [41] proposed the use of nanosized transistors for detecting the charge of polarized mixed-valence molecules. Fig. 1.8(a) shows a schematic representation of a bis-ferrocene molecule with one of the two ferrocene units inserted in the gap between a hypothetic gate and the substrate. The presence of an eventual charge on the ferrocene would lead to a variation of the charge profile of the transistor with consequent modulation of the gate capacitance, see Fig. 1.8(b). An alternative approach recently proposed and discussed in [43] consists in using bistable molecules which present a different vibrational behavior when polarized in the two stable states. Fig. 1.8(c) shows a 1,1,2-trifluorononа-1,8-diene, this molecule presents two stable states with different asymmetric geometries and, consequently, asymmetric vibrational modes. In principle, the charge detection can be performed by measuring the molecule vibrational spectrum, which varies according to the encoded state, see Fig. 1.8(d). Finally, Single-Electron Transistor (SET), eventually realized at the molecular scale, looks promising for the sensing close charges [44]. SET devices demonstrate they can detect charges in possible quantum dots in the vicinity of the transistors. An eventual SET realized at the

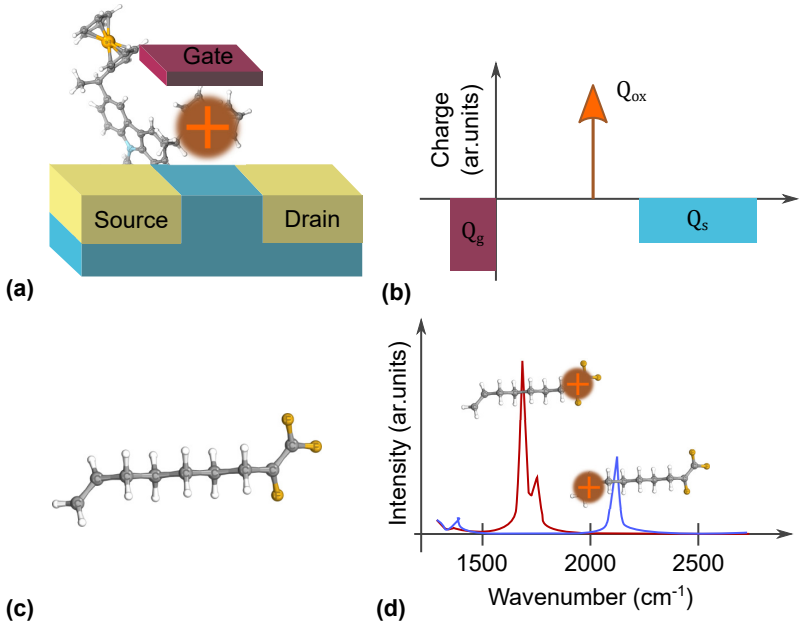

Fig. 1.8 Readout systems for molecular FCN: (a) Transistor-based readout system. The ferrocene group of a bis-ferrocene molecule is positioned in the gate dielectric of a transistor. (b) Charge diagram of a transistor readout system with the ferrocene charge positioned in the gate dielectric of a transistor. The charge Q_{ox} is representative of the oxidation of the bis-ferrocene molecule. (c) Bistable 1,1,2-trifluorononа-1,8-diene cation, proposed in [43]. (d) Vibrational spectrum of a 1,1,2-trifluorononа-1,8-diene in the two stable states, the vibrational spectrum varies with the position of the charge, making the readout possible by exploiting spectroscopy techniques [43].

molecular scale may be potentially used to measure the charge on a molecule, thus providing readout capabilities.

1.3.3 Fabrication of Molecular FCN

Notwithstanding some FCN technologies have already been experimentally demonstrated, for instance, aluminum metallic-dot QCA cells have been measured at the cryogenic temperature in [45]. Magnetic FCN technology has also been demonstrated experimentally by measuring the propagation of information in an NML wire [46]. However, a molecular prototype is still missing due to the needed very high nanopatterning resolution and the difficulties in sensing the charge of molecules. Several molecules have been deposited to study the deposition and chemical characteristics of the molecules. The bis-ferrocene and the dyferrocenyl-carborane, which have been synthesized ad-hoc for implementing FCN, are possible examples [20, 21, 37].

Some steps have also been performed towards realizing a prototype, especially concerning the technological techniques. Hydrogen Depassivation Lithography (HDL) and nanoshaving are, for instance, promising for the nanopatterning of SAMs [47], and also Scanning Tunnelling Microscopy (STM) demonstrates auspicious results [48]. Finally, electron beam lithography and DNA nanopatterning have been used successfully to realize the prototype of a molecular circuit [49]. Concerning the realization of electrodes, for the clocking and drive structures, several techniques permit the realization of very thin nanowires [50–52]. Fascinating steps have also been performed in IBM concerning the charge imaging of single molecules using Kelvin-Probe Microscopy [27].

Fabrication of organic thin films

Most of the molecules involved in molecular FCN might be deposited on substrates through the realization of SAM [21, 37], thus by realizing patterned organic thin films. In the last decades, organic thin films have become of high interest in the field of nanotechnology, biotechnology, and molecular electronics, as they often exhibit optical, electrical, optoelectronic, mechanical, chemical, and other properties which are very interesting in the application standpoint and which are not accessible with inorganic materials [53]. SAMs are very organized organic molecular assemblies formed spontaneously on surfaces by adsorption (i.e., adhesion of atoms on a surface) [54, 55]. The most famous case of SAM is the deposition of sulfur-ended alkyl chains terminated by sulfur elements on gold substrates.

Each molecule involved in the generation of the SAM is generally composed of two parts, as depicted in Fig. 1.9(a): the head group and the functional group, as depicted in Fig. 1.9(a). The ‘head’ is a chemical group that strongly reacts with the substrate, favoring the adhesion of the molecule, thus the formation of the SAM. The ‘functional’ group depends on the final application of the created SAM.

Concerning the possible head groups, the thiols are organosulfur compounds R-SH (R represents an alkyl or an organic substituent) that generally present good affinity with metal substrates such as gold. Silanes are compounds with four substituents on silicon, and at least an organic compound (e.g., trichlorosilane $SiHCl_3$, tetramethylsilane $Si(CH_3)_4$, and tetraethoxysilane $Si(OC_2H_5)_4$), which are generally used on non-metal oxide surfaces. Fig. 1.9(b) shows the thiol, the tetramethylsilane and the tetraethoxysilane, whereas Fig. 1.9(c) shows the tetraethoxysilane. Particu-

larly relevant are also the phosphonates, thus compounds containing $C-PO(OH)_2$ or $C-PO(OR)_2$ groups, shown in Fig. 1.9(d). It is important to mention amphiphiles, molecules obtained as the union of an apolar group with a polar one of more or less the same size. These molecules are important because they permit the use of some SAM fabrication techniques that will be discussed in the next paragraphs.

The head groups are typically connected to molecular chains, which end with functional groups that can vary their physical/chemical properties as a response to possible external stimuli, consequently varying the property of the surface. This phenomenon is often used to create biosensors. Consequently, the choice of the molecule depends both on the type of used substrate with the corresponding needed reaction (technological perspective) and on the final application (application perspective). The most common molecule which is used for the creation of Self-Assembled Monolayer is the alkanethiol, which is a molecule composed of an alkyl chain $(C-C)^n$, a tail group, and a $S-H$ head group. Fig. 1.9(d) shows the ferrocenyl-hexanethiol (6-(ferrocenyl)hexanethiol, $C_{16}H_{22}FeS$), an example of a molecule often used for the creation of SAM. In this specific case, the hexanethiol constitutes the head group, as it is supposed to chemically bond with a gold substrate, whereas the ferrocene group is the functional group. This molecule is often used to create molecular diodes.

Concerning the realization of SAMs, several techniques are available. The first example is the Langmuir and Langmuir-Blodgett (LB) film, whose realization is schematically depicted in Fig. 1.10. First, a molecular layer of amphiphiles is deposited on the water surface in an unorganized manner. The polar 'head' is submerged in the water, whereas the 'tail' is on the surface since it is apolar. Then, the molecular layer is pressed by two plates so that the density of the molecules increases, thus pushing the organization of the layer. An immersed substrate is then pulled out from the water, promoting the adhesion of the Langmuir monolayer on the solid surface and creating the so-called LB film.

Other techniques are possible to fabricate SAMs, such as the Organic Molecular Beam Deposition (OMBD) and Organic Molecular Beam Epitaxy (OMBE), which exploit the evaporation in Ultra-High Vacuum (UHV) conditions, similarly to the techniques used for the deposition of inorganic layers [56]. In OMBD, a flux of molecules impacts a substrate kept at a high temperature. The equipment necessary for OMBD is costly and challenging to maintain and control. Finally, the SAM can be realized by depositing organic molecules in a solution or from a gas phase. The

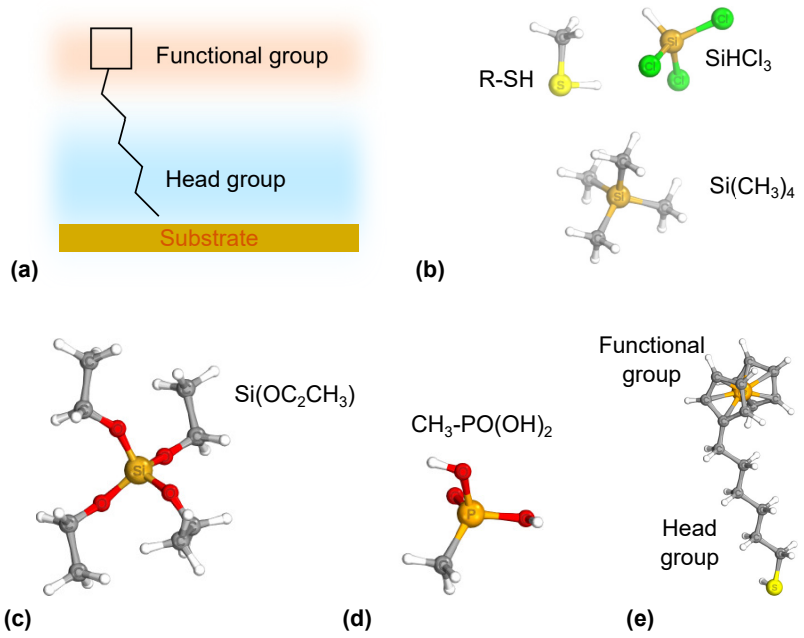

Fig. 1.9 (a) Basic scheme of the typical molecule used in the realization of SAMs, with 'head' anchoring the molecule on the substrate and 'functional' groups. (b) Thiol ($R-SH$), trichlorosilane ($SiHCl_3$), and tetramethylsilane ($Si(CH_3)_4$). (c) Tetraethoxysilane ($Si(OC_2H_5)_4$). (d) Phosphonate group ($C-PO(OH)_2$). (e) 6-(ferrocenyl)hexanethiol ($C_{16}H_{22}FeS$).

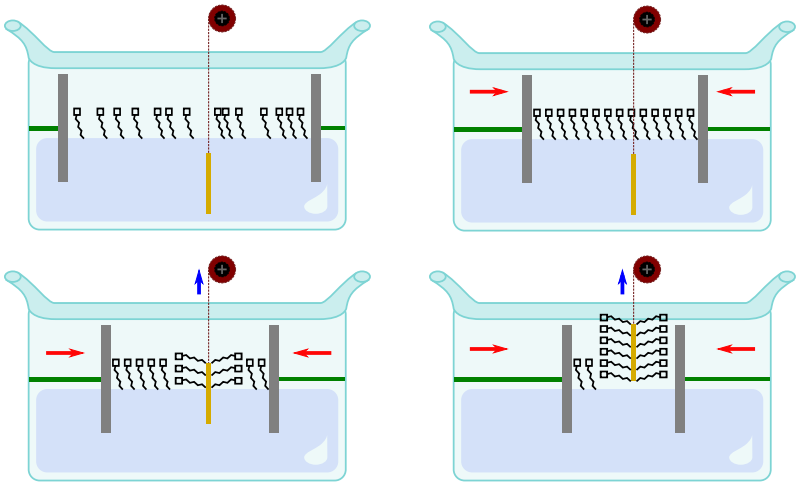

Fig. 1.10 Complete procedure for the realization of a LB thin film.

head reacts with the substrate chemically, thus promoting the adsorption of the head with the substrate. The alkanethiol-gold surface reaction is an example of SAM realized through a solution. Indeed, the SAM can be realized by immersing the gold surface in a solution composed of alkanethiol in a solvent. The sulfur group of the alkanethiol reacts with the gold substrate to link with the gold atoms.

Organic monolayers can be considered an ensemble of molecules regularly organized on a substrate. To characterize the monolayers quantitatively, we must consider the nanoscale structure and distinguish two different aspects:

- **The molecule position and alignment with the substrate**: the molecules deposit with a tilt angle between the molecule and substrate.
- **The organization of molecules on the substrate**: it defines the so-called overlayer structure, which is the two-dimensional organization of the organic monolayer, eventually following a precise substrate-dependent ordering. The overlayer structure can be described with the so-called Wood's notation.

1.4 The analysis of FCN circuits

Contrarily to standard CMOS electronics, the simulation of molecular technologies is generally far from being mature enough to satisfy the high requirements of Computer-Aided Design (CAD) tools. From a theoretical perspective, the analysis of molecules

should be performed with *ab initio* calculation, which is a numerical technique used to evaluate the Schröedinger equation characterized by a very high computational cost. Therefore, the use of *ab initio* calculation is limited to the analysis of single molecules or systems composed of a few molecules [17, 23, 57]. In addition, *ab initio* tools generally permit the use of a single static uniform electric field, which makes challenging the analysis of multi-clock region circuits, where circuits require the application of many electric fields on the same circuit, which eventually vary with time. The simulation of entire circuits is not possible with a fully *ab initio* calculation. Details regarding this computational technique will be given in Section 2.

A first attempt to simplify the analysis of molecular FCN devices was performed in [58], where the charge distribution of a molecular wire was performed by calculating the charge distribution on each molecule alone, in the same order of the wire, with *ab initio* calculation. The first molecule of the wire was analyzed in the presence of a point charge driver forcing a specific polarization of the first molecule. In turn, the obtained charge distribution was used as the driver molecule of the following molecule in the *ab initio* analysis. In general, the procedure is iterated along with the wire. The obtained charge distribution of the i-th molecule, under the influence of a point charge driver (molecule $i-1$) is used to realize the driver for the following molecule ($i+1$) in the *ab initio* calculation. This method was the first attempt to simplify the *ab initio* calculation. The computational cost is reduced since only single molecules were simulated, and computationally manageable point charges emulate adjacent molecules. However, from a practical perspective, the molecules of the wire cannot be considered dependent only on the charge distribution of the previous molecule. Indeed, when a molecule charge distribution is changed from an adjacent molecule, it generates an electric field that impacts the charge distribution of the influencing molecule. In general, all the molecules in a circuit interact and influence other molecules. Therefore, the need for a self-consistent procedure is straightforward.

A first self-consistent algorithm was proposed in [59, 42]. The method has been established in the so-called MoSQuiTo methodology and will be enhanced and discussed intensely in the methodology Section 3. The iterative procedure relies on a characterization performed with an *ab initio* tool, yet the interaction is evaluated with electrostatic equations, making the computational effort manageable and compatible with design requirements. The self-consistent procedure was already used to demonstrate the propagation of the information on molecular wires by

considering a possible non-ideal rough substrate, demonstrating the link between the substrate characteristics and the device performance [60].

Concerning the general QCA paradigm, authors in [4] proposed an iterative procedure to evaluate the propagation of the information in QCA wires. In addition, QCADesigner [61] is a tool that is often used in the context of the general QCA paradigm without specifically addressing a precise QCA technology. Generally speaking, QCADesigner offers the possibility to evaluate the polarization of any QCA cell inserted in a group of other cells by exploiting the Two-state approximation [62] and the concept of Kink Energy. Details on the theory will be discussed in Section 2. The cell is generally composed of four quantum dots, following the historical definition of the QCA. Thus, the software does not natively consider the molecular implementation of the paradigm, yet the agreement between the cell physics and the two-molecule system should be guaranteed in terms of geometry and physical characteristics if one wants to use QCADesigner. Also, many molecules should be modeled with the quantum dots (i.e., the complete cell is composed of six quantum dots), which requires the use of a three-state approximation [36], still not implemented in QCADesigner. The Two-State Approximation (TSA) model implemented in QCADesigner permits the analysis of general QCA devices, which can be eventually implemented with molecules. However, a tool that validates the final device with molecular granularity is needed to assess the molecular FCN technology since it is necessary to ensure a correct link between the physics of the molecule and the circuit. The tool and the model must consider molecular physics, geometry, and the eventual technological parameters. QCADesigner has been recently enhanced also to evaluate the power dissipation [63, 64].

Another tool it is worth mentioning is a tool for the simulation of atomic silicon quantum-dot circuits, named Silicon Quantum Atomic Designer (SiQAD) [65], and NMLSim [66], for the simulation of NML technology.

1.4.1 ToPoliNano and MagCAD

Other tools have also been proposed for the analysis of FCN devices. It is worth mentioning: TOrino POLItecnico NANOtechnology (ToPoliNano) and MagCAD, which consist of a complete suite for providing design capabilities through Computer-Aided Design (CAD) and Electronic Design Automation (EDA) tools [67].

ToPoliNano [68] is a tool that allows the design and the simulation of emerging FCN technologies following an approach similar to the one of CMOS. Indeed, ToPoliNano starts from a VHSIC (Very High Speed Integrated Circuits) Hardware Description Language (VHDL)/Verilog description of the circuit and generates the circuit layout according to technology-related constraints and design rules. This tool also integrates the Fiction design tool [69]. Besides the design and simulation, MagCAD [70, 71] is a tool that allows the drawing of FCN devices and is fully compatible with ToPoliNano. ToPoliNano and MagCAD currently support magnetic FCN, even though molecular FCN is currently under integration [67] and part of the work in this thesis favored the integration of the molecular characteristics into the ToPoliNano framework.

1.4.2 The MoSQuiTo methodology

This thesis uses MoSQuiTo methodology to study and analyze the molecular FCN molecules, devices, and circuits with minimal exploitation of *ab initio* calculation, thus reducing the computational cost. The methodology was proposed in [18] as a two-step procedure for the analysis and the modeling of the molecule. Recently, MoSQuiTo was completed in [25] by including a third step regarding the interaction among molecules and the circuit analysis. The three steps are discussed in the following sections.

Ab initio calculation

Computational chemistry analysis permits the analysis of the molecule and allows evaluating the molecule conformation energy and geometry at the equilibrium or in a dynamic regime. Chapter 2 gives a brief description of the theory behind *ab initio* calculation. In addition, it is possible to evaluate the so-called charges obtained by fitting the Molecular Electrostatic Potential (MEP), see Section 2.1.4 which represents the charge distribution of a molecule in a precise state. The molecule, composed by N atoms, can be therefore approximated by atomic charges with values $\{q_1, \cdots, q_N\}$ in positions $\{\boldsymbol{r}_1, \cdots, \boldsymbol{r}_N\}$. Fig. 1.11(a) shows the diallyl-butane approximated with a set of atomic charges (q_i). The atomic charges can also be used to evaluate the dipole moment (μ) of a molecule, to a reference point ($\boldsymbol{r}_0$), with good precision [25]:

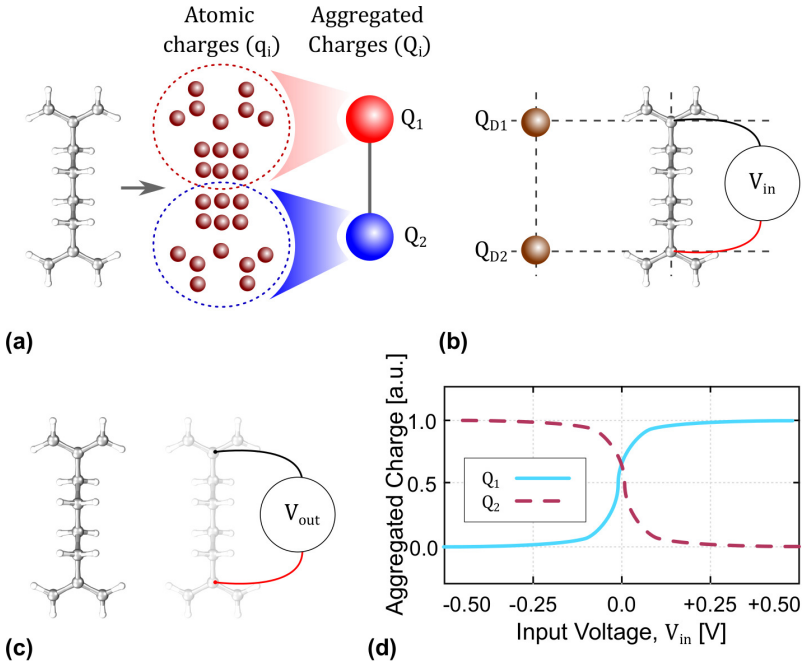

Fig. 1.11 The MoSQuiTo methodology: (a) Construction of the Aggregated Charge for a diallyl-butane molecule; the molecule is analyzed with ab initio calculation to obtain the atomic charges, q_i, which are then grouped into the Aggregated Charges, Q_i. (b) Definition of the input voltage, V_{in}, of a molecule obtained by evaluating the voltage generated by a point-charge driver system composed of charges Q_{D1} and Q_{D2}. (c) Definition of the output voltage, V_{out}, of a molecule obtained by evaluating the voltage generated by the diallyl-butane molecule. (d) Vin-Aggregated Charge Transcharacteristics of a molecule, obtained by linking the Aggregated Charge with the Input Voltage.

Table 1.2 Hartree Atomic Units

Quantity	**Value in SI units**	**Value in other units**
Charge	1.602×10^{-19} C	
Dipole Moment	8.478×10^{-30} C m	2.542×10^{9} D
Electric Field	5.142×10^{11} V m^{-1}	
Energy	4.359×10^{-18} J	
Length	5.292×10^{-11} m	0.529 Å
Polarizability	1.649×10^{-41} C m^2 V^{-1}	
Time	2.419×10^{-17} s	
Voltage	27.211 V	

$$\boldsymbol{\mu} = \sum_i q_i(\boldsymbol{r}_i - \boldsymbol{r}_0) \tag{1.2}$$

Electric fields may be applied to evaluate the molecule response to external stimuli that may be the response of external electrodes (e.g., inputs or clock electrodes) or other molecules. In the latter case, point charges may be used to model possible molecules in precise charge configurations. Fig. 1.11(b) shows a point charge driver system, composed of two charges Q_{D1} and Q_{D2} intended to influence a diallyl-butane molecule.

This work makes use of the ORCA package [72, 73]. ORCA is an *ab initio* quantum chemistry tool which contains modern electronic structure methods. The free version is available for academic use[1]. ORCA package permits the exploitation of parallel computing to speed up the calculation. Parallel computing is available through Open MPI[2]. Geometries may be generated with Avogadro[3].

Notice that, in computational chemistry, dealing with sub-nm elements, quantities are generally expressed with particular units named Hartree Atomic Units (abbreviated as *au* or *a.u.*), which are chosen according to four fundamental physical constants to facilitate the description of electron properties. Particularly, Table 1.2 reports the main quantities and corresponding SI values.

[1] ORCA forum, official website - Accessed on 18 August 2022
[2] Open MPI, official website - Accessed on 18 August 2022
[3] Avogadro, official website - Accessed on 18 August 2022

Figures of merit

Ab initio calculation outputs consist of chemical quantities describing the electronic properties of the molecule and the eventual wavefunction. To provide an electronics description of the molecule, with proper input and output, the second step of the methodology post-processes the information obtained from *ab initio* calculation to provide quantities that can be used by software and electronics engineers to describe the information propagation and elaboration. The MoSQuiTo methodology provides a set of figures of merit that allow studying the switching capabilities of molecules and their eventual influence on neighbor molecules [25]. Mainly, it provides a framework to consider molecules as electronic devices. Indeed, the molecule is considered a black box with a precise charge distribution, named Aggregated Charge (AC), which represents the status of a molecule. The aggregated charge is obtained from the distribution of atomic charges by grouping them into specific groups, which mimic the electrostatic behavior of the molecule. Fig. 1.11(a) shows the procedure to derive aggregated charges Q_1 and Q_2 from the atomic charges obtained from ab initio calculation. The aggregated charge represents the charge distribution of the molecule and its electrostatic behavior. Indeed, it is possible to evaluate with good approximation the molecule dipole moment with good precision [25]. In particular, the atomic charges are generally normalized with respect the electron charge (e=1.602 176 634 $\times 10^{-19}$ C). The generic aggregated charge (Q_i) is linked with the corresponding atomic charge (q_i) as:

$$e \cdot Q_i = q_i$$

The dipole moment can be evaluated by rewriting Equation (1.2):

$$\boldsymbol{\mu} = e \sum_i Q_i (\boldsymbol{r}_i - \boldsymbol{r}_0) \tag{1.3}$$

Additionally, it is possible to use the aggregated charge to evaluate the voltage ($V(\boldsymbol{r})$) generated by the molecule. In the generic case the molecule is composed by N_{AC} charges in positions $R_1, \cdots, R_{N_{AC}}$ the voltage may be evaluated as:

$$V(\boldsymbol{r}) = \frac{e}{4\pi\varepsilon_0} \sum_{\alpha=1}^{N_{AC}} \frac{Q_\alpha}{|\boldsymbol{r} - R_\alpha|}$$

Where $\varepsilon_0 = 8.854\,187\,812\,8 \times 10^{-12}\,\mathrm{F\,m^{-1}}$ is the vacuum permittivity. The aggregated charge also represents the molecule status variable considered an electronics device. Therefore, input and output quantities may be defined by integrating the electric field. In particular, the Input Voltage (V_{in}) is the voltage received by a molecule, which can be evaluated by integrating the electric field generated by other molecules or external electrodes $\boldsymbol{E}(\boldsymbol{r})$ on a path (γ) connecting the two active dots:

$$V_{in} = \int_{\gamma} \boldsymbol{E}(\boldsymbol{r}) d\boldsymbol{r}$$

Fig. 1.11(b) shows a schematic representation of the input voltage evaluated by integrating the electric field generated by a point-charge driver system. In the same way, it is also possible to define the output voltage as the voltage received by a fictitious molecule, evaluated by integrating the electric field generated by the molecule under consideration, see Fig. 1.11(c).

Notice that it is possible to evaluate the atomic charges with ab initio calculation by stimulating it with a precise point charge driver and, consequently, the aggregated charge. There is a strict link between the aggregated charge and the input voltage. By linking these two quantities, it is possible to define the so-called Vin-Aggregated Charge Transcharacteristics (VACT), which represents the link between the input and the status of the molecule considered an electronic device. Fig. 1.11(d) depicts a possible VACT. Notice the particular trend of the VACT, which tends to be linear in the central region, whereas the charge saturates for a high voltage. For this purpose, the central region of the VACT is generally referred to as *linear region*, whereas for high voltages, the term *saturation region* is generally used. From the VACT, it is also possible to evaluate the output voltage from the aggregated charge, therefore linking the input to the output in the so-called Vin-Vout Transcharacteristics (VVT) [25]. The mentioned quantities provide a complete description of the molecule and its electrostatic behavior and can be used to study the interaction among molecules.

Circuit level analysis

Once the molecule is well characterized from an electronics perspective, a molecular FCN circuit can be considered a group of connected molecules. In the simplest case of a wire, one may imagine that the input of a single molecule is the output voltage of the previous molecule. However, the input voltage of a specific Molecule Under

Test (MUT) depends on the charge distribution of all the circuit molecules. Once the MUT input voltage and the consequent MUT aggregated charges are evaluated, the molecule generates an electric field that influences other molecules and changes molecule charge distributions. It is necessary to develop a self-consistent procedure to obtain a meaningful evaluation of circuit charge distribution. In particular, in this thesis, the self-consistent procedure is integrated into a complete simulation tool which is named Self-Consistent ElectRostatic Potential Algorithm (SCERPA) [74, 35]. It permits the analysis and the design of molecular FCN circuits by considering the link between the physics of the molecule and the system-level characteristics of the circuit. This work also makes use of MagCAD [70, 71], which is interfaced with SCERPA to facilitate the drawing of FCN devices.

Chapter 2

Theoretical Background

This chapter describes the theoretical basics necessary to understand the concepts contained in this thesis and to provide the electronics engineer with a possible background to understand molecular physics and computational chemistry. First, it discusses the basics of computational chemistry regarding static properties of molecules, obtained by solving the Schroedinger equation with *ab initio* tools. The Hartree-Fock (HF) and Density Functional Theory (DFT) computational methods are discussed to provide a complete view of the *ab initio* world to the electronics engineer, both for the time-independent and time-dependent problem. Then, the focus is moved to evaluating molecular properties essential to analyze molecules and derive properties necessary for modeling molecular Field-Coupled Nanocomputing (FCN) electronics devices, which can be generally obtained by solving the Schrödinger equation for the molecule, which is a computationally expensive task. In particular, molecular vibrations and the effect of the electric fields (i.e., the polarizability) are analyzed. Finally, the chapter also briefly describes the Two-State Approximation (TSA) theory to provide a link for Quantum-dot Cellular Automata (QCA) literature.

2.1 The time-independent quantum problem

In the *ab initio* perspective, the molecule is considered a group of atoms from the computational chemistry perspective. Each atom of the molecule is composed by:

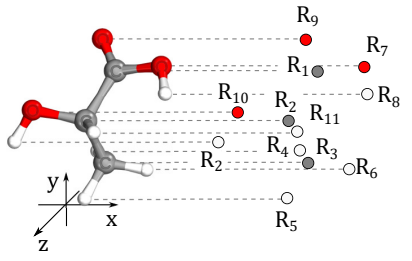

(a)

C - R1 = (-0.2501, +3.4429, -0.0836)
C - R2 = (-1.0194, +2.1490, +0.2050)
C - R3 = (-0.5255, +1.0610, -0.7486)
H - R4 = (-0.7146, +1.3634, -1.7782)
H - R5 = (-1.0480, +0.1232, -0.5498)
H - R6 = (+0.5431, +0.8798, -0.6286)
O - R7 = (+0.9276, +3.5599, +0.5877)
H - R8 = (+1.0248, +2.8517, +1.2341)
O - R9 = (-0.5869, +4.2714, -0.8709)
O - R10 = (-2.3930, +2.4220, +0.0498)
H - R11 = (-0.8152, +1.8449, +1.2426)
H - R12 = (-2.8540, +1.6035, -0.1513)

(b)

Fig. 2.1 Perspective of the *ab initio* calculation: (a) 2-Hydroxypropanoic acid (Lactic acid) $C_3H_6O_3$ represented in the 3D space. (b) Cartesian coordinates in angstrom of the lactic acid nuclei.

- Nuclei, composed by neutrons (mass 1.67×10^{-27} kg - Charge 0 a.u.) and protons (mass 1.67×10^{-27} kg - Charge 1 a.u.)
- Electrons (mass 9.31×10^{-31} kg - Charge -1 a.u.)

The molecule can be studied with Quantum Mechanics (QM) as a set of N_N positive nuclei, with position $\boldsymbol{R}_i = \{X_i, Y_i, Z_i\}$ and charge $Q_i \cdot e$, and a set of N_e electrons, with position $\boldsymbol{r}_i = \{x_i, y_i, z_i\}$ and charge $-e$. Fig. 2.1(a) shows an example of molecule (lactic acid) represented as a group of nuclei with coordinates $\boldsymbol{R}_i$. Fig. 2.1(b) shows the cartesian coordinates of the nuclei. The time-independent QM problem can be written as:

$$\widehat{H}\Psi = E\Psi$$

where $\widehat{H}$ is the molecular Hamiltonian, E is the eigenvalue and Ψ is the so-called molecular wavefunction, which can be written as a function of nuclear and electron coordinates:

$$\begin{aligned}\Psi = \Psi(R,r) =& \Psi(X_1, Y_1, Z_1, \cdots, X_{N_N}, Y_{N_N}, Z_{N_N}, x_1, y_1, z_1, \cdots, x_{N_e}, y_{N_e}, z_{N_e}) \\ =& \Psi(\boldsymbol{R}_1, \cdots, \boldsymbol{R}_{N_N}, \boldsymbol{r}_1, \cdots, \boldsymbol{r}_{N_e})\end{aligned}$$

The quantity $|\Psi(\boldsymbol{R},\boldsymbol{r})|^2$ is the probability to find the molecule in a precise status where the nuclei and the electrons have coordinates $\boldsymbol{R}$ and $\boldsymbol{r}$ respectively. Instead, the so-called molecular Hamiltonian ($\widehat{H}$) can be expressed as it follows:

$$\widehat{H} = \widehat{T}_N + \widehat{T}_e + \widehat{V}_{NN} + \widehat{V}_{Ne} + \widehat{V}_{ee}$$

Where $\widehat{T}_N$ and $\widehat{T}_e$ are the kinetic contributions for nuclei and electrons respectively, whereas $\widehat{V}_{NN}$, $\widehat{V}_{Ne}$, and $\widehat{V}_{ee}$ are the potential energies associated to nuclei-nuclei, nuclei-electrons and electrons-electrons interactions, respectively. Other terms (e.g., magnetic effects and the effects of external electric fields) may be inserted but neglected for the scope of this discussion.

Notice that the proton mass is 1.67×10^{-27} kg, whereas the electron mass is 9.31×10^{-31} kg. Consequently, the kinetic energy of nuclei is negligible, and one can imagine the electrons moving in an average potential generated by nuclei. This approximation leads to an equivalent QM problem related to the electron only:

$$[\widehat{T}_N + \widehat{V}_{Ne} + \widehat{V}_{ee}]\Psi_{el}(r,R) = E\Psi_{el}(r,R)$$

The nuclei are considered frozen: the electron wavefunction Ψ_{el} still depends on nuclear coordinates, but not on the nuclear velocities. This concept is known as Born-Oppenheimer Approximation (BOA). The quantity $|\Psi(\boldsymbol{R},\boldsymbol{r})|^2$ is the probability of finding the electrons in a precise position r considering the nuclei in frozen coordinates R. The nuclei, considered point charges, generate an electrostatic potential: the electrons sense that electrostatic potential.

By evaluating the energy of the molecule as a function of the nuclei coordinates, we can define the so-called Potential Energy Surface (PES) as:

$$E_{PES}(\boldsymbol{R}) = E(X_1, Y_1, Z_1, \cdots, X_{N_N}, Y_{N_N}, Z_{N_N})$$

The PES may show several local minima, which represent the possible conformation geometries of the molecule. For instance, a bistable molecule will show two minima in the PES. The procedure to find the geometry minimizing the PES value is known as *Geometry Optimization*. By considering the BOA, the final QM problem for the only electrons becomes:

$$[\widehat{T}_e + \widehat{V}_{NN} + \widehat{V}_{Ne} + \widehat{V}_{ee}]\Psi_{el}(\boldsymbol{r},\boldsymbol{R}) = E\Psi_{el}(\boldsymbol{r},\boldsymbol{R})$$

Which can be expanded as:

$$\left[-\sum_i \frac{\hbar^2}{2M_i}\nabla^2 \boldsymbol{r}_i - \sum_i \sum_j \frac{Z_i e^2}{4\pi\varepsilon_0 |\boldsymbol{R}_i - \boldsymbol{r}_j|} + \frac{1}{2}\sum_i \sum_j \frac{e^2}{4\pi\varepsilon_0 |r_i - r_j|} + \right.$$
$$\left. + \sum_i \sum_j \frac{Z_i Z_j e^2}{4\pi\varepsilon_0 |\boldsymbol{R}_i - \boldsymbol{R}_j|}\right] \Psi_{el}(r,R) = E\Psi_{el}(\boldsymbol{r},\boldsymbol{R}) \quad (2.1)$$

2.1.1 Linear combination of atomic orbitals and Hartree-Fock method

One can imagine that the molecular wavefunction depends on the wavefunction of each electron. In isolated atoms, electrons lie in atomic orbitals. Similarly, in molecules, each electron lies in a Molecular Orbital (MO), and one may suppose the wavefunctions of atoms somehow combine to create the molecular orbitals and the eventual electron wavefunction. The most trivial combination is the so-called Hartree product, where the electron wavefunction (Ψ_{el}) is created by supposing the product of atomic orbitals (Ψ_i).

$$\Psi_{el} = \prod_i \Psi_i(x_i, y_i, z_i) = \Psi_1(x_1, y_1, z_1) \cdot \cdots \cdot \Psi_{N_e}(x_{N_e}, y_{N_e}, z_{N_e})$$

In the most simple case of a two-MO molecule, with two MOs (Ψ_1 and Ψ_2) and two electrons in positions $\boldsymbol{r}_1$ and $\boldsymbol{r}_2$, the Hartree product is written as:

$$\Psi_{el} = \Psi_1(\boldsymbol{r}_1) \cdot \Psi_2(\boldsymbol{r}_2) = \Psi_1(x_1, y_1, z_1) \cdot \Psi_2(x_2, y_2, z_2)$$

This is the most trivial combination, which is generally not used since it does not consider anti-symmetry principle. Indeed, if one imagines to have the two electrons in the same position $\bar{r} = (\bar{x}, \bar{y}, \bar{z})$, it comes out that:

$$\Psi_{el}(\bar{r}) = \Psi_1(\bar{x}, \bar{y}, \bar{z}) \cdot \Psi_2(\bar{x}, \bar{y}, \bar{y})$$

That generally is a non-null term, implicating a probability of finding two electrons in the same position instantaneously, which is impossible. Therefore, the so-called Slater-Determinant is a second more common possibility to express the electron wavefunction. Considering a number N of MOs, it may be expressed as:

$$\Psi_{el} = \frac{1}{\sqrt{N!}} \begin{vmatrix} \Psi_1(x_1,y_1,z_1) & \cdots & \Psi_N(x_1,y_1,z_1) \\ \cdots & \cdots & \cdots \\ \Psi_1(x_N,y_N,z_N) & \cdots & \Psi_N(x_N,y_N,z_N) \end{vmatrix}$$

For two MOs, thus $N = 2$:

$$\Psi_{el} = \Psi_1(x_1,y_1,z_1)\Psi_2(x_1,y_1,z_1) - \Psi_2(x_2,y_2,z_2)\Psi_1(x_2,y_2,z_2)$$

In this case, if the two electrons are in the same position $\bar{r}$, it comes out:

$$\Psi_{el}(\boldsymbol{r}) = \Psi_1(\bar{x},\bar{y},\bar{z})\Psi_2(\bar{x},\bar{y},\bar{z}) - \Psi_2(\bar{x},\bar{y},\bar{z})\Psi_1(\bar{x},\bar{y},\bar{z}) = 0$$

Which means that the probability of finding two electrons in the same position is null.

At this point, we have to solve the QM problem and derive the expression of the MO wavefunctions. To do this we exploit the so-called Linear Combination of Atomic Orbitals (LCAO), that is, we express the molecular orbital Ψ_{MO} as a combination of atomic orbitals $\Psi_{AO,i}$, weighted with coefficients c_i, centered on atoms:

$$\Psi_{MO}(x,y,z) = \sum_{i=1}^{N_e} c_i \Psi_{AO,i}(x - X_i, y - Y_i, z - Z_i)$$

Quantum chemistry tools have to find the set of c_i minimizing the energy: this is the so-called Hartree-Fock method. We can express the energy of the system by using the variational principle:

$$E = \frac{\int \Psi_{el} \widehat{H}_{el} \Psi_{el}^* dV}{\int \Psi_{el} \Psi_{el}^* dV}$$

2.1.2 Basis sets

The remaining unknown quantity is the expression of the atomic orbital. The physically best-motivated orbital is the so-called Slater Type Orbital (STO) (it is a solution of the Schrödinger equation). STO functions are precise, yet they are computationally challenging to treat and difficult to integrate numerically. For this reason, the atomic orbital of atom i is generally approximated as a sum of Gaussian functions:

$$\Psi_{AO,i}(x,y,z) = \sum_{j=1}^{N_e} k_j G_j(x,y,z)$$

Where G is the so-called Gaussian Type Orbital (GTO). The idea is to fit the STO orbital with a set n of GTO orbitals. Therefore, one defines the so-called STO-nG basis set, that is, n Gaussian functions fitting for the STO orbital (STO-3G, STO-4G, STO-5G, ..., STO-nG).

STO-nG orbitals provide a precise description of atoms in normal conditions. However, the atomic orbitals may be stretched due to external stimuli. For example, an electric field may polarize the molecule, deforming the electron cloud in a specific direction. Symmetrical Gaussian/Slater orbitals cannot account for this effect. For this purpose, so-called *polarization functions* are introduced, which are functions modeling higher momentum orbitals (orbitals that should not be naturally occupied). For instance, in the hydrogen atom (H), only $s-type$ orbitals are generally occupied. Therefore, a nonsymmetrical orbital is created by adding a $p-type$ orbital (generally not occupied) and mixing it with an $s-type$ orbital, which allows the electron to go further from the nuclei in specific directions.

A second important set of functions are the *diffuse functions*, which are GTOs with a small exponent used to describe the regions far from nuclei. These functions are needed to describe better long-distance effects, such as van der Waals interactions.

Notice that the most important orbitals playing a relevant role in the chemical reactions are the valence orbitals; therefore, it makes no sense to express all the orbitals with the same number of GTOs. Here come the Split-valence Basis sets, which are typically expressed with the notation:

$$X - YZg$$

Where X represents the number of STOs used for the core orbitals. Two sets of atomic orbitals represent the valence orbitals. The first set is approximated by Y GTOs, whereas Z GTOs approximate the second one. Some examples of possible basis sets are:

- $3-21G$ – 3 GTOs for the core orbitals, valence orbitals are split into two orbitals, one composed of 2 GTOs, one with one orbital
- $3-21G*$ – Polarization functions on heavy atoms
- $3-21G**$ – Polarization functions on heavy atoms and hydrogen
- $3-21+G$ – Diffuse functions on heavy atoms
- $3-21++G$ – Diffuse functions on heavy atoms and hydrogen
- $3-21+G**$ – Polarization functions on heavy atoms and hydrogen, as well as diffuse functions on heavy atoms

Also, very widely-used basis sets are the Split-Valence *Ahlrichs basis sets* SV, SVP, DZ, TZV, TZVP, QZVP, and the *Karlsruhe basis sets*, redefined from Ahlrichs basis sets, def2-SVP, def2-TZVP, def2-QZVP, def2-QZVPPD. In particular, def2-SVP splits the basis set into core and valence orbitals. The core and the valence orbitals are represented by a single set of functions (Gaussian orbitals). Def2-TZVP splits the basis set into core and valence orbitals. The valence orbitals are three sets of functions (Gaussian orbitals).

2.1.3 Density Functional Theory

DFT is an alternative approach to the HF method, which is a computational technique based on the so-called electron density (ρ). This quantity can be written as:

$$\rho(\boldsymbol{r}) = \int \cdots \int |\Psi(\boldsymbol{r}_1, \boldsymbol{r}_2, \cdots, \boldsymbol{r}_{N_e})|^2 d\boldsymbol{r}_1 \cdots dr_{N_e}$$

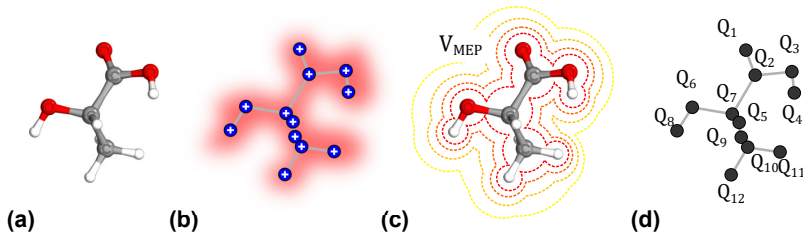

Fig. 2.2 CHELPG method: (a) Lactic acid. (b) Representation of the lactic acid in terms of positive nuclei and negative electron cloud. (c) Schematic representation of the MEP generated by the lactic acid. (d) Charges obtained by fitting the MEP throught the CHELPG method of the lactic acid.

The DFT theory reveals that the molecule energy can be written as a function of the electron density $E = E[\rho(\boldsymbol{r})]$. Mathematically, it can be expanded into two contributions:

$$E = E'[\rho] + Functional$$

Where $E'[\rho]$ is a closed-form equation describing the energy-density relation (for a set of N_e non-interacting electrons). The second term (functional, partially empirical) incorporates the terms not (yet) included in the relationship. The problem becomes similar to the HF and can be solved by finding the electron density ρ that minimizes the molecule energy.

2.1.4 Molecular electrostatic properties

The molecule is composed of positive (nuclei) and negative (electrons) charges. Fig. 2.2(a) shows the lactic acid, together with the positive charges of the nuclei and the negative cloud caused by the electrons, Fig. 2.2(b). Thus, the molecule naturally generates an electrostatic potential which is named Molecular Molecular Electrostatic Potential (MEP):

$$V_{MEP}(\boldsymbol{r}) = \frac{1}{4\pi\varepsilon_0}\sum_{N_N}\frac{eQ_i}{|\boldsymbol{R}_i - \boldsymbol{r}|} - e\int\frac{\rho(\boldsymbol{r})}{|\boldsymbol{r}' - \boldsymbol{r}|}d\boldsymbol{r}'$$

Fig. 2.2(c) shows a representative potential generated by the lactic acid. It is possible to evaluate a set of N normalized charges (Q_i) generating the same potential through a fitting. This technique is usually known as the CHarges from

ELectrostatic Potentials using a Grid-based method (CHELPG) method [75]. The voltage generated by each point charge can be written with electrostatic equations:

$$V_C(\boldsymbol{r}) = \frac{e}{4\pi\varepsilon_0} \sum_{i=1}^{N} \frac{Q_i}{|\boldsymbol{r}_j - \boldsymbol{r}_i|}$$

The error one should minimize is the defined as the difference between the MEP potential V_{MEP} and the voltage generated by the point charges V_C :

$$\varepsilon^2 = [V_{MEP}(\boldsymbol{r}) - V_C(\boldsymbol{r})]$$

By minimizing the error, a set of normalized charges $\{Q_1, \cdots, Q_N\}$ can be obtained. This set of charges, shown in Fig. 2.2(d) for the lactic acid, generates an electrostatic potential that agreeably fits the potential generated initially by the molecule ($V_C \approx V_{MEP}$). The set of charges describes the electrostatic behavior of the molecule.

2.2 The time-dependent characteristics of molecules

So far, the molecules have been considered: static in the time-domain, at cryogenic temperature, strictly ensuring the BOA. On the other hand, the nuclei and the electron have some kinetic energy and show dynamic properties in an actual situation depending on the temperature (i.e., interaction with the external environment). In particular, dynamics properties may be related to nuclei, as in the case of molecular vibrations, or electrons, as in the case of electron transfer or dynamic polarizability.

In the case of molecular FCN technology, both dynamic properties are important indeed: nuclei movements may impact the capability of the molecule to encode information and influence neighbors molecules, whereas electron dynamic properties are crucial in assessing the fundamental capabilities of the molecular switch in terms of switching velocity. However, both the topics, thus nuclear and electron movement, are still poorly studied in the literature on molecular FCN. Therefore, this thesis introduces some analysis concerning the nuclei. Therefore, this section briefly discusses and describes some theoretical background about electron dynamics,

even though the study of electron dynamics and molecular FCN is left as a future perspective of this thesis work.

2.2.1 Molecular vibrations

As already said, molecules are not frozen in space, yet, the atoms tend to move due to thermal noise. In particular, the higher the temperature, the higher the kinetic energy of the atoms, providing some periodic nuclear movements known as *molecular vibrations*. In a molecule composed of N atoms, each atom is characterized by three cartesian coordinates. Thus, the entire molecule is composed of $3N$ coordinates. Considering that each atom may move in the three directions, there are $3N$ degrees of freedom involving translation, rotations, and vibrations. In any case, some rotations and translations do not produce variations in the internal coordinates of the molecule. Indeed, if the entire molecule is translated in the three directions, the molecule is preserved. Also, the rotation of the entire molecule on the mass center does not produce any variation in the internal coordinates. To sum up, it comes out that, for non-linear molecules, the number of vibrational modes is $3N-6$. On the other hand, if the molecule is linear, the rotation on its principal axis should not be considered: the number of vibrations is $3N-5$.

To proceed further with the theoretical discussion and the types o molecular vibrations, it is necessary to define the so-called polarizability of the molecule. In particular, the molecule is composed of positive nuclei and negative charges. However, according to the electronegativity of the atoms and other physical properties, the center of positive and negative charges is not always the same, making the molecule polar. Then, polar molecules exhibit a natural electrical dipole moment ($\boldsymbol{\mu}$). The dipole moment can generally be natural or induced by an external electric field ($\boldsymbol{E}$). By considering, for simplicity, the neutral molecule (i.e., with a null dipole moment), an eventual electric field generates a dipole moment. If the electric field is sufficiently small, the dipole moment can be evaluated linearly [76]:

$$\boldsymbol{\mu} = \alpha \boldsymbol{E} \tag{2.2}$$

Where α is the so-called polarizability tensor and describes the attitude of a molecule to generate a dipole moment as a response to an electric field. The polarizability can be written in matrix form as:

$$\begin{pmatrix} \mu_x \\ \mu_y \\ \mu_z \end{pmatrix} = \begin{pmatrix} \alpha_{xx} & \alpha_{xy} & \alpha_{xz} \\ \alpha_{yx} & \alpha_{yy} & \alpha_{yz} \\ \alpha_{zx} & \alpha_{zy} & \alpha_{zz} \end{pmatrix} \begin{pmatrix} E_x \\ E_y \\ E_z \end{pmatrix}$$

The term $\{\alpha_{ij}\}$ represents the attitude of the molecule to polarize on the direction i (i.e. to increase μ_i) as a consequence of the field component along the j direction (E_j). In general, the field mainly generates a dipole moment which is orientered in the same direction, therefore, the equation can be often approximated as:

$$\begin{pmatrix} \mu_x \\ \mu_y \\ \mu_z \end{pmatrix} = \begin{pmatrix} \alpha_{xx} & 0 & 0 \\ 0 & \alpha_{yy} & 0 \\ 0 & 0 & \alpha_{zz} \end{pmatrix} \begin{pmatrix} E_x \\ E_y \\ E_z \end{pmatrix} \tag{2.3}$$

Polarization and dipole moments are fundamental in the discussion of molecular vibrations. Indeed, one can distinguish two types of molecular vibrations according to the electrostatic behavior and consequences of molecular vibrations. Molecular vibrations vary the position of nuclei and, consequently, the dipole moment and/or the polarizability. Generally speaking, the molecule polarizability increases with the size of the molecule, whereas the dipole moment increases with the asymmetry of the molecule. In general, vibrations changing the dipole moment are associated with the so-called **Infrared Active** modes. For these molecules, the dipole moment has an oscillatory behavior with a frequency corresponding to the frequency of the vibrational modes.

In some other cases, the molecular vibration mainly varies the molecule size periodically. In these cases, the molecular vibration varies the molecule polarizability rather than the dipole moment. The polarizability follows the oscillatory movement of the vibrational mode. The mode is named *Raman Active* mode and is used in the Raman spectroscopy to identify molecular species. In particular, the polarizability can be written as:

$$\alpha = \alpha_0 + \alpha_1 \sin(2\pi\nu t)$$

Where ν is the frequency of the vibrational mode, α_0 is the equilibrium polarizability, whereas α_1 is the polarizability induced by the vibrational mode. In particular, if

an electric field with frequency f_E is applied to the molecule, the dipole moment becomes:

$$\mu = \alpha E = [\alpha_0 + \alpha_1 \sin(2\pi\nu t)]\,[E_0 \sin(2\pi f_E t)]$$

According to trigonometry:

$$\mu = \alpha_0 E_0 \sin(2\pi f_E t) + \frac{\cos[2\pi(f_E - \nu)t] - \cos[2\pi(f_E + \nu)t]}{2}$$

Therefore, the incidence of an electric field at frequency f_E produces three frequency contributions in the dipole moment:

- Rayleigh scattering: a dipole moment oscillating at the frequency of the electric field f_E
- Stokes scattering: a dipole moment oscillating at the frequency $f_E - \nu$
- Anti-stokes scattering: a dipole moment oscillating at the frequency $f_E + \nu$

In the context of molecular FCN, it is necessary to evaluate and take vibrational modes into account. Indeed, the infrared active modes may vary the charge distribution of the molecules, eventually impinging on the encoding capabilities of the molecules, whereas Raman active modes may vary the polarizability of the molecule, eventually impinging on the switching capabilities.

2.2.2 Dynamic computational chemistry

So far, the chemical problem was analyzed from a static standpoint without considering the time explicitly. Molecules were considered at the ground state. In the DFT perspective, the wavefunction of a molecule can be considered as function of the electron density (ρ):

$$\Psi = \Psi(\rho(\boldsymbol{r}))$$

By moving to the dynamic domain, the wavefunction can be written as:

$$\Psi(t) = \Psi(\rho(\boldsymbol{r}), t, \Psi_{t=0})$$

Where t represents the time variable, thus $\Psi_{t=0}$ is the wavefunction at time $t = 0$. It is worth asking whether the BOA is still valid or not. In general, there are three types of analysis concerning dynamic regimes:

D1 Nuclear movement is relevant concerning the scope of the analysis, whereas the electrons can be considered at the ground state. An example is the study of molecular vibrations, where one is generally interested in the movement of nuclei, and the study of electron wavefunction dynamics is not strictly relevant.

D2 Nuclear movement is not relevant concerning the scope of the analysis. Electrons cannot be considered at the ground state. This study focuses on the movement of the electron cloud. For example, the analysis of polarization dynamics is mainly affected by electron dynamics rather than nuclear movements, which are far slower.

D3 Both the nuclear and electronic movements are relevant to the scope of the analysis, and the dynamics of the molecule must be considered thoroughly. For example, it is necessary to consider nuclear and electronic movements when studying electron transfer since it results from a nuclear movement.

Accordingly, three different techniques are essential in studying molecule dynamics, depending on the analysis type.

Molecular dynamics is the most trivial case of study concerning the dynamics of molecules. In particular, this method permits the study of nuclear movement (i.e., D1), whereas the electrons are generally considered in the ground state. The Molecular Dynamics (MD) does not require ab initio calculation since it bases the evaluation on a mechanical model (Force Fields), which allows the engine to consider nuclear movements well. Alternatively, for small systems, ab initio calculation can be integrated into the calculation to improve the potentialities of the methods. This method is known as Ab Initio Molecular Dynamics (AIMD).

When the nuclear dynamics is not relevant, but the scope of the analysis regards the movement of electrons only, thus D2, it is necessary to employ ab initio calculation to evaluate the dynamics of the wavefunction. One possibility consists

in the use of the so-called Real-Time Time-Dependent Density Functional Theory (RT-TDDFT), which permits the study of electron dynamics by considering the nuclei frozen in a precise position [77]. This study allows, for instance, to estimate the dipole moment of a molecule when subjected to an external electric field [78]

Finally, when both the nuclear and electron movements are relevant for the scope of the analysis, thus D3, techniques such as the Ehrenfest Molecular Dynamics (MD) permits to consider the movement of nuclear and electron coordinates fully. Notice that Ehrefest MD is often unnecessary since electrons and nuclei have different kinetic scales that permit separating the two dynamic regimes.

This thesis does not deal with electron movement, but it is necessary to stress that the study of electron dynamics is significant in assessing molecular FCN technology. Introducing the time in the molecular FCN analysis would permit studying the dynamic properties of molecular FCN devices and circuits. Therefore, the study of electron dynamics is left as future work of this thesis work.

2.2.3 (Ab initio) Molecular Dynamics

Notwithstanding electron dynamics will not be explicitly considered in this thesis, a first dynamic analysis is performed by studying the effect of molecular vibrations. Molecular dynamics can be generally used to study molecular vibrations, the kinetics of some chemical reactions, and the kinetics of molecules (e.g., under the influence of electric fields).

In the MD perspective, each molecule is considered a group of atoms with mass equal to the element mass. Instead, chemical bonds are represented by mechanical springs connecting atoms and characterized by a precise stiffness parameter k. For example, Fig. 2.3(a) shows the water molecule (H_2O) and the equivalent MD model composed of three masses (two hydrogen atoms and one oxygen atom). Two springs with stiffness k_{OH} represent the Oxygen-Hydrogen bond, which has length R_0 at the thermal equilibrium. In the MD model, R_0 is the length of the spring at the thermal equilibrium. A third spring with stiffness k_{HHO} and standard length (angle) Θ_{HHO} can also be used to model the H-H interaction. In this case, the spring is not linear, yet it describes an interaction that may involve an angular movement (e.g., water bending vibration). The effect of the spring may be evident when discussing force fields and the energy aspects of the mechanical model.

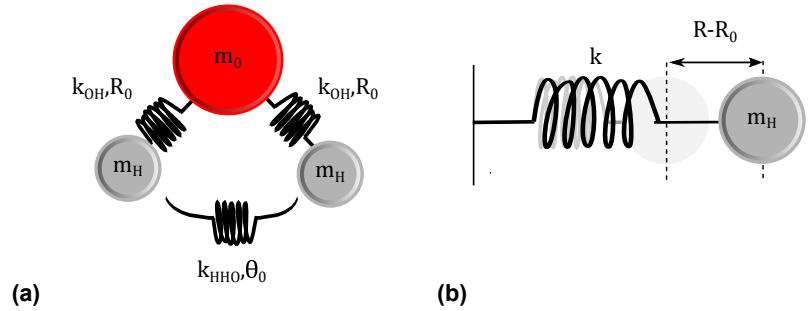

Fig. 2.3 Molecular dynamics perspective: (a) Water molecule (H_2O) represented in the MD perspective; the atoms are substituted by spheres with mass equal to the atomic mass (M_H is the Hydrogen (H) mass, whereas m_0 is the Oxigen (O) mass; k_{OH} and R_O represent the O−H bond force and equilibrium parameters, whereas k_{HHO} and Θ_O represent the angular interaction between the two Hydrogen atoms with the Oxygen atom. (b) Spring-Mass model used to represent a chemical bond in MD.

Indeed, to understand molecular dynamics basics, it is possible to consider the model composed of a single atom connected with a constrained spring, Fig. 2.3(b). At the equilibrium, the distance between the atom and the constraint (spring length) is R_0. If the atom is pulled at a distance R, a mechanical force $F = -k(R-R_0)$ acts on the atom, increasing the mechanical system energy to $W = \frac{1}{2}k(R-R_0)^2$. Notice that, in general, the force (F) acting on the atom may be written as:

$$F = -k(R-R_0) = -\frac{\partial W}{\partial R}$$

The term $\partial W/\partial R$ is generally named *gradient*. The gradients are often obtained from ab initio calculation or databases known as **Force Fields**. In particular, if the gradients are evaluated runtime (AIMD), the calculation allows a better description of the system under analysis since gradients are evaluated directly in the considered system, whereas gradients obtained from databases rely on particular cases. AIMD is also known as Bohr-Oppenheimer Molecular Dynamics (BOMD). Indeed, the wavefunction is generally obtained following the techniques presented in this chapter, thus minimizing the molecule energy. Notice that AIMD is much more computationally expensive than normal MD since requiring *ab initio* calculation. The force F_i acting on a generic i-th atom in position $\boldsymbol{R}_i = (X_i, Y_i, Z_i)$ is evaluated from the PES:

$$\boldsymbol{F}_i = -\frac{\partial W}{\partial \boldsymbol{R}} = \frac{\partial}{\partial \boldsymbol{R}} E(X_1, Y_1, Z_1, \cdots, X_i, Y_i, Z_i, \cdots, X_{N_N}, Y_{N_N}, Z_{N_N})$$

The system dynamics may be then evaluated with classical mechanics, following Newton's law:

$$\boldsymbol{F}_i = -m_i \boldsymbol{a}_i$$

Where m_i and $\boldsymbol{a}_i$ are the mass and the acceleration of the i-th atom, respectively. The equation may be therefore rewritten as:

$$\left(-\frac{\partial E_{PES}}{\partial \boldsymbol{R}_i}\right) = m_i \left(\frac{d^2 \boldsymbol{R}_i}{dt^2}\right) \qquad k\left(\boldsymbol{R}_i - \boldsymbol{R}_{i0}\right) = m_i \frac{d^2 \boldsymbol{R}_i}{dt^2}$$

Where $\boldsymbol{R}_{i0}$ is the equilibrium position of i-th atom. The velocity $\boldsymbol{v}_i$ of the atom can be obtained by integrating:

$$\boldsymbol{v}_i = \frac{d\boldsymbol{R}_i}{dt} = \int_0^t \frac{d^2 \boldsymbol{R}_i}{dt'^2} dt' = \boldsymbol{v}(t) + \boldsymbol{v}_{i0}$$

Where $\boldsymbol{v}_{i0}$ is the initial velocity of the atom and is generally obtained from thermodynamics according to the simulation temperature T_0 according to a Maxwell-Boltzmann distribution:

$$v_{i0} = \sqrt{\frac{2k_B T_0}{m_i}} \tag{2.4}$$

k_B is the Boltzmann constant. The temperature is not defined at the molecular scale, yet it represents how the system interacts with the external environment. Indeed, the introduction of the temperature implicitly states that the system is coupled with an external bath with temperature T_0. Notice that the system has a specific potential energy that it will try to minimize to reach an equilibrium condition. However, if energy is conserved, the system increases its kinetic energy and atom velocities. Thus, according to Equation (2.4), a velocity increase implies a temperature increase. A thermostat must be introduced to control the temperature oscillations, thus simulating the kinetics of chemical reactions at a constant temperature. The most simple thermostat is the Berendsen thermostat (implemented in the ORCA tool). A coupling coefficient τ limits the temperature increase and reduces numerical errors.

$$\frac{dT}{dt} = \frac{1}{\tau}(T_0 - T)$$

In general, concerning normal *ab initio* molecular dynamics, the simulation is related to gas phase, where the gas law ($PV = nRT$) holds. Three possible simulation scenarios, mentioned for the sake of completeness, are possible:

- NVE: number of particles (n) system volume (V) and system energy (E) are kept constant;
- NVT: number of particles (n) system volume (V) and system temperature (T) are kept constant;
- NPT: number of particles (n) system pressure (P) and system temperature (T) are kept constant.

2.3 Quantum approximation of the QCA cell

The two-state approximation is a model describing quantum systems existing in a superposition of two states. These two states are described by two eigenfunctions ψ_0 and ψ_1. In general, the wavefunction of the quantum system may be written as:

$$\psi = c_0\psi_0 + c_1\psi_1$$

Where $|c_0|^2$ and $|c_1|^2$ are the probability of finding the quantum states in the two states. In particular, following the vector Dirac's notation, the system can be described in the basis of the two eigenstates $|0\rangle$ and $|1\rangle$ as:

$$|\psi\rangle = c_0|0\rangle + c_1|1\rangle$$

In this scenario, it comes out that all the possible observables, such as the Hamiltonian, are 2×2 Hermitian matrices. The TSA can be used to model a bistable molecule showing two states ψ_a and ψ_b. The wavefunction of the system is $\psi = c_a\psi_a + c_b\psi_b$. In particular, following the procedure reported in [22], the Hamiltonian operator can be written as:

$$\begin{pmatrix} H_{aa} & \gamma \\ \gamma & H_{bb} \end{pmatrix}$$

Where γ is the matrix element describing the coupling between the two states. Whereas H_{aa} and H_{bb} are the two-state adiabatic energies and can be evaluated as:

$$H_{aa} = \langle \psi_a | H | \psi_a \rangle \qquad H_{bb} = \langle \psi_b | H | \psi_b \rangle$$

In the case $H_{aa} = H_{bb}$, the two adiabatic energies are generally named H_0 and known as on-side energy. By measuring the polarization of the molecule as $P = c_a^2 - c_b^2$, it is possible to solve the QM problem and find an expression describing the polarization of a bistable molecule as a response of a charge driver composed by two point charges at a distance L, described with polarization P_D. The procedure is fully described in [22]. The polarization can be written as:

$$P = \frac{2}{1 + \left\{ \beta P_D + \sqrt{\beta^2 P_D^2 + 1}^2 \right\}} - 1, \quad \beta = \frac{(2-\sqrt{2})e^2}{8\pi\varepsilon_0 \gamma L}$$

Molecules, when composed of three dots and three stable states, can be described with a three-state approximation [36, 79]. A similar procedure can also be used to describe the polarization of a generic QCA cell described with the TSA. For example, the polarization P of a cell, influenced by a driver cell with polarization P_D can be written as:

$$P = \frac{E_k}{\sqrt{1 + \left(\frac{E_k}{2\gamma} P_D \right)}} \tag{2.5}$$

E_k is the so-called Kink Energy, evaluated as the difference between the energy of the two-cell system when encoding the same and the opposite logic.

$$E_k = E_{00} - E_{01} = E_{11} - E_{10} \tag{2.6}$$

In a circuit, the (2.5) can be generalized to evaluate the polarization of a generic cell (i-th) as a response to the polarization of other circuit cells, indicated with index j. In general, the interaction between i and j cell is described by the Kink Energy ($E_k^{\{i,j\}}$) evaluated according to Equation (2.6) where E_{00} and E_{01} (equivalently, E_{11}

and E_{10}) are evaluated by considering i-th cell encoding logic 0, whereas j-th cell encoding logic 0 and 1 respectively.

$$P_i = \frac{E_k^{\{i,j\}} \sum_j P_j}{\sqrt{1 + \left(\frac{E_k^{\{i,j\}}}{2\gamma} \sum_j P_j \right)}}$$

The equation is currently implemented into QCADesigner and solved in an iterative procedure to evaluate the information propagation and elaboration in general QCA circuits. γ is the tunneling potential, which is eventually influenced by the clock to guide the information propagation. It is essential to highlight that the Equation (2.6) holds only for the general QCA paradigm. Indeed, specific technologies such as the molecular FCN may be such that $E_{00} - E_{01} \neq E_{11} - E_{10}$, making the use of QCADesigner controversial and requiring a more physical simulation of the validation of the functional behavior of the device [13].

Chapter 3

Modelling the molecules and the molecular interaction

This chapter models and analyses through *ab initio* calculation molecules proposed for the realization of molecular FCN. It proposes an automatic procedure to characterize molecules, then it analyses and models either monostable or bistable molecules, providing information about the effect of the static electric field generated by molecules or external electrodes. The molecules are studied both in the static and dynamic regime, eventually considering the effect of molecular vibrations and evaluating the impact on the encoding of the information in molecules. This chapter also fully describes a model for evaluating the molecule ground state energy, which is based on physical-chemistry theories. The model is validated through *ab initio* calculation.

3.1 Characterization of FCN molecules

Many molecules are proposed to implement molecular Field-Coupled Nanocomputing (FCN) devices in the literature, yet no current molecule fits all the requirements to be effectively used to accomplish computation. For this purpose, a tool to automatically characterize molecules favors the assessment of the technology by facilitating the characterization of eventual molecules in a batch system. In this thesis, a MATLAB tool interfacing with ORCA is developed to characterize molecules automatically. The tool consists of three steps:

- Molecule geometry optimization
- Molecule response evaluation
- Result analysis

All the steps are independent and can be used stand-alone. In addition, each step generates the output files necessary to insert the molecule in the SCERPA algorithm or archive the molecule data in a future database of molecules.

3.1.1 Molecule geometry optimization

The first step performs the geometry optimization of the molecule by starting from the given coordinates. The coordinates of a molecule can be obtained from several sources:

- By writing the cartesian coordinates directly, when available in the literature or the case of elementary molecules (e.g., H_2, H_2O).
- By drawing it by hand using the Avogadro tool (used in this work) or similar software. Eventually, a first optimization based on molecular mechanics may be performed.
- By using geometries obtained from previous *ab initio* optimizations. Eventually, input geometry may be obtained post-processing other geometries (e.g., for the analysis of an intermediate geometry between two molecular conformations)
- By downloading the molecule from online databases such as ChemSpider [1].

The *ab initio* method can be entirely customized in the characterization tool by choosing between Density Functional Theory (DFT) and Hartree-Fock (HF) methods. DFT functionals, basis sets, and additional corrections (e.g., D3 correction) can also be selected. The user chooses the charge and the multiplicity. The input file also enables setting the computational resource by indicating the ORCA path and the number of cores requested for the calculation.

[1] http://www.chemspider.com/

3.1.2 Molecule response

The second step of the tool takes the coordinates obtained from the first step optimization, then it aligns the molecule with the x, y, and z-axis and characterizes the molecule under the influence of an electric field. The script may also use an external geometry if required, bypassing the geometry optimization step. In particular, it allows studying the molecule in the *FIELD* system, where the field is uniform, and in the *SWITCH* system, where the field is similar to the one generated by molecules. The field is generated by using point charge systems. In particular, the distances for the point charges, the field span granularity, and the maximum values of fields and charges can be set from the script. Eventually, the calculation can also be performed under different clock field values.

3.1.3 Result analysis

The third step analyses the obtained Vin-Aggregated Charge Transcharacteristics (VACT) by showing the user the characterization results. In particular, the scripts automatically evaluate the molecule input voltage, and group the atomic charges to evaluate the aggregated charges. The number of dots composing the molecule can be chosen from two to three. In particular, if two aggregated charges are chosen, naming q_i an eventual charge with coordinates $(x_{q_i}, y_{q_i}, z_{q_i})$ the two groups DOT1 (Q_1) and DOT2 (Q_2) are chosen following the rule:

$$Q_1 = \{\forall q_i : x_{q_i} < 0\} \tag{3.1}$$

$$Q_2 = \{\forall q_i : x_{q_i} \geq 0\} \tag{3.2}$$

If three DOTs are chosen, the script requires the definition of a threshold x_{th} and groups the molecule following the rule:

$$Q_1 = \{\forall q_i : x_{q_i} < -x_{th}\} \tag{3.3}$$

$$Q_2 = \{\forall q_i : x_{q_i} > +x_{th}\} \tag{3.4}$$

$$Q_3 = \{\forall q_i : |x_{q_i}| \leq x_{th}\} \tag{3.5}$$

The script also permits for a user-defined aggregated charge grouping.

Finally, the script outputs:

- The VACT associated with each clocking field.
- The orbital energies as a function of the input voltage.
- The *ab initio* Self-Consistent Field Energy of the molecule as a function of the input voltage.
- The atoms used in the evaluation of the aggregated charges. These groups can be a starting point for user-defined aggregated charge definition.

3.2 Ideal molecules

As already stated, many molecules have been proposed to implement the FCN paradigm. Therefore, in order to derive general considerations, ideal reference molecules which can be neutral, oxidized, or zwitterionic, briefly described and discussed in Section 1.3.1, can be idealized. Examples of ideal molecules have been used in published works to derive general expressions regarding the bistability of the molecular FCN propagation [5] and the effects of molecular species on the molecular FCN circuits [13]. In particular, the ideal molecules are modeled in this work as a group of $N_{AC} = 3$ aggregated charges. Fig. 3.1(a) shows the geometrical representation of the ideal molecule. The charges Q_1 and Q_2, with distance w, will be the active dots. Thus, the two aggregated charges permitting the information encoding are Q_1 and Q_2. Instead, the charge Q_3 is necessary for the NULL state and for taking into account the possible counterion making the molecule neutral. Q_3 is positioned between Q_1 and Q_2, lowered by a quantity h concerning the active dot plane, see Fig. 3.1(a). In the case of an ideal molecule, the charge switching (i.e., the VACT) between active dots is modeled through the equation:

$$Q_1 = \frac{1}{1 + e^{\sigma V_{in}}}, \qquad \sigma = \frac{4\alpha}{ew^2} \tag{3.6}$$

Which represents a Fermi-like function, well imitating the typical switching behavior of molecules, see [22, 25]. Notice that α represents the molecule polarizability,

which will be discussed in Section 2.2.1 and represents the tendency of a molecule to become polar as a response to the electric field. Notice that, by defining the dipole moment according to Equation (1.3):

$$\mu = e(Q_2 - Q_1)\frac{w}{2} \tag{3.7}$$

For oxidized and zwitterionic molecules, $Q_1 + Q_2 = 1$, thus it is possible to derive Q_2 as $Q_2 = 1 - Q_2$ and expand the equation with Equation (3.6). Thus, it is possible to rewrite Equation (3.7) and obtain a linear relation between the input voltage (V_{in}) and the dipole moment (μ). In particular, for small input voltages:

$$\mu \approx \alpha \left(\frac{V_{in}}{w}\right), \qquad V_{in} \to 0$$

In the case of a uniform electric field, the term V_{in}/w is the value of the electric field; thus, the relation between the dipole moment and the field is directly proportional to α, that is, the molecule polarizability. Eventually, the output voltage may also be evaluated to study the intermolecular interaction:

$$V_{out} = \frac{e}{4\pi\varepsilon_0}(Q_1 - Q_2)\left(\frac{1}{d} - \frac{1}{\sqrt{d^2 + w^2}}\right) = -\frac{\alpha}{2\pi\varepsilon_0 w^2}\left(\frac{1}{d} - \frac{1}{\sqrt{d^2 + w^2}}\right)V_{in} \tag{3.8}$$

In particular, the VACT of the three molecular species are obtained from Equation (3.6). Table 3.1 schematically reports all the equations for the three molecular electrostatic species. Fig. 3.1(b) reports the VACT of the oxidized molecule obtained fixing $\sigma = 10$, whereas Fig. 3.1(c) reports the VACT of the neutral molecule. Finally, Fig. 3.1(d) reports the VACT of the zwitterionic molecule. The latter molecule may be, from an electrostatic point of view, confused with the counterioned molecule in the case [13].

3.3 Analysis of the bistable diallyl-butane molecule

Concerning the modeling of FCN molecules, this work starts by considering one of the most famous and used molecules for modeling purposes: the diallyl-butane

Table 3.1 Model of Oxidized, Neutral and Zwitterionic ideal molecules.

	Oxidized molecule	**Neutral molecule**	**Zwitterionic molecule**
$\mathbf{Q_1}$	$\frac{1}{1+e^{\sigma V_{in}}}$	$\frac{1}{1+e^{\sigma V_{in}}} - 0.5$	$\frac{1}{1+e^{\sigma V_{in}}}$
$\mathbf{Q_1 + Q_2}$	1	0	+1
$\mathbf{Q_3}$	+1	0	0
$\mathbf{Q_1 + Q_2 + Q_3}$	+1	0	0

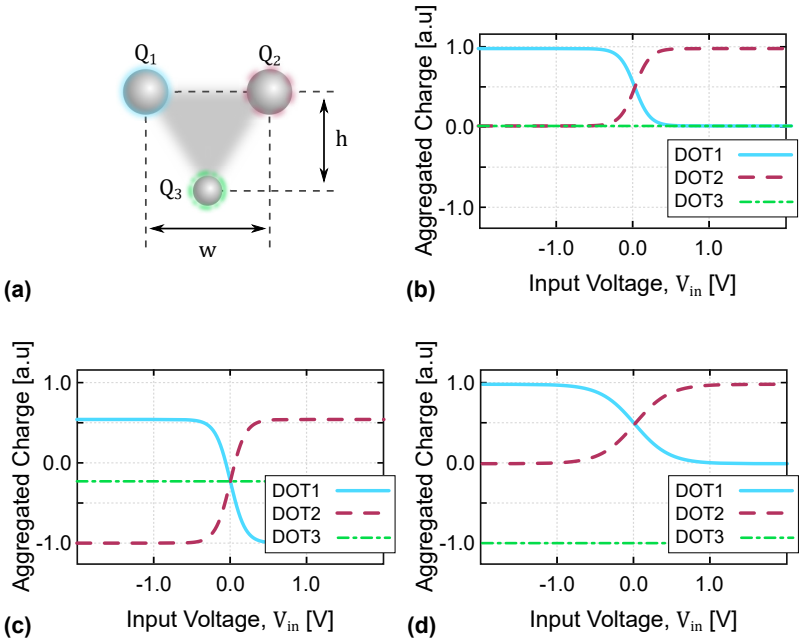

Fig. 3.1 Ideal molecules: (a) Geometry of the ideal molecule. (b) VACT of the oxidized ideal molecule with $\sigma = 10$ in the HOLD state. (c) VACT of the neutral ideal molecule with $\sigma = 10$ in the HOLD state. (d) VACT of the zwitterionic/counterionied ideal molecule with $\sigma = 10$ in the HOLD state.

molecule, previously shown in Fig. 1.6(a). The analysis starts by evaluating the geometry of the bistable molecule. Therefore, the focus is moved on the stability analysis and on the electrostatic characteristics to study its encoding capabilities and assess the methodology for modeling molecules. This molecule has been initially considered in the literature as a bistable molecule [17], then it was recently identified with monostable characteristics [30]. Therefore, this work firstly uses diallyl-butane as a bistable molecule to demonstrate the modeling procedure of bistable molecules, then the molecule is analyzed in its monostable nature by using more recent computational methods. In general, two computational methods are exploited:

M1 Bistable method: the molecule is analysed using Unrestricted Hartree-Fock method with basis sets STO-3G.

M2 Monostable method: the molecule is analysed using Density Functional Theory, CAM-B3LYP functional, Unrestricted Kohn-Shann, def2-TZVPP basis set and D3 correction.

The Code A.1.1 reports the geometry of the molecule obtained with M1 whereas Code A.1.2 reports the geometry of the molecule obtained with M2. Fig. 3.2(a) reports the coordinates of the molecule optimized with the two methods together with a label indicating the number of the atom. It is possible to notice that the atoms almost overlap with the two methods, indicating the presence of two very similar geometries. For the sake of clarity and completeness, the distance between each atom is evaluated and displayed in Fig. 3.2(b). Notwithstanding the distance between atoms is lower than 0.01 nm, this section will demonstrate that the switching of the molecule is completely different in the two configurations. This result clarifies that it is necessary to pay particular attention to the geometry optimization of molecules since small variations in the atom positions may impact the molecule final behavior. In particular, a non-symmetrical geometry of the molecule, in terms of atom positions, may promote asymmetry in the electron wavefunction, thus generating a possible dipole moment.

Indeed, Table 3.2 reports the dipole moment (μ) evaluated for the two geometries. Notwithstanding the geometrical similarities, the dipole moment is completely different and demonstrates the different characteristics of the molecule configurations. Indeed, the molecule optimized with M1 shows a clear charge localization that creates

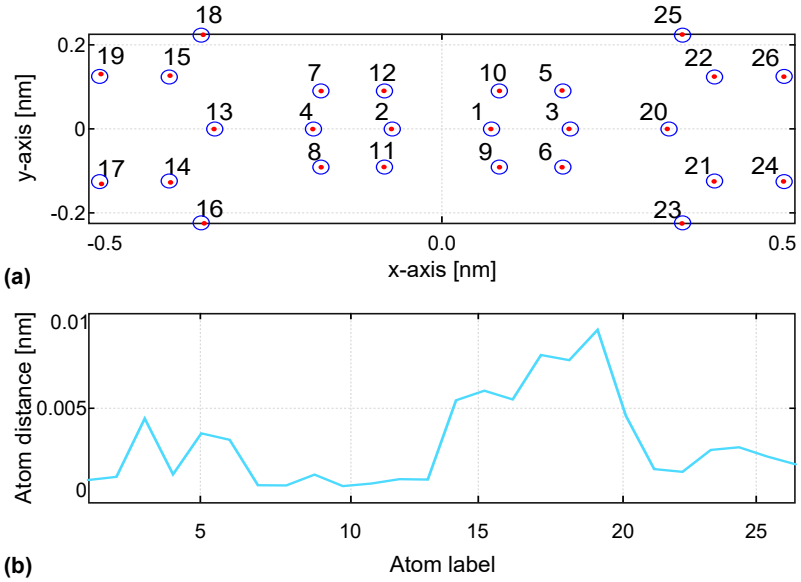

Fig. 3.2 Geometry of the diallyl-butane molecule: (a) Position of the atoms using methods M1 and M2. (b) Distance among atoms using the two methods M1 and M2.

Table 3.2 Dipole moment of the diallyl-butane

Method	μ_x **[a.u.]**	μ_y **[a.u.]**	μ_z **[a.u.]**
M1	-6.64065	0.00129	0.52758
M2	-0.00046	0.00003	0.00004

a dipole in the $-x$ direction, consistent with literature [17]. The molecule analyzed with M1 fits the definition of a bistable molecule normally polarized with no applied electric field. On the contrary, the dipole moment evaluated using geometry and methods associated with M2 is null. Notice that M2 better considers the electron correlation, thus providing reliable results. The obtained results are consistent with the literature. Indeed, M1 predicts a localization of the charge, whereas M2 predicts non-polar molecule characteristics [30].

The diallyl-butane is first analyzed with method M1 for completeness and historical reasons. Then, the molecule is characterized by studying the response to electric fields following the procedure proposed in [17]. The study consists in optimizing the molecule that is supposed to be bi-stable, thus polar in a stable state and deriving the opposite state by mirroring the molecule coordinates. Therefore, the mean state is derived by averaging the two configurations and the transcharacteristics by analyzing the mean state under the influence of electric fields. Denoting $\boldsymbol{R}_i^{\{1\}}$ the coordinate of an i-th nucleus of the stable state, the opposite state is obtained as:

$$\boldsymbol{R}_i^{\{2\}} = \boldsymbol{R}_i^{\{1\}} \begin{pmatrix} -1 & 0 & 0 \\ 0 & 1 & 0 \\ 0 & 0 & 1 \end{pmatrix} \tag{3.9}$$

Whereas the mean state $R_i^{\{0\}}$ is obtained as:

$$\boldsymbol{R}_i^{\{0\}} = \frac{1}{2}\boldsymbol{R}_i^{\{1\}} + \frac{1}{2}\boldsymbol{R}_i^{\{2\}} \tag{3.10}$$

The two configurations are analyzed using a single-point calculation and M1 computational methods. From an energy perspective, the two opposite states have similar energies ($-383.051\,103\,037$ a.u. and $-383.051\,103\,024$ a.u.), whereas the averaged state shows higher energy ($-383.011\,715\,227$ a.u.), which is somehow expected, being the geometry not optimized.

According to Lent et al., the molecule can oscillate between the stable state ($R^{\{1\}}$ or $R^{\{2\}}$) and the meta-stable ($R^{\{0\}}$) state due to a temperature variation [17]. Then, the molecule response to the electric field can be studied at the averaged point since, at any moment, the molecule nuclei can be in the configuration ($R^{\{0\}}$), thus permitting electrons to switch from $R^{\{1\}}$ to $R^{\{2\}}$ (or vice versa).

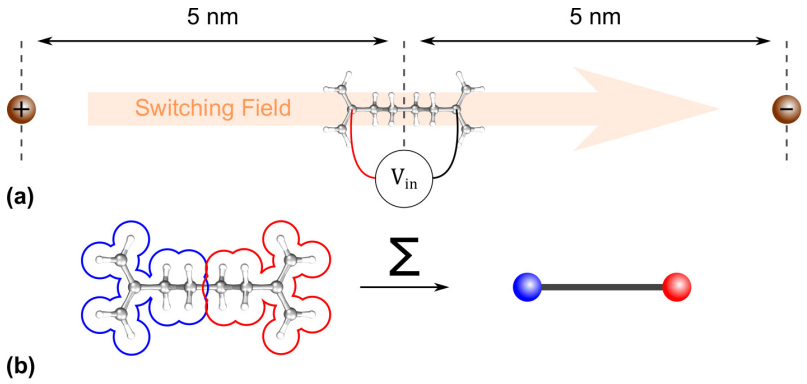

Fig. 3.3 Scheme of the diallyl-butane bistable analysis: (a) Basic schematic used for the generation of a switching field by using point charges. (b) Consitution of the Aggregated Charges for the diallyl-butane

The molecule is studied in the $R^{\{0\}}$ configuration under the influence of a static electric field to analyze the encoding and switching capabilities. The ORCA package does not permit the application of static fields. Therefore, the static fields are obtained by background point charges $\pm Q$ positioned at d =5 nm from the molecule center of mass. The generated *Switching Field* (E_{SW}) is:

$$E_{SW} = \frac{2eQ}{\pi\varepsilon_0 d^2}$$

Fig. 3.3(a) shows the molecule under the influence of two point charges generating a switching field. The two atoms of the allyl groups constitute the evaluation points of the input voltage. Thus the input voltage is obtained by integrating the field on a path connecting the two allyl groups according to Equation (1.4.2).

The diallyl-butane is analyzed with the ORCA package using UHF/STO-3G, and the CHELPG method is applied to evaluate the atomic charges. For each calculation, the atomic charges are summed to constitute the aggregated charge according to Fig.3.3(b), and the input voltage V_{in}. Fig. 3.4(a) shows the result of the calculation. It is possible to see the bistable switching of the molecule, DOT1, and DOT2, perfectly alternate for opposite fields, demonstrating the capability of the diallyl-butane to encode eventual information. Considering bistable molecules, it is also interesting to see the frontier orbitals, shown in 3.4(b). In particular, the Highest Occupied Molecular Orbital (HOMO)/Lowest Unoccupied Molecular Orbital (LUMO) gap reduces around the null voltage point, eventually favoring the molecule switching at this point.

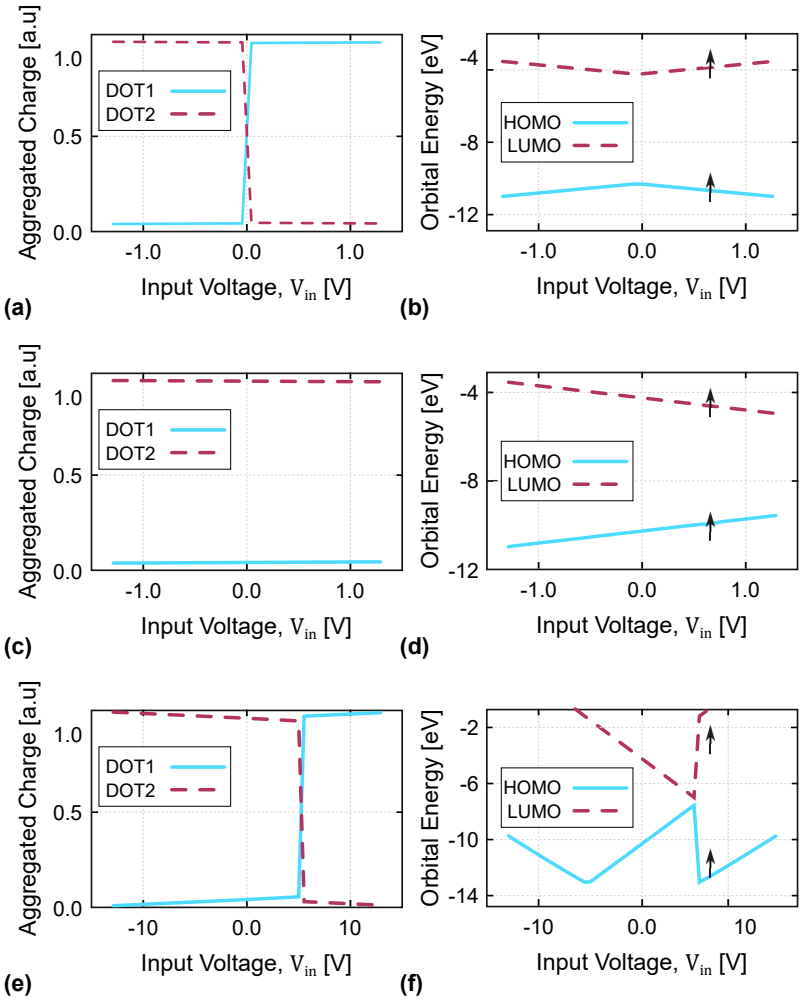

Fig. 3.4 Analysis of the diallyl-butane using bistable method: (a) VACT of the diallyl-butane molecule by using no initial orbital guess in each *ab initio* calculation. (b) HOMO/LUMO energy levels of the diallyl-butane molecule by using no initial orbital guess in each *ab initio* calculation. (c) VACT of the diallyl-butane molecule by using a biased initial orbital guess in each *ab initio* calculation. (d) HOMO/LUMO energy levels of the diallyl-butane molecule by using a biased initial orbital guess in each *ab initio* calculation. (e) VACT of the diallyl-butane molecule by using a biased initial orbital guess in each *ab initio* calculation and high electric fields (f) HOMO/LUMO energy levels of the diallyl-butane molecule by using a biased initial orbital guess in each *ab initio* calculation and high electric fields.

The reported analysis is evaluated without considering the possible memory effects of the bistable molecule. From a computational perspective, it means each *ab initio* calculation is independent of others.

Algorithm 1 Analysis of the diallyl-butane using M2 with memory effects.

```
Define input voltage vector V = [V(1),...,V(N)]
Build diallyl-butane ORCA input file with random guess for the initial orbitals;
Evaluate Background charges associated to V(1);
Launch ORCA calculation;
Save resulting orbitals orb(1);
for i in [2,N] do
    Build diallyl-butane ORCA input file with orb(i-1) for the initial orbitals;
    Evaluate Background charges associated to V(i);
    Launch ORCA calculation;
    Save resulting orbitals orb(i);
end for
```

It is interesting to see what happens when introducing memory effects. Therefore, the molecule is evaluated by forcing the initial orbital configuration of each calculation to the last evaluated point. The calculation will be more rapid, yet, the solution will be biased with an electron configuration which depends on the previous calculation. The calculation is performed in batch mode using the ORCA package; the resulting orbital of each calculation is taken as the initial guess for the next point, following the pseudocode reported in Code 1.

The obtained result demonstrates interesting characteristics related to molecule bistability. If the molecule orbital configuration is initially set to a stable state, the molecule does not switch with a small field. Fig. 3.4(c) shows a constant charge on the two DOTs. Concerning the frontier orbitals, thus the HOMO and LUMO orbitals, the HOMO/LUMO gap reduces by increasing the switching field, yet it is not minimum in the null voltage point. The field is not enough to overcome the energy barrier separating the two states, and the switching of the molecule can be expected for high electric fields. By evaluating the slope of the HOMO/LUMO gap, it comes out that a possible degeneration of the HOMO and LUMO levels may appear around 5 V. This guess is confirmed by a second analysis, where the molecule is stimulated with higher electric fields. Fig. 3.4(e) shows the VACT of the diallyl-butane molecule evaluated for a larger set of input voltages. As expected, the obtained result clearly shows a switching phenomenon at 5 V. Fig. 3.4(f) shows

the energy levels. The HOMO/LUMO gap reduces at its minimum, at 5 V, further confirming the expectations.

It is necessary to stress that the use of an initial guess in the *ab initio* calculation may strongly impact the obtained VACT, thus mandating awareness in the choice of the computational method employed in the analysis of the bistable molecules. Notice that the analysis performed by considering memory effect does not reproduce a ground state situation. It can be demonstrated by analyzing the molecule energy during the calculation. Fig. 3.5(a) shows the Self-Consistent Field (SCF) energy of the ab initio calculation with no memory effect. The energy is symmetric to the zero voltage point. This result is important, in general, also for monostable molecules. Indeed, signs of asymmetry in the energy profile will result in a possible memory effect and a non-ground state situation that may be an unwanted configuration. Fig. 3.5(b) shows the energy trend of the calculation performed with memory effect. In this case, the energy increases with the switching field, highlighting a situation that is not symmetric and which is generally not on the ground state. Notice that the energy profile is discontinuous at 5 V, thus in the vicinity of the molecule switch, consistently with the analysis reported in Fig. 3.4(e) and Fig. 3.4(f). Finally, this analysis suggests it is essential to evaluate the energy of the calculation in *ab initio* characterization to discover possible errors introduced by the computational method or the presence of bistable characteristics.

To conclude the bistable analyses, it is also interesting to comment on the aberration in the HOMO level shown in Fig. 3.4(f) around -5 V. Indeed, the energy of the HOMO level appears to increase when decreasing the applied voltage suddenly. The aberration may be understood by analysing the energy and the shape of HOMO and HOMO-1 levels. Fig. 3.6 shows the energy of the HOMO and HOMO-1 orbitals around the aberration point together with the orbital shapes evaluated at $V_{in} = -6.057$ V and $V_{in} = -4.477$ V.

With a switching field lower than the aberration, therefore $V_{in} = -4.477$ V, the electron (negatively charged) is localised in the HOMO on one of the two allyl groups, creating a dipole moment which is contrarily oriented concerning the switching field. From an electrostatic perspective, the HOMO level is favoured: the higher the switching field, the lower the orbital energy. On the contrary, the HOMO-1 energy level mainly locates the electron charge on the opposite molecule side, creating a dipole moment oriented along the switching field. From an electrostatic standpoint,

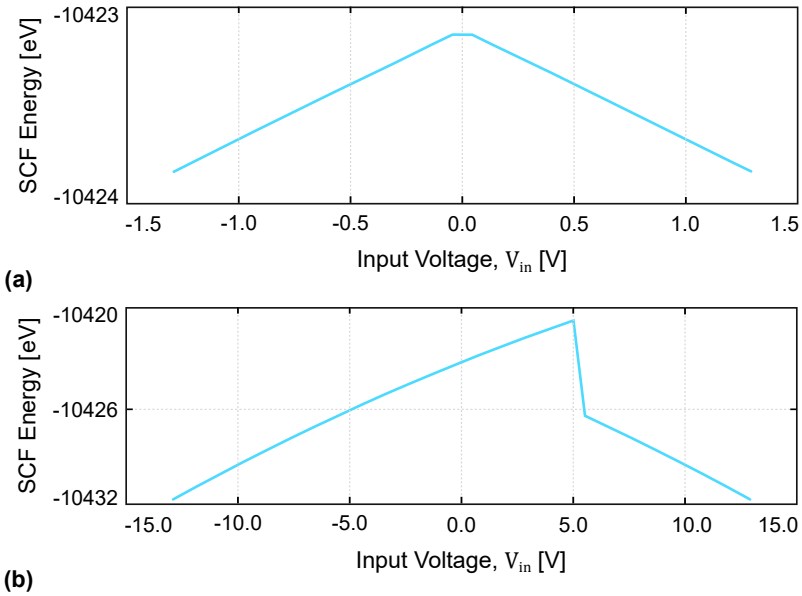

Fig. 3.5 SCF Energy of the diallyl-butane using bistable method: (a) SCF energy of the diallyl-butane molecule by using no initial orbital guess in each *ab initio* calculation. (b) SCF energy of the diallyl-butane molecule by using a biased initial orbital guess in each *ab initio* calculation.

the HOMO-1 orbital is not favoured. Thus HOMO-1 energy is supposed to increase by increasing the switching field.

To sum up, by increasing the switching field, the HOMO level decreases the energy, whereas the HOMO-1 level increases the energy. Thus, the HOMO/HOMO-1 energy separation reduces by increasing the switching field, finally degenerating in the aberration shown in Fig. 3.4(f) and replicated in Fig. 3.6 concerning the HOMO level. Indeed, at around -5 V, the HOMO-1 energy increases enough to equalise the HOMO energy, which is also decreased for the electrostatic interaction with the switching field. Finally, for $V_{in} = -6.057\,\mathrm{V}$, the HOMO-1 and the HOMO level shapes have been swapped, indicating the orbital swapping. The orbital considered HOMO-1 for lower voltage is now HOMO and maintains its increasing trend since it is electrostatically discouraged.

3.3.1 Double-Well analysis

To complete the analysis of the diallyl-butane in the bistable framework, the double-well of the molecule is evaluated. Several *ab initio* calculations are performed by

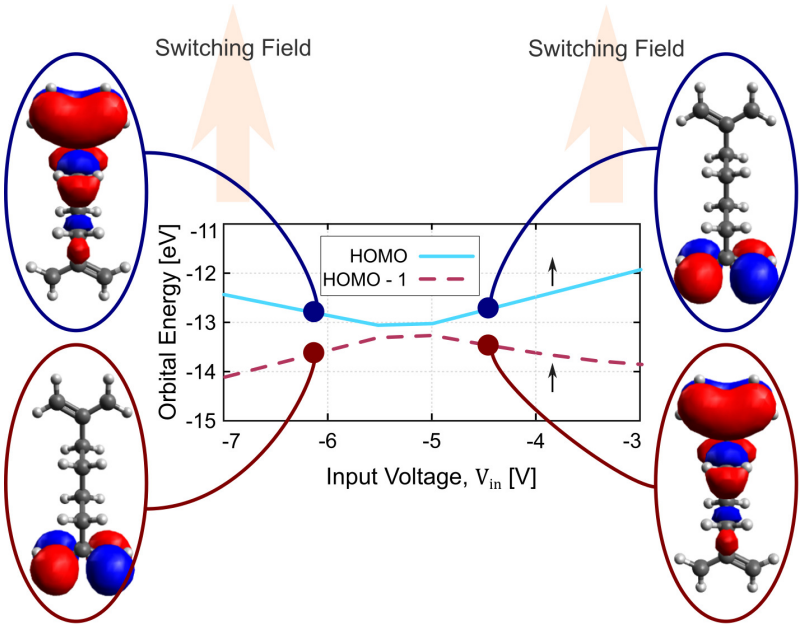

Fig. 3.6 Aberration in the diallyl-butane electronic structure using the bistable method: energy and shape of the HOMO and HOMO-1 orbitals.

varying the geometry of the molecule. The coordinate of the diallyl-butane nuclei are varied as a linear combination between the two opposite states:

$$R_i = \frac{1+\alpha}{2} R_i^{\{2\}} + \frac{1-\alpha}{2} R_i^{\{1\}}$$

Where α is a linear parameter named *Linear Coordinate*. Notice that:

$$R_i = \begin{cases} R_i^{\{1\}}, & \text{when} \quad \alpha = -1 \\ R_i^{\{0\}}, & \text{when} \quad \alpha = 0 \\ R_i^{\{2\}}, & \text{when} \quad \alpha = +1 \end{cases}$$

The molecule energy is evaluated for each nuclear configuration by setting the orbitals to the two stable states orbital configurations: $orb(R^{\{1\}})$ is the ground state orbital associated with $R^{\{1\}}$, whereas $orb(R^{\{2\}})$ is the ground state orbital associated to $R^{\{2\}}$. The SCF procedure is suppressed in the *ab initio* calculation to avoid energy minimization and to study the molecule energy out from the ground state. Fig. 3.7 shows the obtained double well. The results show the two configurations $R^{\{1\}}$ and $R^{\{2\}}$ to be well separated in terms of energy. In particular, 0.2 eV is necessary to jump from the ground state to the excited state when the configuration is in the stable

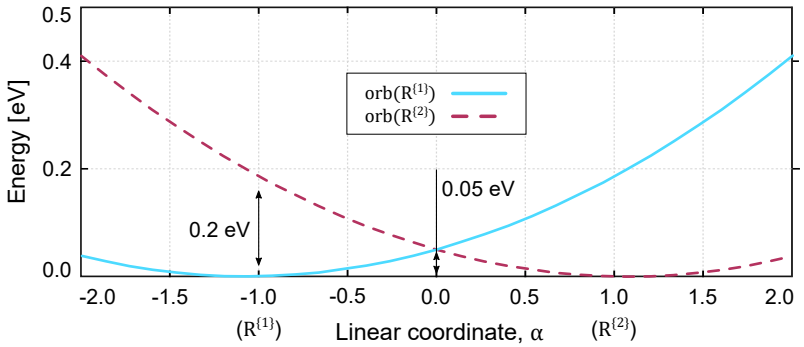

Fig. 3.7 Double-well of the diallyl-butane

points (i.e., $\alpha = \pm 1$), whereas 50 meV is the energy barrier between the two well evaluated at $\alpha = 0$, that is, in the middle of the switch (i.e., $R_i^{\{0\}}$, where the VACT is valuated). In this condition, the molecule energy is the same, whatever the orbital configuration is, motivating and justifying the analysis of the transcharacteristics in this point for bistable molecules.

3.4 Molecule-level analysis of the monostable diallyl-butane molecule

So far, the diallyl-butane cation was considered a bistable molecule to introduce bistable modeling. At this point, the real monostable nature of the diallyl-butane is studied to introduce the modeling of monostable molecules, following method M2. Some of the results in this section are also published in [31, 80].

The geometry of the diallyl-butane molecule is first optimized using the Kohn-Sham approach and Becke-Johnson damping scheme (D3) [81, 82]. To correctly consider the electron correlation and evaluate the diallyl-butane with monostable characteristics, the DFT method is performed by using the CAM-B3LYP DFT functional, suggested by [30] with a def2-TZVPP [83] basis set. The optimization converges to a geometry, reported in A.1.1, similar to the one with bistable characteristics. The energy of the monostable molecule is $-390.205\,728\,967\,7$ a.u. (the optimization of the bistable diallyl-butane converged to $-383.011\,715\,227$ a.u.). At the equilibrium, the cation shows a small dipole moment:

$$\boldsymbol{\mu} = (-0.0023, 0.000025, 0.000076) \text{ a.u.}$$

demonstrating the non-polar nature of the diallyl-butane. The non-polar characteristics of the molecule are consistent with physical chemistry theories since symmetric geometries lead to symmetric wavefunction with a consequent null dipole moment.

3.4.1 The vibration spectrum of the diallyl butane cation

Before proceeding with the analysis of the transcharacteristics, it is interesting to study also the molecule dynamics and the possible effects related to temperature. Therefore, the vibrational spectrum of the molecule is obtained by using DFT, with CAM-B3LYP functional and def2-TZVP basis set. Table 3.3 reports the vibrational modes of the molecule. As reported in Section 2.2.1, each mode can be Raman or InfraRed Active and influence polarizability and dipole moment, respectively. For this purpose, the diallyl-butane molecule is analyzed in a 500 fs timeframe to study the charge on the molecule in the time domain and discover eventual effects introduced by molecular vibrations.

Fig. 3.8(a) shows the obtained aggregated charges in the examined time for different temperatures. The figure reports the DOT1 aggregated charge (Q_1) only, even though (Q_2) can be reconstructed by considering the cationic nature of the molecule (i.e., $Q_1 + Q_2 = 1$ a.u.).

As expected, molecular vibrations make the molecular charge oscillate. Nevertheless, the mean values of the two dots are $\bar{Q}_1$=0.513 a.u.. and $\bar{Q}_2$=0.4867 a.u., which are close to the equilibrium value obtained with the single-point calculation. Fig. 3.8(b) also shows the Fast Fourier Transform (FFT) transform of the obtained charge profile. It is interesting to notice that the peaks have frequencies comparable with two of the vibrational modes of the diallyl-butane. Hence this is a clear effect demonstrating the molecular vibrations influences the charge distribution of the molecule, eventually impacting the final information encoding of molecular FCN cells.

Regarding the effect of the temperature, one may expect that a temperature growth increases the kinetic energy of nuclei, thus the effects of molecular vibrations. It is worth mentioning that, whatever the temperature is, the average of the molecule

Table 3.3 Vibrational modes of the diallyl-butane (source: [80])

N	**Wavenumber (k) [cm^{-1}]**	**Frequency (f) [THz]**
9	78.55	2.3565
14	317.71	9.5313
17	416.20	12.4860
19	445.05	13.3515
24	628.03	18.8409
27	897.50	26.9250
29	922.45	27.6735
34	1003.16	30.0948
35	1010.29	30.3087
36	1037.92	31.1376
37	1056.60	31.6980
42	1160.02	34.8006
45	1334.70	40.0410
48	1386.29	41.5887
50	1415.36	42.4608
52	1428.78	42.8634
55	1499.81	44.9943
57	1524.16	45.7248
59	1545.37	46.3611
60	1570.72	47.1216
63	3050.97	91.5291
66	3080.81	92.4243
67	3090.68	92.7204
69	3126.66	93.7998
70	3181.40	95.4420
76	3286.39	98.5917

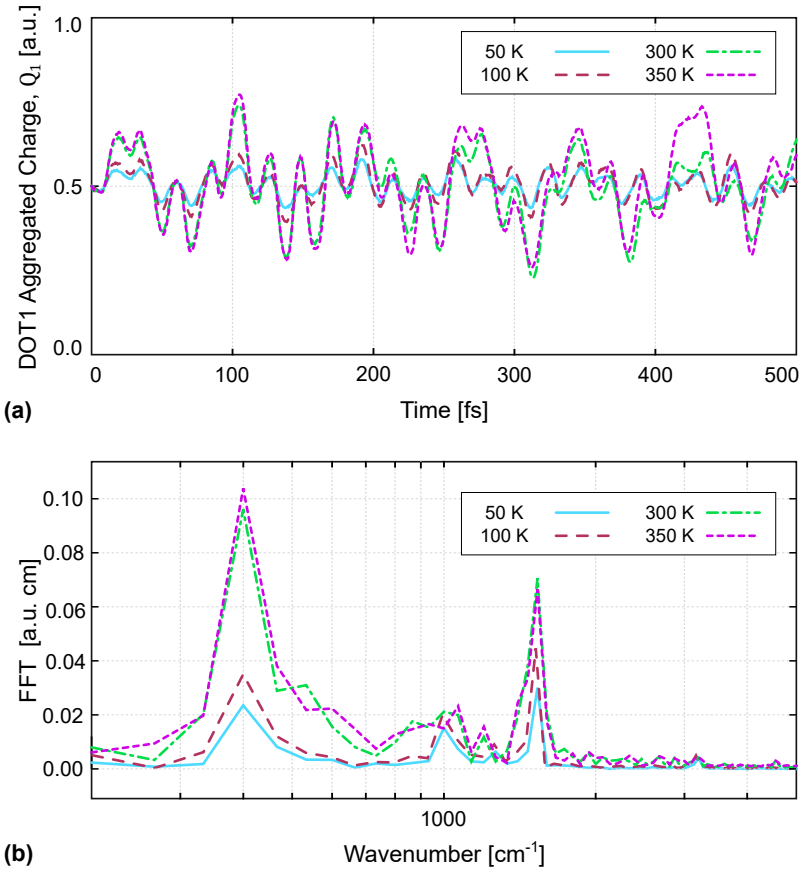

Fig. 3.8 Effect of temperature on the diallyl-butane: (a) Aggregated Charge (Q_1) dynamics in a 500 fs timestep at different temperatures. (b) Fast-Fourier Transform of the aggregated charge dynamics.

charge is always kept constant to the transcharacteristics value. The charge variation is, in any case, reduced with low temperature. Table 3.4 reports the average DOT charges evaluated at different temperature and the associate standard deviation (σ). The reported results demonstrate:

- The average charge is always close to the equilibrium value
- The higher is the temperature and the higher is the fluctuation of the diallyl-butane charge.

Table 3.4 Temperature effects on diallyl butane charge distribution (source: [80])

Temperature (T)	**Aggregated Charge [a.u.]**		σ
[K]	$\bar{Q}_1$	$\bar{Q}_2$	a.u.
50	0.5046	0.4954	0.0317
100	0.5057	0.4943	0.0470
200	0.5285	0.4715	0.0877
300	0.4973	0.5027	0.1015
350	0.5133	0.4867	0.1174

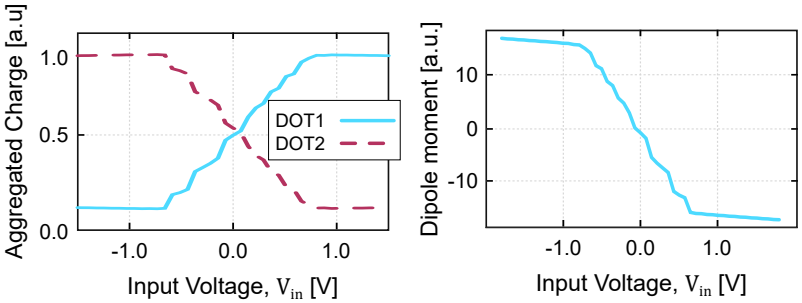

Fig. 3.9 Effect of static electric fields on the monostable diallyl-butane molecule

3.4.2 The effects of external electric fields

To study the response of the diallyl-butane cation, the VACT is evaluated by exposing the molecule to electric fields. First, the molecule is analyzed with the system reported in 3.3, where the value of point charges is varied following the same procedure used with method M1. Nevertheless, the geometry is acquired from the optimization procedure associated with M2, thus using CAM-B3LYP/def2-TZVPP.

Fig. 3.9 shows the obtained VACT and the dipole moment, clearly indicating the charge switching. Notice that in this case, the memory effect was considered in the evaluation of the transcharacteristics. Nevertheless, the response is symmetric, thus assessing the monostable characteristics of the molecule. The molecule correctly switches between the two charge configurations, and no stable state is found. This VACT describes the response of the molecule to a static electric field that external electrodes may generate, e.g., write-in electrodes [19].

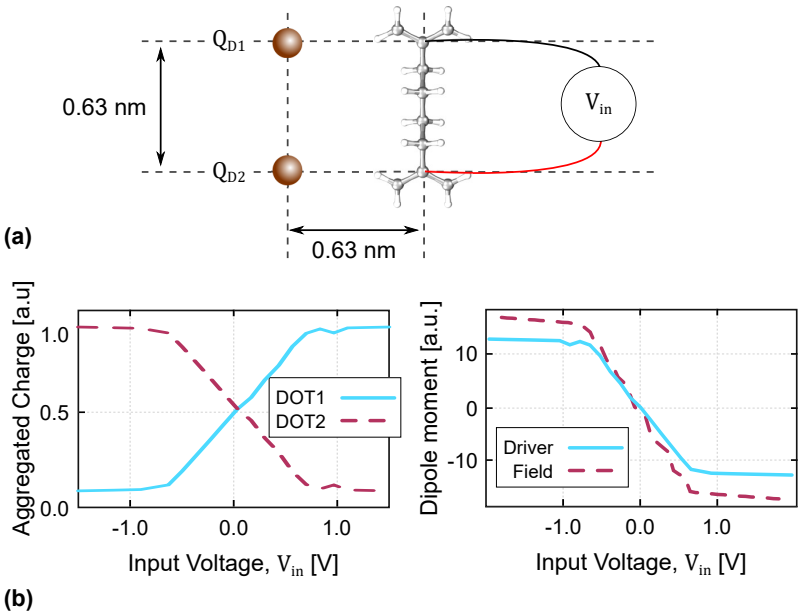

Fig. 3.10 Effect of a driver molecule on the monostable diallyl-butane molecule: (a) Point charge system used to evaluate the VACT. (b) VACT and dipole moment of the diallyl-butane cation. The dipole moment is reported both using the point charge driver and the uniform field.

3.4.3 The effects of a driver molecule

The just performed analysis can investigate the influence of static electric fields. However, in a circuit, electric fields are generated by molecules and are far from perfect static uniform fields. Indeed, molecules generate fields that follow the molecule shape, thus non-uniform in the space, significantly if evaluated in the near field. Therefore, studying the diallyl-butane cation response to other molecules is necessary. The VACT is now obtained with *ab initio* calculation by exposing the molecule under the influence of a driver, which is emulated by two point charges representing the aggregated charges of a polarized molecule. Fig. 3.10(a) shows the used system with two-point charges Q_{D1} and Q_{D2} positioned at a distance matching the molecule width (0.63 nm, that is, the distance between the diallyl-butane allyl groups). The value of point charges is varied as done for the previous evaluations, and the molecule is analyzed using proper M1 calculation configuration, thus using CAM-B3LYP/def2-TZVPP.

Fig. 3.9(b) shows the obtained VACT and dipole moment. The field generated by the point charge is less uniform, leading to a weaker driver-molecule coupling

which slightly reduces the interaction concerning the previous evaluation, performed with a more uniform field generated by two far point charges, see Fig. 3.9. The dipole moment reduction impinges on the switching and encoding capabilities of the molecule since the charge localization and the consequent ability of the molecule to generate electric fields reduce.

Finally, an Ab Initio Molecular Dynamics (AIMD) calculation at 300 K is also performed by fixing two point charges emulating the presence of a driver to complete the study of the molecule response. Two charges $Q_{D1} = 0.8$ a.u. and $Q_{D2} = 0.2$ a.u. are considered and the diallyl-butane charge dynamics is evaluated. Fig. 3.11 shows the obtained result. The two aggregated charges separate in the time domain, demonstrating the encoding of the molecule. In addition, the average charge at 300 K are 0.1177 a.u. and 0.8823 a.u., which are similar to the ones obtained at the thermal equilibrium with single-point calculation (Q_1=0.1840 a.u. and Q_2 =0.8160 a.u.). The obtained results demonstrate the encoding of the information at ambient temperature and the validity of the transcharacteristics concerning molecular vibrations and temperature.

Notice that, so far, molecular vibrations of single molecules have been considered in this chapter. Even though there is considerable research on single-molecule spectroscopy [84, 29], typical laboratory experiments evaluate the vibrational spectra of molecular ensembles composed of numerous molecules. Consequently, the vibrational frequencies obtained by *ab initio* calculation evaluated in this work may differ from practical measurements. Furthermore, this work demonstrates that molecular vibrations influence the charge dynamics of the molecule. Yet, the VACT model proposed in this work demonstrates robustness to molecular vibrations since it predicts, in the shown cases, the correct charge distribution of the molecule even in the presence of molecular vibrations. Therefore, notwithstanding a possible difference between simulation and experimental vibrational frequencies, the VACT model can be used to effectively model the charge distribution of a molecule used for molecular FCN applications, and vibrational modes do not represent a current problem for the encoding of the information. The obtained results motivate further studies concerning the robustness of the information propagation to molecular vibrations and, equivalently, to possible charge noise. Some work has already been started in [85], demonstrating the possible achievement of the molecular FCN propagation in noisy wires.

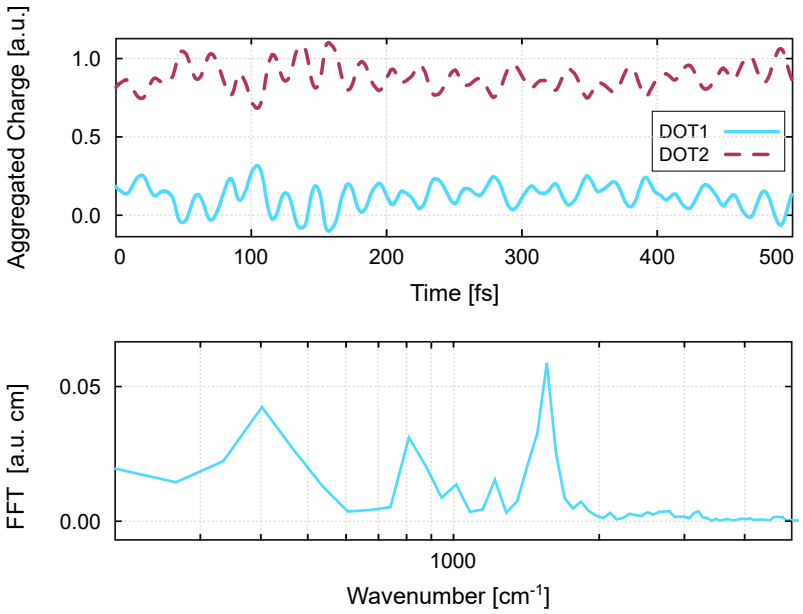

Fig. 3.11 AIMD simulation results of a diallyl-butane cation under the influence of a driver molecule. The figure reports the aggregated charge distribution in a 500 fs time frame and the associated Fast-Fourier Transform.

3.5 The energy model of a monostable molecule

This section briefly reports the model described in [31] to model the energy of circuits and systems composed of monostable molecules. In particular, the system energy is subdivided into two parts: the *internal energy* is related to the conformation energy of the molecule and the possible polarization given by external electric fields, eventually generated by electrodes or other molecules. Secondly, the *interaction energy* takes into account the interaction between a molecule and possible external electrostatic stimuli such as other molecules or electric fields. All the contributions are briefly described in the following sections. In the discussion, the capital letter W will reference an energy contribution related to more than one molecule, whereas the small letter w is used when dealing with single molecules.

3.5.1 Internal energy

The internal energy of a molecule is here defined as the energy related to the interaction between electrons and nuclei of the same molecule. For the scope of the molecular FCN paradigm, this energy can be subdivided into conformation energy

and polarization energy. The **conformation energy**, indicated with the symbol w_0, is the energy of the non-interacting molecule at the equilibrium, and it is evaluated in the absence of external stimuli. In particular, being the molecule monostable, the conformation energy represents a minimum in the Potential Energy Surface and is evaluated at the electronic ground state. Consequently, any perturbation to the molecule generally increases the total energy of the molecule. The conformation energy can be evaluated by solving the Schröedinger equation [86] or by exploiting ab initio calculation. In general, the energy is evaluated as

$$w_0 = \frac{\langle \Psi_{mol} | \hat{H}_{mol} | \Psi_{mol} \rangle}{\langle \Psi_{mol} | \Psi_{mol} \rangle}$$

where Ψ_{mol} is the molecular wavefunction and $\hat{H}_{mol}$ is the molecular hamiltonian operator. In the case of a circuit composed of N molecules, the total conformation energy can be evaluated as:

$$W_0 = \sum_{i=1}^{N} w_0^{\{i\}}$$

If there is only a single molecular species, thus all the molecules of the circuit are equal, w_0 is constant, and the total conformation energy (W_0) may be evaluated as:

$$W_0 = N \times w_0$$

Recent studies also pointed out the possibility to realize circuits with several molecules to achieve particular functions [87]. In this case, if the multi-molecule circuit is realized with M molecular species, identified with index k:

$$W_0 = \sum_{k=1}^{M} N_k \times w_0^{\{k\}}$$

where N_k is the number of molecules of species k in the circuit, with $w_0^{\{k\}}$ the specific conformation energy.

Concerning the diallyl-butane molecule, the conformation energy value has been reported in 3.4 (w_0=−390.205 728 967 7 a.u.). As already mentioned, w_0 represents

an energy minimum for the monostable molecule. Therefore, if w^* is the energy of a monostable molecule at a certain moment, the following relationship always holds:

$$w^* \geq w_0$$

When an external electric field is applied to the molecule (due to external electrodes or other molecules), the interaction increases the molecular energy by a quantity w_μ, here named **polarization energy**. The energy w_μ is associated with the field impact on the molecule, which polarizes the molecule, thus creating a dipole moment μ. Considering that the molecule often exhibits an equilibrium dipole moment μ_0, the dipole moment can be written as:

$$\boldsymbol{\mu} = (\mu_x + \mu_{0,x}, \mu_y + \mu_{0,y}, \mu_z + \mu_{0,z})$$

The modeling of polarization energy is crucial for monostable molecules. Indeed, the standard two-state approximation used to model the energy of bistable molecules cannot succeed in this operation since the polarized states are high-energy states in monostable molecules rather than energy minima [31]. The energy w_μ represents the energy that the molecule needs to reshape the electron cloud to respond to an external electric field. This mechanism is also responsible for the encoding and propagation of digital information.

The relation between the applied field and the energy is, in general, quadratic [76]. Therefore, it is often common to represent the molecule-field interaction with a mechanical system composed of a spring and a charge [31]. In this condition, also considering the possible linearity of the dipole moment concerning the electric field, seeEquation (2.3), it is possible to write the polarization energy of the molecule as:

$$w_\mu = \frac{(\mu_x - \mu_{0,x})^2}{2\alpha_{xx}} + \frac{(\mu_y - \mu_{0,y})^2}{2\alpha_{yy}} + \frac{(\mu_z - \mu_{0,z})^2}{2\alpha_{zz}} \tag{3.11}$$

Concerning the diallyl-butane molecule, according to [31], the polarizability may be evaluated directly using the ORCA package or by a linear approximation of the dipole-electric field relationship. In particular, molecule response is studied in [31] with DFT calculation by stimulating the molecule with electric fields on the order of 0.001 a.u. to obtain the polarizability matrix of the diallyl-butane:

$$\boldsymbol{\alpha} = \begin{pmatrix} 2837.5818 & -0.1008 & -4.5466 \\ -0.1008 & 129.7067 & 0.0016 \\ -4.5466 & 0.0016 & 79.9294 \end{pmatrix} \text{ a.u.}$$

Notice that the higher terms create the diagonal of the polarizability tensor, highlighting an isotropic tendency of the diallyl-butane molecule. Each component of the electric field mainly influence the molecule generating a dipole moment in the same direction. That means, by denoting the field as $\boldsymbol{E} = (E_x, E_y, E_z)^T$:

$$\boldsymbol{\alpha} \approx \begin{pmatrix} 2837.58 & 0 & 0 \\ 0 & 129.71 & 0 \\ 0 & 0 & 79.93 \end{pmatrix} \text{ a.u.} \qquad \boldsymbol{\mu} = \boldsymbol{\alpha E} \approx \begin{pmatrix} \alpha_{xx} E_x \\ \alpha_{yy} E_y \\ \alpha_{zz} E_z \end{pmatrix}$$

Notice that, among the polarizability tensor components, α_{xx} is the most interesting since it is the one supplying encoding and switching capabilities to the molecule.

3.5.2 The interaction energy

The interaction energy of a molecule is here defined as the energy related to the interaction between electrons and nuclei of a certain molecule with external electrostatic stimuli. For the scope of the molecular FCN paradigm, molecules can interact with other molecules to permit the propagation and elaboration of digital information and electric fields to permit clock and driver capabilities. Thus, the interaction energy can be subdivided into intermolecular energy and electric field interaction energy. Notice that, within the Molecular Simulator Quantum-dot cellular automata Torino (MoSQuiTo) methodology, the molecule is represented as a group of atom-centered point charges $\{q_i\}$. If two molecules, identified as m_i and m_j, interact each other, the electrostatic interaction w_{mm} can be evaluated with electrostatic equation as:

$$w_{mm}^{\{i,j\}} = \frac{1}{4\pi\varepsilon_0} \sum_{\alpha \in m_i} \sum_{\beta \in m_j} \frac{q_\alpha q_\beta}{|r_\alpha - r_\beta|} \tag{3.12}$$

In a circuit composed of N molecules, all the molecules interact with each other. Thus, the total interaction energy is obtained as:

$$W_{mm} = \frac{1}{2} \sum_{i,j \in [1,N], j \neq i} w_{mm}^{\{i,j\}}$$

Finally, the molecule may also interact with external fields generated by driver and clock electrodes. Therefore, the field polarizes the molecule, thus inducing a dipole moment $\boldsymbol{\mu}$ which rises the energy by a quantity w_E related to the dipole moment-field interaction:

$$w_E = -\boldsymbol{\mu} \cdot \boldsymbol{E} \tag{3.13}$$

The electric field interaction energy is not subordinated to a polarization-induced dipole moment, yet it is also present in the case of a non-neutral molecule, thus when the dipole moment is present at the equilibrium (μ_0). Also, notice the minus sign in Equation (3.13). If the dipole moment and the electric field vectors are concordant, the energy is negative, justifying the tendency of a molecule to polarize by aligning the dipole moment with the electric field. Finally, notice that the dipole moment should not be evaluated from *ab initio* calculation, yet it can be obtained with good precision from the charges obtained by fitting the electrostatic potential, following Equation (1.2), or from the aggregated charges, following Equation (1.3).

3.5.3 Validation of the energy model and analysis of the diallyl-butane

The complete validation of the molecule energy model is reported in [31]. Here, two essential case studios are reported for completeness: the interaction between an electric field and a diallyl-butane cation and between two diallyl-butane cations.

Case studio: interaction between an electric field and a diallyl-butane cation

When molecules are exposed to external electric fields, which external electrodes can generate, the main energy contributions playing a role in the energy perspective are:

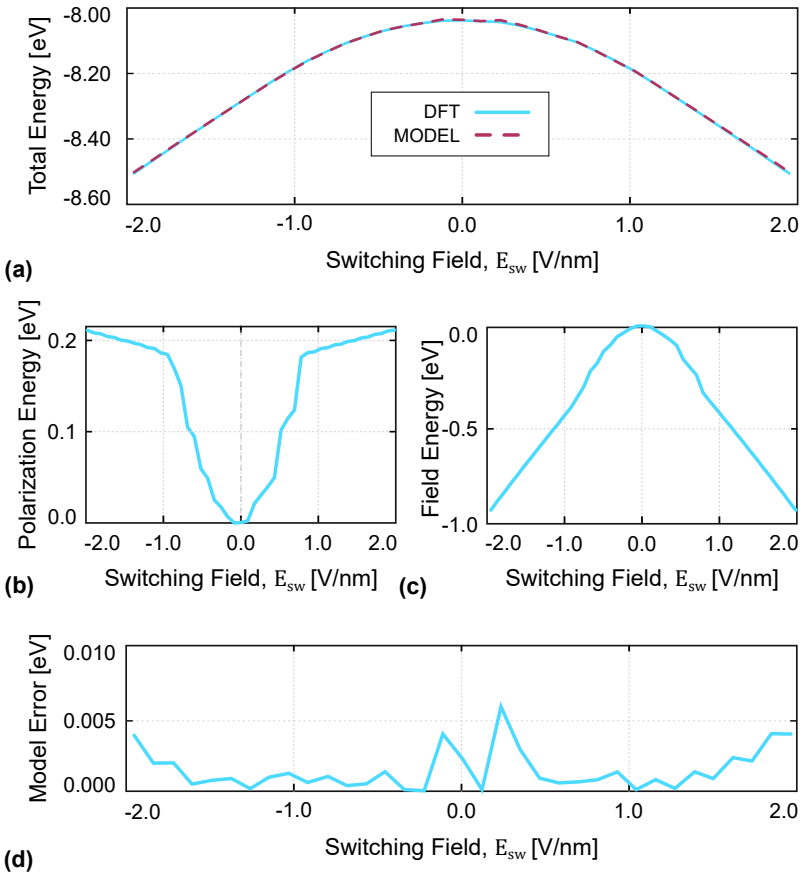

Fig. 3.12 Validation of the polarization energy model: (a) Total energy of a diallyl-butane molecule evaluated by varying an applied switching field with DFT calculation and with the described energy model. (b) Polarization energy, w_μ. (c) Field energy, w_E. (d) Absolute error in the value $W_{TOT} - w_0$ evaluated with the DFT calculation and the described energy model.

- The conformation energy W_0: a molecule is present in the analyzed system. The cation contributes with proper conformation energy to compose the final total energy.
- The polarization energy W_μ: the molecule is exposed to an electric field. Thus it can polarize and create a dipole moment, rising its internal energy.
- The electric field interaction energy W_E: the molecule is polar (after field-induced polarization) and interacts electrostatically with the external field.

In this section, all the calculations performed to derive the dipole moment in a uniform electric field reported in Fig. 3.9(b) are analyzed from the energy perspective. In particular, the *ab initio* SCF energy is evaluated in each calculation. Fig. 3.12(a) reports the SCF energy obtained from the ORCA calculation. Therefore, the total energy of the molecular system is evaluated as:

$$W_{TOT} = w_0 + w_\mu + w_E \tag{3.14}$$

In particular, w_0 is a known quantity, whereas w_μ and w_E are polarization and electric field interaction energy contributions. The mentioned contributions are evaluated with the energy model. w_μ, thus the polarization energy, is evaluated with Equation (3.11). Fig. 3.12(b) reports the polarization energy as a function of the applied switching field. It is worth highlighting the parabolic-like behavior of the energy, which is a distinctive characteristic of the monostable molecule. The higher the applied electric field, the higher the polarization of the molecule (i.e., the reshape of the electron cloud), which increases the internal energy of the molecule.

Fig. 3.12(c) reports the electric field interaction energy evaluated with the model, (w_E), evaluated with Equation (3.11), which is due to the interaction between the molecule dipole moment and the applied electric field. As expected, the energy decreases by increasing the applied electric field. Indeed, the higher the electric field, the higher the concurrent dipole moment, thus decreasing the term $-\boldsymbol{\mu} \cdot \boldsymbol{E}$ of the electric field interaction energy.

Finally, Fig. 3.12(a) also reports the total energy evaluated with Equation (3.14). Notice that, for the sake of clarity, the energy reported in Fig. 3.12(a) does not consider the conformation energy, therefore, the curve reports the value $W_{TOT} - w_0$. The energy computed with the electrostatic model well fits with DFT calculation

result, thus validating the energy model. In addition, Fig. 3.12(d) also reports the error between the two energy trends, which appears lower than 0.01 eV in the range $\pm 2\,\mathrm{V\,nm^{-1}}$.

Case studio: interaction between two diallyl-butane cations

When several molecules are present in the same molecular circuit, the molecules interact electrostatically, eventually creating dipole-dipole interaction and polarization effects. The reported case studio considers two molecules positioned at a specific intermolecular distance denoted as d. The primary energy contributions playing a role in the energy perspective are:

- The conformation energy $W_0 = 2w_0$: two molecules are present in the analyzed system. The two cations are equal and contribute the same conformation energies to compose the final total energy.
- The polarization energy W_μ: the molecules are exposed to the electric field generated by the molecules themselves. Thus they can polarize and create a dipole moment, rising molecule internal energies.
- The intermolecular interaction energy w_{mm}: the two molecules are composed of charged electrons and nuclei, which naturally electrostatically interact with each other. In addition, the molecules may also be polar, charged, or may create a dipole moment to respond to the intermolecular interaction, eventually impacting the electrostatic intermolecular interaction.

In this case studio, the energy of the molecular system is evaluated by varying the intermolecular distance (d). In particular, since only an intermolecular interaction is present and no electric field exists in the molecular system, the total energy is firstly evaluated as:

$$W_{TOT} = 2w_0 + w_{mm} \tag{3.15}$$

Again, w_0 is a constant term, whereas w_{mm} is evaluated with Equation (3.12). The intermolecular interaction energy is a pure electrostatic contribution that decreases by distancing the two molecules, i.e., increasing d. By assuming the energy expressed

according to Equation (3.15), the intermolecular contribution may be evaluated as $W_{TOT} - 2w_0$. Fig. 3.13(a) reports the energy ($W_{TOT} - 2w_0$) evaluated with both DFT calculation and the energy model. Fig. 3.13(b) also reports the error between the two curves. The electrostatic nature of the intermolecular energy contribution is evident; indeed, the energy decreases by increasing the distance. The more distant the molecules are, the lower the electrostatic interaction between the two molecules.

From a quantitative point of view, the energy model predicts a trend similar to the DFT calculated intermolecular energy, validating the theoretical model. However, a small error between the two calculated curves may be associated with a possible polarization of the molecules. Indeed, the calculation of the intermolecular interaction was performed by considering the molecule charge distribution at the thermal equilibrium. The eventual polarization of the molecules was not considered since external electrodes do not bias the molecules. Eventually, the model can be refined by also evaluating the polarization energy:

$$W_{TOT} = 2w_0 + w_{mm} + W_\mu \tag{3.16}$$

Where W_μ is the polarization energy associated with the polarization of both the two molecules, thus:

$$W_\mu = w_\mu^{\{1\}} + w_\mu^{\{2\}}$$

Again, Fig. 3.13(a) reports the energy ($W_{TOT} - 2w_0 - W_\mu$) evaluated with the energy model according to Equation (3.16). In this case, the error is further reduced with respect to the previous case, and the evaluated energy becomes more precise concerning the DFT calculation, see Fig. 3.13(b).

3.6 Characterisation of the bis-ferrocene molecule

Notwithstanding only molecules composed of two aggregated charges have been analyzed with the MoSQuiTo method, the procedure to derive aggregated charges is general enough to permit the characterization of molecules with more aggregated charges. Therefore, the MoSQuiTo method is also compatible with molecules permitting the exploitation of the clock field through a third DOT.

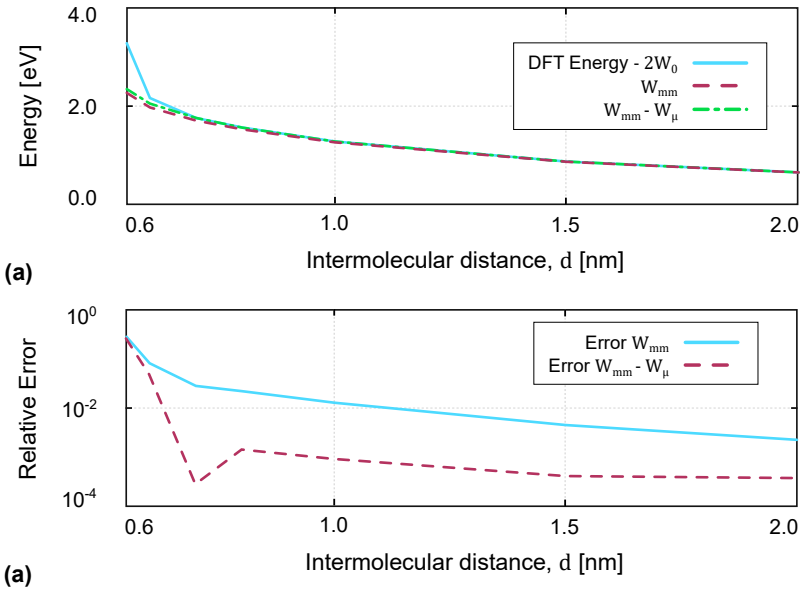

Fig. 3.13 Validation of the intermolecular energy model: (a) Energy between two diallylbutane molecules positioned at a distance d evaluated with DFT, and with the energy model by considering the intermolecular contribution only, w_{mm}, or both the intermolecular interaction and the polarization energies, $w_{mm} + w_{\mu}$. (b) Error between the described energy model in the evaluation of the energy, with respect to the DFT calculation, when considering the intermolecular contribution only, w_{mm}, or both the intermolecular interaction and the polarization energy, $w_{mm} + W_{\mu}$.

Furthermore, the following chapters of this work make extensive use of the bis-ferrocene molecule for the implementation of molecular FCN circuits since it is one of the molecules permitting the realization of clocked molecular devices [42]. This work skips the *ab initio* characterization of the bis-ferrocene molecule that was previously done in [18] by using Gaussian 09 [88] with B3LYP DFT functional and LANL2DZ basis set. Following analyses are also reported in [35].

The bis-ferrocene molecule is generally grouped into three charges: the two ferrocene units create the active dots, thus Q_1 and Q_2, whereas the carbazole and the hexanethiol create the third dot Q_3 permitting the encoding of the NULL state. Fig. 3.14(a) shows the bis-ferrocene molecule and the groups used to model the molecule with three aggregated charges.

When supposing the molecule to be oxidized, the charge completely aggregates on the two ferrocene units, permitting encoding capabilities when it is in the HOLD state. On the contrary, an external clock field may force the charge to aggregate on the carbazole, eventually ensuring the NULL state.

As usual, the molecule is characterized in a driver-molecule system to study the intermolecular interaction, thus the capabilities of the molecule to propagate and elaborate information. Different from previously analyzed molecules, concerning the bis-ferrocene molecule, it is necessary to introduce the clocking field, which is a static field in the x-axis, see Fig. 3.14(a). The molecule is first simulated in the presence of a $+2\,\mathrm{V\,nm^{-1}}$ electric field to favor the molecule charge to locate on the active dots. Fig. 3.14(b) reports the VACT of the molecule with $+2\,\mathrm{V\,nm^{-1}}$. For comparison, the molecule is also analyzed with no clocking field. Fig. 3.14(c) reports the obtained VACT. Interestingly, thanks to the $+2\,\mathrm{V\,nm^{-1}}$ clocking field forcing the charge to occupy the ferrocene units, the molecule shows a large charge separation between Q_1 and Q_2 in the linear and the saturation regions of the VACT. Also, the sum of the active dot charges is almost unitary, thus equal to the oxidation charge, meaning that most of the charge is located in the two ferrocene groups ($Q_1 + Q_2 \approx 1$).

Concerning the molecule with no electric field applied, Fig. 3.14(c), the charge is reduced in the saturation and central regions. Notice that the switching phenomenon is still evident. Thus, the molecule is, in principle, able to encode information without a positive clock field. Nevertheless, the charge on the two ferrocene units is reduced.

In the latter case, Fig. 3.14(d), the charge separation between the two active dots is strongly reduced, and the switching phenomenon is wholly suppressed. The negative $-2\,\mathrm{V\,nm^{-1}}$ clocking field inhibits the molecule switching and encoding capabilities. In comparison, the positive clocking field may seem unnecessary since the molecule permits charge localization also with $0\,\mathrm{V\,nm^{-1}}$, even though with reduced charge separation, the negative clocking field is essential to provide RESET capabilities.

These results generally demonstrate the possibility of using the bis-ferrocene molecule to perform molecular FCN calculations. Indeed, the molecule localizes the charge in the active dots when the HOLD field is applied. Then, the information may be deleted with the negative clocking field. Therefore, this molecule represents a good candidate for implementing molecular circuits; thus, it will be used in the following chapters as a reference molecule to demonstrate the functionalities of molecular FCN circuits.

For this purpose, to reduce unwanted effects related to the non-neutrality of the molecule, the bis-ferrocene molecule can be coupled with a counterion that screens the molecule from an electrostatic standpoint. Furthermore, from a model point of view, the charge of the DOT3 may be modified by reducing it from a quantity one making the total bis-ferrocene charge equal to 0 a.u..

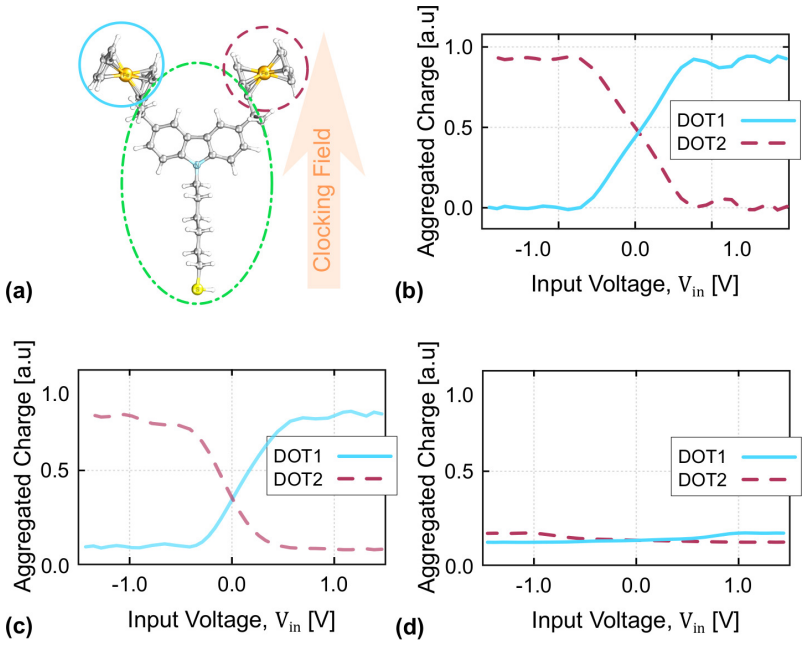

Fig. 3.14 Characterisation of the bis-ferrocene molecule: (a) Functional groups used to derive the distribution of the four aggregated charges and representation of the clocking field. (b) VACT evaluated for a clocking field E_{clk} =+2 V nm^{-1}. (c) VACT evaluated with no clocking field. (d) VACT evaluated for a clocking field E_{clk} =−2 V nm^{-1}.

Chapter 4

Modelling the molecular interaction in FCN circuits: SCERPA

This chapter fully describes the mathematics behind the Self-Consistent Electrostatic Potential Algorithm (SCERPA), proposed as a tool for the physical-aware analysis and design of molecular Field-Coupled Nanocomputing (FCN) clocked devices and circuits. First, the chapter discusses the Self-Consistent ElectRostatic Potential Algorithm (SCERPA) tool limits by evaluating the procedure convergence conditions and computational costs. Then, it introduces and assesses approximation techniques for speeding up the evaluation procedure, eventually favoring the integration of the proposed tool in current CAD software such as TOrino POLItecnico NANOtechnology (ToPoliNano). Finally, it describes the organization and the MATLAB implementation of the SCERPA tool code and the main aspects and features regarding its usability from the design perspective.

For the sake of clarity, it is worth anticipating the key indices that will be used in the following sections:

- α represents the index of a molecule charge, it spans in the range $[1, N_{AC}]$, with N_{AC} number of aggregated charges
- τ represents a timestep, it spans in the range $[0, \tau_T]$
- k represents a step of the iterative procedure, it spans in the range $[0, \infty]$, where $k = \infty$ represents a convergence state

- i and j are used to indicate molecules of the circuit and span in the range $[0,N]$.

The mentioned convention will be used in the entire section to help the reader understand the math beyond the SCERPA algorithm.

4.1 Theoretical derivation of the SCERPA equation

A generic molecular FCN circuit composed of N molecules is described as a set of $N_{AC} \times N$ aggregated charges. $Q_{\alpha,j}$ is the charge representing DOT-α of the j-th molecule, in the position $R_{\alpha,j}$. The voltage V generated by all circuit molecules to a general position $\boldsymbol{r}$ can be written as:

$$V(\boldsymbol{r}) = \frac{e}{4\pi\varepsilon_0} \sum_{j=1}^{N} \sum_{\alpha=1}^{N_{AC}} \frac{Q_{\alpha,j}}{|\boldsymbol{r} - R_{\alpha,j}|} \tag{4.1}$$

Then, the input voltage evaluated at i-th molecule can be obtained as the voltage difference evaluated between the two active dots:

$$V_{in,i} = V(\boldsymbol{R}_{1,i}) - V(\boldsymbol{R}_{2,i}) = \frac{e}{4\pi\varepsilon_0} \sum_{j=1, j\neq i}^{N} \sum_{\alpha=1}^{N_{AC}} \left[Q_{k,j} \left(\frac{1}{|\boldsymbol{R}_{1,i} - \boldsymbol{R}_{\alpha,j}|} - \frac{1}{|\boldsymbol{R}_{2,i} - \boldsymbol{R}_{\alpha,j}|} \right) \right]$$

The contribution of eventual driver molecules ($\boldsymbol{V}_D$), which are molecules with fixed charges, can be added:

$$V_{in,i} = \frac{e}{4\pi\varepsilon_0} \sum_{j=1, j\neq i}^{N} \sum_{\alpha=1}^{N_{AC}} \left[Q_{\alpha,j} \left(\frac{1}{|\boldsymbol{R}_{1,i} - \boldsymbol{R}_{\alpha,j}|} - \frac{1}{|\boldsymbol{R}_{2,i} - \boldsymbol{R}_{\alpha,j}|} \right) \right] + V_{D,i} \tag{4.2}$$

The voltage contributing to the i-th molecule input voltage ($V_{in,i}$) depends on the charge distribution of other molecules ($Q_{\alpha,j}$). Other molecule charges, in turn, are related to their input voltage ($V_{in,j}$). Then, by introducing the Vin-Aggregated Charge Transcharacteristics (VACT), the charge $Q_{\alpha,j}$ of j-th molecule is linked to the molecule input voltage $V_{in,j}$ and the clock field $E_{clk,j}$:

$$Q_{\alpha,j} = Q_\alpha(V_{in,j}, E_{clk,j})$$

Then the Equation (4.2) may be rewritten as:

$$V_{in,i} = \frac{e}{4\pi\varepsilon_0} \sum_{j=1, j\neq i}^{N} \sum_{\alpha=1}^{N_{AC}} \left[Q_\alpha(V_{in,j}, E_{clk,j}) \left(\frac{1}{|\boldsymbol{R}_{1,i} - \boldsymbol{R}_{k,j}|} - \frac{1}{|\boldsymbol{R}_{2,i} - \boldsymbol{R}_{\alpha,j}|} \right) \right] + V_{D,i} \tag{4.3}$$

Or, synthetically:

$$V_{in,i} = F_i \left(V_{in,1}, V_{in,2}, \cdots, V_{in,i-1}, V_{in,i+1}, \cdots, V_{in,N}, V_{D,i}, E_{clk,1}, \cdots, E_{clk,i-1}, E_{clk,i+1}, \cdots, E_{clk,N} \right)$$

Or, by introducing the superscript $\backslash x$ notation, it can be written as

$$V_{in,i} = F_i(\boldsymbol{V}_{in}^{\backslash i}, V_{D,i}, \boldsymbol{E}_{clk}^{\backslash i})$$

Where the $\backslash x$ denotes the exclusion of a generic x-index in a vector, as an example, $\boldsymbol{V}_{in}^{\backslash i}$ denotes the vector containing all the V_{in} in the range $[1, N]$ excluding $V_{in,i}$:

$$\boldsymbol{V}_{in}^{\backslash i} = \begin{pmatrix} V_{in,1} \\ \vdots \\ V_{in,i-1} \\ V_{in,i+1} \\ \vdots \\ V_{in,N} \end{pmatrix}$$

Given a predefined clock field, driver voltage, and an initial guess, the SCERPA algorithm iterates Equation (4.3) by evaluating at each time step k the voltage $V_{in,i}^{\{k\}}$ until convergence is reached. By defining a certain convergence tolerance, ε_{max}, the iterative procedure is stopped when:

$$|V_{in,i}^{\{k\}} - V_{in,i}^{\{k-1\}}| < \varepsilon_{max}$$

In general, in an ideal case, the solution may be intended as $V_{in,i}^{\{\infty\}}$, formally defined as:

$$V_{in,i}^{\{\infty\}} = \lim_{k\to\infty} V_{in,i}^{\{k\}}$$

The problem may be finally formalized by introducing the vector representation of voltages:

$$\begin{pmatrix} V_{in,1} \\ \vdots \\ V_{in,i} \\ \vdots \\ V_{in,N} \end{pmatrix} = \begin{pmatrix} F_1(V_{in,2}, V_{in,3}, \cdots, V_{in,N}, V_{D,1}, E_{clk,2}), \cdots, E_{clk,N} \\ \vdots \\ F_i\left(\boldsymbol{V}_{in}^{\setminus i}, V_{D,i}, \boldsymbol{E}_{clk}^{\setminus i}\right) \\ \vdots \\ F_N(V_{in}, V_{in,2}, \cdots, V_{in,N-1}, V_{D,N}, E_{clk,1}, \cdots, E_{clk,N-1}) \end{pmatrix}$$

That means:

$$\boldsymbol{V}_{in} = \mathbf{F}(\boldsymbol{V}_{in}, \boldsymbol{V}_D, \boldsymbol{E}_{clk}) \tag{4.4}$$

For the sake of shortness will be used in some cases as $\boldsymbol{V}_{in} = \mathbf{F}(\boldsymbol{V}_{in})$, without explicitly specifying the clocking and driver dependencies:

$$\boldsymbol{V}_D = \begin{pmatrix} V_{D,1} \\ \vdots \\ V_{D,i} \\ \vdots \\ V_{D,N} \end{pmatrix} \qquad \boldsymbol{E}_{clk} = \begin{pmatrix} E_{clk,1} \\ \vdots \\ E_{clk,i} \\ \vdots \\ E_{clk,N} \end{pmatrix}$$

Equation (4.4) can be solved numerically as a fixed-point problem by guessing an initial value $\boldsymbol{V}_{in}^{\{0\}}$ and by evaluating $\boldsymbol{V}_{in}^{\{1\}} = \mathbf{F}(\boldsymbol{V}_{mol}^{\{0\}})$. Then the procedure is iterated by evaluating $(k+1)$-th step as:

$$\boldsymbol{V}_{in}^{\{k+1\}} = \boldsymbol{F}\left(\boldsymbol{V}_{in}^{\{k\}}\right)$$

Until convergence is reached, and, that means for the step $\hat{k}$ such that:
$|\boldsymbol{V}_{in}^{\{\hat{k}\}} - \boldsymbol{V}_{in}^{\{\hat{k}-1\}}| < \varepsilon_{max}$. Finally assuming the solution to be $V_{in}^{\{\infty\}} = V_{in}^{\{\hat{k}\}}$.

4.2 The convergence of the SCERPA algorithm

In order to study the convergence of the algorithm, the problem may be considered a fixed-point numerical problem whose equation is:

$$V_{in,i}^{\{k+1\}} = F_i(V_{in,1}^{\{k\}}, \cdots, V_{in,i-1}^{\{k\}}, V_{in,i+1}^{\{k\}}, \cdots, V_{in,N}^{\{k\}})$$

The convergence of a fixed-point method, according to [89], is ensured if $\|J_{\mathbf{F}}\|_2 < 1$, where $J_{\mathbf{F}}$ denotes the Jacobian matrix of function $\mathbf{F}$:

$$\{J_{\mathbf{F}}\}_{i,j} = \frac{\delta F_i}{\delta V_{in,j}}$$

It is worth highlighting that the voltage associated with the i-th molecule depends on the charges of all the molecules a part for itself. Therefore, the diagonal elements of the Jacobian are null. Notice also that, if molecules are equal, the effect caused by i-th molecule to the j-th molecule is the same effect caused by j-th molecule to the i-th molecule, hence:

$$\{J_{\mathbf{F}}\}_{i,j} = \frac{\delta F_i}{\delta V_{in,i}} = 0 \qquad \{J_{\mathbf{F}}\}_{i,j} = \frac{\delta F_i}{\delta V_{in,j}} = \frac{\delta F_j}{\delta V_{in,i}} = \{J_{\mathbf{F}}\}_{j,i}$$

The Jacobian matrix appears to be symmetric and with null diagonal terms. Finally, the components of the Jacobian may be evaluated by differentiation.

$$\{J_{\mathbf{F}}\}_{i,j} = \frac{\delta F_i}{\delta V_{in,j}} = \frac{e}{4\pi\varepsilon_0} \sum_{\alpha=1}^{N_{AC}} \left[\left(\frac{1}{|\boldsymbol{R}_{1,i} - \boldsymbol{R}_{\alpha,j}|} - \frac{1}{|\boldsymbol{R}_{2,i} - \boldsymbol{R}_{\alpha,j}|} \right) \frac{\delta Q_\alpha(V_{in,j})}{\delta V_{in,j}} \right]$$

It may be understood that the higher the Jacobian element, the more difficult the numerical procedure convergence. Notice that, so far, clocking field and driver effects have not been considered for discussing the convergence since it mainly depends on V_{in} oscillations between one k-step and another. Clock field (E_{clk}) and driver effects (V_D) are constant in each k-step, thus do not influence convergence directly. Nevertheless, some secondary dependence can be associated with these two contributions and should be considered to evaluate the Jacobian element correctly. Considering the results reported in [25]

- The driver contribution may move the starting point of the iterative procedure, which is generally reflected on a point on the molecule transcharacteristics. The Jacobian element is directly proportional to the trans-characteristics slope, generally showing its maximum slope in the central region, thus with small input voltage.
- The effect of the clock generally varies the slope of the transcharacteristics, which is generally maximized for active clocks (i.e. clocks permitting the information encoding and propagation). Generally, the active clock represents the worst case for SCERPA convergence.

Finally, to discuss the algorithm convergence in the worst-case considering clocking and driver effects, it is necessary to consider the central region of the transcharacteristics for an active clock. The aggregated charge of α-dot evaluated for zero input voltage (i.e., to maximize the slope and with the worst-case driver effect) and for the clocking field providing the maximum slope is here named $Q_\alpha(0)$. The first derivative to the input voltage V_{in} in the same driver-clock conditions is named $Q'_\alpha(0)$. Therefore, to evaluate convergence, it is useful to approximate the transcharacteristics following a linear approximation:

$$Q_\alpha(V_{in,j}) \approx Q_\alpha(0) + \left.\frac{\delta Q_\alpha(V_{in,j})}{\delta V_{in}}\right|_{V_{in,j}=0} \cdot V_{in,j} = Q_\alpha(0) + Q'_\alpha(0) V_{in,j}$$

Then:

$$\frac{\delta Q_\alpha(V_{in,j})}{\delta V_{in,j}} = \frac{\delta}{\delta V_{in,j}} \left\{ Q_\alpha(0) + Q'_\alpha(0) V_{in,j} \right\} = Q'_\alpha(0)$$

Hence, the Jacobian matrix element is:

$$\{J_G\}_{i,j} = \frac{\delta F_i}{\delta V_{in,j}} \approx \frac{1}{4\pi\varepsilon_0} \sum_{\alpha=1}^{N_{AC}} \left[\left(\frac{e}{|\boldsymbol{R}_{1,i} - \boldsymbol{R}_{\alpha,j}|} - \frac{1}{|\boldsymbol{R}_{2,i} - \boldsymbol{R}_{\alpha,j}|} \right) Q'_\alpha(0) \right]$$

This equation shows that the self-consistent procedure convergence depends on the distances among charges and the transcharacteristics slope. It follows that:

- Larger intermolecular distances decrease the Jacobian elements, favoring the convergence.
- Larger VACT slope increases the Jacobian elements, discouraging the convergence of the SCERPA algorithm

To better study the algorithm convergence, it is worth analyzing the particular case of a perfectly aligned molecular wire with N molecules. For simplicity, it is assumed that N is an even natural number so that $N/2$ represents the number of cells. Molecules are indicated with index $i \in [1echeck, N]$, and the value of index i is consistent with its physical position in the wire. Molecule i is supposed to be adjacent to molecules $i-1$ and $i+1$ for $i \in [2, N-1]$. The circuit under analysis is reported in Fig. 4.1(a). It is also supposed that the distance between two dots of the same molecule is constant for all molecules and named w while the distance between two molecules is $|j-i|d$. The molecules are considered composed of three aggregated charges ($N_{AC} = 3$). The third DOT is positioned between DOT1 and DOT2, beyond their plane with distance $w/2$, see Fig. 4.1(b). In particular, the quantity σ is defined as the ratio between intermolecular distance and interdot distance.

$$\sigma = \frac{d}{w}$$

The influence of molecule $i+1$ to molecule i is the same of the molecule $i+j$ influencing $i+j-1$, in other terms, the influence between adjacent molecules is the same independently on what the molecule under consideration is. The distances may be evaluated as:

$$\left(\frac{1}{|\boldsymbol{R}_{1,i} - \boldsymbol{R}_{1,j}|} - \frac{1}{|\boldsymbol{R}_{2,i} - \boldsymbol{R}_{1,j}|} \right) = \frac{1}{|j-i|d} - \frac{1}{w\sqrt{1 + (|j-i|\sigma)^2}}$$

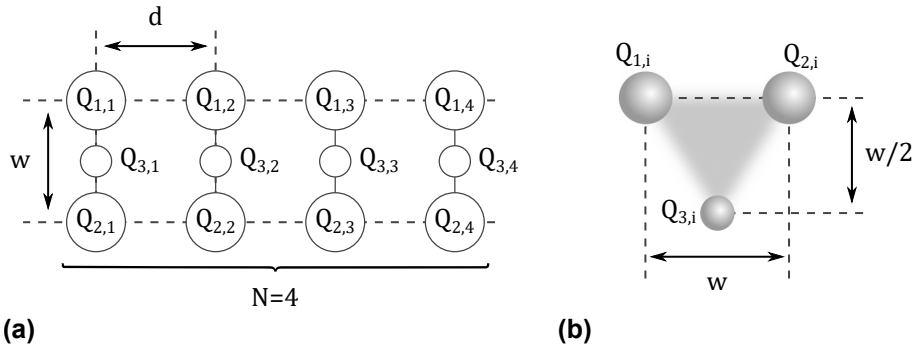

Fig. 4.1 Scheme used for the evaluation of the SCERPA convergence: (a) Molecular wure composed by 4 molecules (N=4) with intermolecular distance d. (b) Model of the molecule composed by three Aggregated Charges with geometrical quantities.

$$\left(\frac{1}{|\boldsymbol{R}_{1,i}-\boldsymbol{R}_{2,j}|}-\frac{1}{|\boldsymbol{R}_{2,i}-\boldsymbol{R}_{2,j}|}\right)=\frac{1}{w\sqrt{1+(|j-i|\sigma)^2}}-\frac{1}{|j-i|d}$$

$$\left(\frac{1}{|\boldsymbol{R}_{1,i}-\boldsymbol{R}_{3,j}|}-\frac{1}{|\boldsymbol{R}_{2,i}-\boldsymbol{R}_{3,j}|}\right)=0$$

The jacobian matrix becomes a symmetric Toeplitz matrix with null terms on the main diagonal.

$$J_F=\begin{pmatrix} 0 & \gamma_1 & \gamma_2 & \gamma_3 & \gamma_4 \\ \gamma_1 & 0 & \gamma_1 & \gamma_2 & \gamma_3 \\ \gamma_2 & \gamma_1 & 0 & \gamma_1 & \gamma_2 \\ \gamma_3 & \gamma_2 & \gamma_1 & 0 & \gamma_1 \\ \gamma_5 & \gamma_4 & \gamma_2 & \gamma_1 & 0 \end{pmatrix}$$

Where:

$$\gamma_n=\gamma_{|j-i|}=\frac{eQ_1'(0)}{4\pi\varepsilon_0}\left(\frac{1}{|j-i|d}-\frac{1}{w\sqrt{1+(|j-i|\sigma)^2}}\right) - \frac{eQ_2'(0)}{4\pi\varepsilon_0}\left(\frac{1}{|j-i|d}-\frac{1}{w\sqrt{1+(|j-i|\sigma)^2}}\right)$$

That can be written as

$$\gamma_{|j-i|} = \frac{eQ_1'(0) - eQ_2'(0)}{4\pi\varepsilon_0}\left(\frac{1}{|j-i|d} - \frac{1}{w\sqrt{1+(|j-i|d^2}}\right)$$

In such conditions, the matrix norm may be written as:

$$\|J_G\|_1 = \max_{j\in[1,N]} \sum_{i=1}^{N} |\{J_G\}_{i,j}|$$

In this case, the spectral norm is not used as required by the convergence condition. Indeed, it can be proven that, in general, $\|\cdot\|_2 \leq \|\cdot\|_1$, then by ensuring $\|J_G\|_1 < 1$ the convergence is ensured, even though nothing can be said if $\|J_G\|_1 > 1$, which requires the spectral norm evaluation. The norm may be easily evaluated considering that $\gamma_n > \gamma_{n+1}$. Finally, in the worst case:

$$\|J_G\|_1 = 2|\gamma_1| + 2|\gamma_2|$$

Where:

$$\gamma_1 = \frac{e}{4\pi\varepsilon_0 w}\left(\frac{1}{\sigma} - \frac{1}{\sqrt{1+\sigma^2}}\right)(Q_1'(0) - Q_2'(0))$$

$$\gamma_2 = \frac{e}{4\pi\varepsilon_0 w}\left(\frac{1}{2\sigma} - \frac{1}{\sqrt{1+(2\sigma)^2}}\right)(Q_1'(0) - Q_2'(0))$$

Then the convergence condition:

$$\|J_F\|_1 < 1 \Longrightarrow |\gamma_1| + |\gamma_2| < \frac{1}{2}$$

That implies:

$$\frac{e|Q_2'(0) + Q_1'(0)|}{4\pi\varepsilon_0 w}\left(\frac{1}{\sqrt{1+\sigma^2}} + \frac{1}{\sigma} + \frac{1}{\sqrt{1+(2\sigma)^2}} + \frac{1}{2\sigma}\right) < \frac{1}{2}$$

The obtained equation completes the understanding of the convergence mechanism concerning circuit dimension. Indeed, the convergence is favored by:

- Increasing the intermolecular distance, making σ large
- Using larger molecules, making w large

Notice that, from an experimental point of view, precise manipulation of the molecules to create a perfect nanowire might be challenging. For this reason, the SCERPA algorithm is developed general enough to permit the study of molecular circuits considering process variations and possible layout non-idealities.

Finally, the algorithm is tested on a wire composed of 3 bis-ferrocene-like molecules at different distances. For the bis-ferrocene molecule, considering the characterization reported in Section 3.6:

$$Q'_1(0) = -1.0928 \times 10^{-19}\,\mathrm{C\,V^{-1}}$$
$$Q'_2(0) = 1.0924 \times 10^{-19}\,\mathrm{C\,V^{-1}}$$
$$Q'_3(0) = 5.6030 \times 10^{-23}\,\mathrm{C\,V^{-1}}$$

Whereas the size of the molecule is w=1 nm. Notice that $Q'_3(0)$, the dot associated with the NULL state, is negligible since the molecule is considered in the HOLD state.

$$Q'_1(0) - Q'_2(0) = -2.1851 \times 10^{-19}\,\mathrm{C\,V^{-1}}$$

The general 3×3 Jacobian for the fixed-point may be written as:

$$J_G = \begin{pmatrix} 0 & \gamma_1 & \gamma_2 \\ \gamma_1 & 0 & \gamma_1 \\ \gamma_2 & \gamma_1 & 0 \end{pmatrix}$$

Table 4.1 reports the spectral norm for several intermolecular distances.

As expected from previous considerations, the method does not converge for short distances, which is a problem for molecular FCN technology. For this purpose, it is possible to improve the algorithm convergence by inserting a damping parameter (ξ). Therefore, the SCERPA equation is modified from Equation (4.6) as:

Table 4.1 Analysis of the SCERPA convergence

Intermolecular distance [nm]	**Jacobian spectral norm**	**SCERPA convergence test**
0.65	2.1072	FAILED
0.80	1.3996	FAILED
1.00	0.8670	PASSED
1.20	0.5689	PASSED

$$V_{in,i}^{\{k+1\}} = \xi V_{in,i}^{\{k\}} + (1-\xi)F_i(V_{in,1}^{\{k\}},\cdots,V_{in,i-1}^{\{k\}},V_{in,i+1}^{\{k\}},\cdots,V_{in,N}^{\{k\}}) = G_i(V_{in,1}^{\{k\}},\cdots,V_{in,i-1}^{\{k\}},V_{in,i+1}^{\{k\}},\cdots,V_{in,N}^{\{k\}})$$

The Jacobian norm is reduced by a quantity $(1-\xi)$ by applying a damping coefficient, favoring the algorithm convergence:

$$\{J_{\boldsymbol{G}}\}_{i,j} = \frac{\delta G_i}{\delta V_{in,j}} = (1-\xi)\frac{\delta F_i}{\delta V_{in,j}} \quad \Longrightarrow \quad \|J_G\|_1 = (1-\xi)\|J_F\|_1 < 1$$

4.3 Introduction of timesteps

So far, Equation (4.3) provides a way to find the charge distribution of circuit molecules in a precise timestep, which is defined with a precise clock field distribution and driver condition. In general, driver and clock fields may vary in the time domain to permit information propagation and elaboration. At the current state, SCERPA supposes that electrode generations mainly influence the velocity of the switch. Therefore, the molecule switch is not taken into account and the time instant can be all considered at the ground state from the point of view of the molecule. Therefore, each time step can be evaluate with the self-consistent procedure. The time is subdived into a set of T timesteps:

$$\{\tau_0,\cdots,\tau,\cdots,\tau_T\}$$

Table 4.2 Analysis of the SCERPA convergence with damping

Damping coefficient	Jacobian spectral norm	SCERPA convergence test
Intermolecular distance, d = 0.65 nm		
0.00	2.1072	FAILED
0.32	1.4329	FAILED
0.56	0.9272	PASSED
Intermolecular distance, d = 0.80 nm		
0.00	1.3996	FAILED
0.32	0.9517	PASSED
0.56	0.6158	PASSED
Intermolecular distance, d = 1.00 nm		
0.00	0.8670	PASSED
0.32	0.5896	PASSED
0.56	0.3815	PASSED
Intermolecular distance, d = 1.20 nm		
0.00	0.5689	PASSED
0.32	0.3869	PASSED
0.56	0.2503	PASSED

Then, driver and clock fields can be discretized in the time domain as:

$$V_{D,i} \longrightarrow V_{D,i}^{\{\tau\}} \qquad E_{clk,j} \longrightarrow E_{clk,j}^{\{\tau\}}$$

According to [74], the charge distribution of the entire circuit is obtained by solving, for each time step (τ), the non-linear system:

$$V_{in,i}^{\{\tau\}} = \frac{e}{4\pi\varepsilon_0} \sum_{j=1, j\neq i}^{N} \sum_{\alpha=1}^{N_{AC}} \left[Q_\alpha(V_{in,j}^{\{\tau\}}, E_{clk,j}^{\{\tau\}}) \left(\frac{1}{|\boldsymbol{R}_{1,i} - \boldsymbol{R}_{\alpha,j}|} - \frac{1}{|\boldsymbol{R}_{2,i} - \boldsymbol{R}_{\alpha,j}|} \right) \right] + V_{D,i}^{\{\tau\}} \tag{4.5}$$

Or, in a synthetic way:

$$V_{in,i}^{\{\tau\}} = F_i(V_{in,1}^{\{\tau\}}, \cdots, V_{in,i-1}^{\{\tau\}}, V_{in,i+1}^{\{\tau\}}, \cdots, V_{in,N}^{\{\tau\}}, V_{D,i}^{\{\tau\}}, E_{clk,i}^{\{\tau\}})$$

For each time step, SCERPA finds the solution of the problem by using an iterative procedure, thus by solving:

$$V_{in,i}^{\{k,\tau\}} = F_i(V_{in,1}^{\{k-1,\tau\}}, \cdots, V_{in,i-1}^{\{k-1,\tau\}}, V_{in,i+1}^{\{k-1,\tau\}}, \cdots, V_{in,N}^{\{k-1,\tau\}}, V_{D,i}^{\{\tau\}}, E_{clk,i}^{\{\tau\}}) \tag{4.6}$$

where F_i denotes the equation Equation (4.3). For the first time step $k = 0$, $\tau = \tau_0$, SCERPA guesses the initial values, formally $k = -1$ be $V_{in}^{\{k=-1\}} = 0$ and computes the driver voltages. Then, in order to accomplish the driver variation at each time step, SCERPA removes the driver contribution of previous time ($V_D^{\{\tau-1\}}$) and apply the driver contribution of the new timestep $V_D^{\{\tau-1\}}$. Formally:

$$V_{in}^{\{0,\tau\}} = V_{in}^{\{\infty,\tau-1\}} - V_D^{\{\tau-1\}} + V_D^{\{\tau\}} \tag{4.7}$$

4.4 Approximations techniques

So far, all the considered equations consider the interaction among all the molecules of the molecular FCN circuits. In particular, according to Equation (4.5), we have to

evaluate $N-1$ electrostatic evaluation for each molecule we have in the circuit in each convergence step (k). That means the computation cost is $O(N^2)$. To reduce the computation cost of the numerical problem, two possible paths are possible:

- Reduce the cost of the electrostatic evaluation
- Reduce the number of electrostatic evaluations in the single step

The equation of the electrostatic evaluation ($V_{ee}^{i,j}$), representing the voltage generated by molecule j to molecule i, can be expressed as:

$$V_{ee}^{\{i,j\}} = \frac{e}{4\pi\varepsilon_0} \sum_{\alpha=1}^{N_{AC}} \left[Q_\alpha(V_{in,j}^{\{\tau\}}, E_{clk,j}^{\{\tau\}}) \left(\frac{1}{|\boldsymbol{R}_{1,i} - \boldsymbol{R}_{\alpha,j}|} - \frac{1}{|\boldsymbol{R}_{2,i} - \boldsymbol{R}_{\alpha,j}|} \right) \right] \tag{4.8}$$

To simplify the operation, three possible directions are possible:

ee_A1 The term $\frac{e}{4\pi\varepsilon_0}$ is constant.

ee_A2 The term $Q_\alpha(V_{in,j}^{\{\tau\}}, E_{clk,j}^{\{\tau\}})$ requires the interpolation of the VACT

ee_A3 The terms $|\boldsymbol{R}_{1,i} - \boldsymbol{R}_{\alpha,j}|$ and $|\boldsymbol{R}_{2,i} - \boldsymbol{R}_{\alpha,j}|$ are constant distances.

Concerning *ee_1*, the constant can be evaluated once as the Coulomb's constant $k_c = \frac{1}{4\pi\varepsilon_0}$. Whereas, the distances, thus *ee_3* may be evaluated at the SCERPA beginning. In general, the distance tensor may be defined as:

$$dist(\alpha, \beta, i, j) = |\boldsymbol{R}_{\alpha,i} - \boldsymbol{R}_{\beta,j}|$$

Equation (4.8) may be thus rewritten as:

$$V_{ee}^{\{i,j\}} = k_c \sum_{\alpha=1}^{N_{AC}} \left[Q_\alpha(V_{in,j}^{\{\tau\}}, E_{clk,j}^{\{\tau\}}) \left(\frac{1}{dist(1, \alpha, i, j)} - \frac{1}{dist(2, \alpha, i, j)} \right) \right]$$

Regarding the interpolation of *ee_2*, the problem is simplified to speed up the algorithm. Indeed, the VACT is implemented in SCERPA through a look-up table

with *NxM* size, where N is the number of input voltage samples and M is the number of clocks. In general, for a given clock, given a specific input voltage V_{in}, the interpolation is a $O(N)$ problem. Therefore, to speed up the optimization, SCERPA assumes:

- All the charges are evaluated on a set of input voltages ($\{V_{in}^{[1]},...,V_{in}^{[M]}\}$) which is the same for all the clock values.
- The set of input voltages is ordered and uniformly spaced.

Under the assumptions mentioned above, the single charge for a specific clock value $E_{clk,j}^{\tau}$ can be evaluated with a linear approximation as

$$Q_\alpha(V_{in,j}^{\{\tau\}},E_{clk,j}^{\{\tau\}}) = \{w\}\cdot Q_\alpha(\lfloor w\rfloor,E_{clk,j}^{\{\tau\}}) + (1-\{w\})\,Q_\alpha(\lfloor w\rfloor+1,E_{clk,j}^{\{\tau\}}) \quad (4.9)$$

With $\{\cdot\}$ and $\lfloor\cdot\rfloor$ representing the fractional part and the floor functions, respectively. w is the named *probe position*:

$$w(V_{in,j}^{\{\tau\}}) = (M-1)\frac{V_{in,j}^{\{\tau\}}-V_{in}^{[1]}}{V_{in}^{[M]}-V_{in}^{[1]}}+1$$

In this regard, the interpolation does not depend on the look-up table size, improving the algorithm efficiency.

4.4.1 Interaction Radius and Active Region modes

So far, all the optimizations have been conducted to simplify the calculation of the single electrostatic interaction, which is currently reduced by decreasing the number of operations per evaluation and improving the convergence procedure, making it independent of the number of VACT samples.

$$V_{in,i}^{\{\tau\}} = \sum_{j=1,j\neq i}^{N} V_{ee}^{\{i,j\}} + V_{D,i}^{\{\tau\}}, \qquad i\in[1,N] \quad (4.10)$$

To further reduce the calculation complexity, it is now necessary to do a step over and consider the number of performed calculations. In particular, in a circuit of N molecules, SCERPA evaluates evaluates $N \times (N-1)$ electrostatic calculations till convergence. By supposing the algorithm converges in $\hat{k}$ steps, the number of calculation performed in a single timestep τ is $N \times (N-1) \times \hat{k}$. In each timestep, the complexity is $O(N^2)$. It is necessary to reduce the number of electrostatic interactions evaluated at each time step to reduce the computational cost. Accordingly, it is important to consider that the equations depend on the distance inversely. The larger the distance among molecules, the smaller the interactions. The input voltage generated by a generic molecule i on a molecule j will be very small when the distance between the two molecules is large.

For this purpose, it is not necessary for each molecule of the circuit to evaluate the electrostatic contributions generated by all the molecules of the circuit. Indeed, neighbor molecules will produce the most important voltage contributions. A maximum interaction radius (d_{IR}) is therefore defined. For each molecule, all the molecules such that $dcc_{\{i,j\}} < d_{IR}$, where $dcc_{\{i,j\}}$ is the center-center distance between two generic molecules, are inserted in the so-called Interaction Radius (IR) list, named *IR list of Molecule i* ($IRList_i$). The number of electrostatic interactions evaluated at each step is now reduced from $N \times (N-1)$ to $N \times dimIRList$. Where $dimIRList$ denotes the number of neighbor molecules. In particular, in the general case of a wire with intermolecular distance d, the dimension of the IR list is finite and equal to $2d_{IR}/d$, and the number of electrostatic interactions lowers to $N \times 2d_{IR}/d$. The computational cost of the interaction reduces to $O(N)$. Notice that the interaction radius is also used in other tools for FCN simulation, such as ToPoliNano [68] and QCADesigner [61].

Generally, the higher the interaction radius (d_{IR}), the more precise and physically consistent the simulation is. On the contrary, a low interaction radius permits a lower calculation complexity, speeding up the calculation. A trade-off between precision and computational complexity is required. Considering the results reported in 5.1.1 and [5], the interaction mainly occurs at a distance equal to six intermolecular distances, which is a suitable d_{IR} parameter. The Equation (4.10) is then modified as:

$$V_{in,i}^{\{\tau\}} = V_{D,i}^{\{\tau\}} + \sum_{j \in IRList_i} V_{ee}^{\{i,j\}}, \qquad i \in [1,N]$$

A second consideration that may permit code optimization is that the molecules generally vary their charge to respond to neighbor molecule effects. Supposing that all the molecules in the vicinity of a precise molecule *i* have null input voltage, the molecule will show a uniform charge distribution and generally do not influence other molecules. In general, the voltage of each molecule varies if and only if neighbor molecules vary. The Active Region mode optimizes the number of molecules considered in the evaluation. In particular, it limits the calculation only to molecules that are effectively supposed to vary:

- Molecules whose input voltage has been changed in the last step.
- Molecules whose neighbor molecules have been polarized in the last step.
- Molecules close to driver molecules which have been changed in the last step
- Molecules whose clock electric field has been changed in the last step

Instead of evaluating the voltage of all the N molecules in the circuit, SCERPA considers a set of molecules, named Active Region list and denoted as *ARList*, with dimension $ARList \leq N$. Finally, the calculation is implemented in SCERPA according to the equation:

$$V_{in,i}^{\{\tau\}} = V_{D,i}^{\{\tau\}} + \sum_{j \in IRList_i} V_{ee}^{\{i,j\}}, \qquad i \in ARList$$

While determining molecules whose clock field has been changed is trivial, the procedure to determine the molecule with varying input voltage is more challenging. For this purpose, a voltage threshold V_{AR} is defined, and all the molecules whose input voltage varies more than the V_{AR} are inserted in the ARList with all the neighbors. Indeed, all the neighbors of an active molecule will undoubtedly have an active molecule in the vicinity. A molecule is inserted in the ARlist if:

$$\left| V_{in,i}^{\{k-1,\tau\}} - V_{in,i}^{\{k-2,\tau\}} \right| > V_{AR} \tag{4.11}$$

Also, in this case, a lower value of the AR threshold would increase the number of molecules considered active, thus improving the algorithm precision. On the other hand, a more significant threshold decreases the precision of the calculation

yet speeds it up. In general, the ARlist may contain all the molecules in the worst case. Therefore, the formal computation complexity remains $O(N)$. Nevertheless, only some molecules will be active in the circuit. Therefore the actual calculation complexity becomes statistically reduced to:

$$O(1) \leq complexity \leq O(N)$$

In the ideal case, only a few molecules will be active. Thus the actual complexity will be close to $O(1)$. Finally, it is worth highlighting that for some reasons that will be clear in the following chapters, related to crosstalk among molecules, it may happen that molecules with null input voltage influence each other and polarize. For this reason, the AR mode is activated at the second SCERPA iteration to avoid evaluation errors related to crosstalk neglection. Therefore, the computational cost of the first iteration is $O(N)$ (the IR mode can be activated).

Finally, SCERPA permits a *refining mode*, which means SCERPA disables AR and IR modes and refines the solution by solving the Equation (4.10) with no approximation when the convergence is reached. The solution is supposed to be the same SCERPA would evaluate using Equation (4.10) only, yet, the computational time is reduced.

To quantitatively analyse the approximation techniques and their effects in terms of calculation time and precision, SCERPA is run on a molecular FCN wire composed by bis-ferrocene molecules using three possible calculation configurations:

- Mode I: IR and AR modes are not exploited
- Mode II: IR and AR modes are enabled, and refining is not exploited.
- Mode II: IR and AR modes are enabled, and refining is enabled.

The obtained total execution time obtained on Intel Xeon E3-12, 2 GHz, single-core are also published in [74] and are shown in Fig. 4.2.

With MODE I, the computational cost of the single step is maximized to $O(N^2)$. Indeed the analysis of a wire composed of 500 molecules requires more than 17 h. The MODE I solution represents the most precise evaluation given by SCERPA. In MODE II, the computational cost of the single step should be reduced to O(1) and

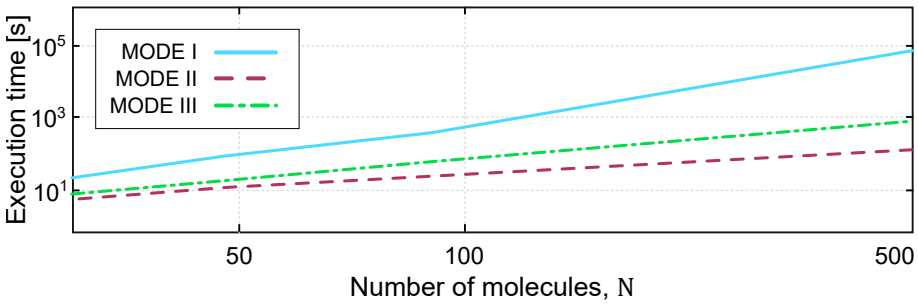

Fig. 4.2 SCERPA computation time

Table 4.3 Analysis of the SCERPA computational cost

	MODE I	**MODE II**	
Number of molecules	**Single Step Time [s]**	**Single Step Time [s]**	**Error, σ [%]**
50	0.477	0.060	0.46
100	1.100	0.063	0.46
500	39.9	0.067	0.45

be essentially independent concerning the number of molecules. Table 4.3 reports the single step execution time for MODE I and MODE II, and the relative error of MODE II evaluated concerning the MODE I solution ($\hat{\boldsymbol{V}}_{in}$) as:

$$\sigma = \frac{\left|\boldsymbol{V}_{in} - \hat{\boldsymbol{V}}_{in}\right|}{\left|\hat{\boldsymbol{V}}_{in}\right|}$$

It can be seen that the execution time is low for MODE II and constant concerning the number of molecules composing the wires. On the contrary, the single-step computational time increases with the number of molecules in MODE I. For comparison, a molecular wire composed of 500 molecules requests 128 s, thus much less than the same evaluation performed with no approximation techniques in MODE I. Furthermore, the error concerning MODE I is lower than 1% independently of the number of molecules. Finally, the computational time is slightly increased with MODE III, yet the error is reduced to zero since the final voltage on all the molecules is consistent with MODE I. Besides, the computational time is reduced since a rough solution is obtained by exploiting the approximations given by AR and IR modes.

4.5 Implementation of the SCERPA algorithm

The current version of SCERPA is implemented as a MATLAB program and subdivided into three independent sections that share predefined files which are intended to be compatible with a future release of ToPoliNano [68]. The three sections are devoted to the layout creation, the calculation engine, and the viewer. The vital files involved in the SCERPA algorithm are:

- The configuration script **.m*: it is used to configure the SCERPA simulation and may embed the layout information.
- The layout file **.qll*: it is used to describe the circuit layout. This file may be omitted if the configuration script describes the layout directly. The file can be generated with MagCAD [71], eventually modified to consider the molecular technology.
- The output step file **.qss* contains the charge distribution of the molecules in each simulation step.
- The table file **.txt*: it contains tabular data containing additional information which can be requested during the simulation.

Fig. 4.3 shows the general working flow of the SCERPA algorithm for a case studio of a wire composed of 10 molecules. The wire can be described using MagCAD to generate the file *Schematic.qll*, or written directly as a matrix in the *ScerpaConf.m*. Additionally, *ScerpaConf.m* contains all the settings necessary for SCERPA for a correct running, including layout, simulation, and viewer configurations. The file is executed by the SCERPA engine, which generates as output files the single-step charge distribution (*Step1.qss*,...,*StepN.qss*) and other requested information in the *table.txt*. All the output files may be read from the viewer, which can generate 1D, 2D, and 3D plots. The following sections will give details about the three sections of the SCERPA algorithm.

Generally, SCERPA is intended to be run with a single MATLAB function named *SCERPA()* which can be run in four different ways:

```
SCERPA('generate',circuit) % mode 1
SCERPA('launch',settings) % mode 2
SCERPA('generateLaunch',circuit,settings) % mode 3
SCERPA('plotSteps',plotSettings) % mode 4
```

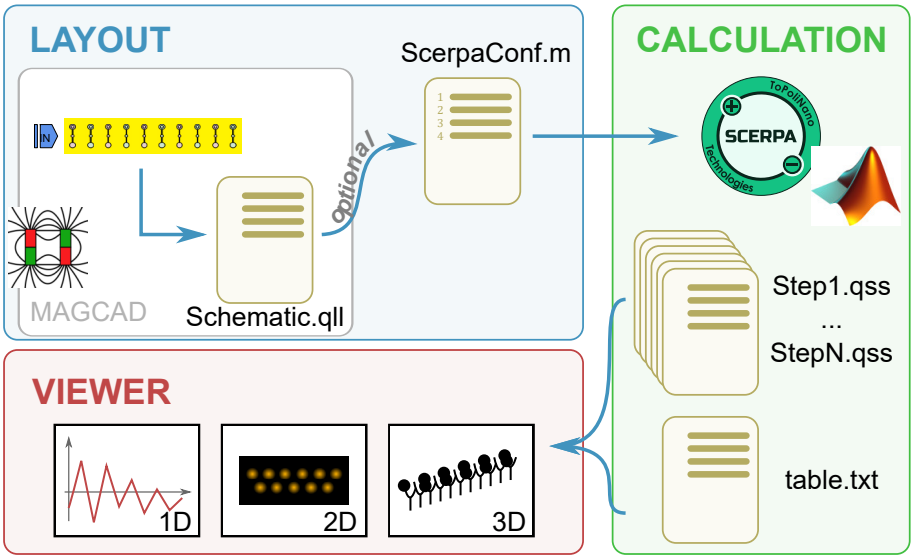

Fig. 4.3 Scheme of the SCERPA tool highlighting the Layout, Calculation, and Viewer sections

In particular:

1. Mode 1: executes the Layout section only and prepares the SCERPA calculation. The *circuit* variable contains all the layout parameters.
2. Mode 2: executes the Algorithm section only. The *settings* variable contains the calculation configuration.
3. Mode 3: it is generally the standard execution mode, and it executes both the layout and the Algorithm sections. The *circuit* variable contains all the layout parameters, whereas the *settings* variable contains the calculation configuration.
4. Mode 4: executes the SCERPA Viewer to post-process simulation data and generates figures. The *plotSettings* variable contains the viewer settings.

Modes 1 and 2 are generally used together when several simulations should be run using the same layout and comparing different calculation configurations.

The following sections will detail the main settings related to the SCERPA tool, which is currently under development. Many functions may be added in the future and are under development. A list of functions, demo files, and available features is

Fig. 4.4 SCERPA logo

available in the SCERPA documentation [90]. Fig. 4.4 shows the current logo used for SCERPA.

The three sections of the SCERPA tool are separated into several folders.

```
SCERPA
├── Algorithm
│   └── ...
├── DemoFiles
│   └── ...
├── Documentation
│   └── ...
├── Layout
│   └── ...
├── Viewer
│   └── ...
└── SCERPA.m
```

In particular, folders *Layout*, *Algorithm*, and *Viewer* are the three section of the SCERPA tool whereas the folders *DemoFiles* and *Documentation* contain some files which can be launched to test the tool and the documentation of the tool. The file *SCERPA.m* is the main function of the tool.

4.5.1 The layout

The layout section permits the definition of the circuit layout, which can be defined directly in the MATLAB input script or using MagCAD. In addition, the Layout

section permits the management of several circuit properties and signals. The layout of the circuit may be defined using MagCAD, thus importing a **.qll* file, or by defining the circuit through a matrix *circuit.structure*. The following code the definition of a 10 molecule FCN wire:

```
circuit.structure = {'Dr_x' '1' '1' '1' '1' '1' '1' '2' '2' '2' '2' 'out_y'};
```

The label *'Dr_x* represents a driver molecule, while 'out_y' is the label representing the output of a circuit. In general, three types of molecules can be inserted into the circuit:

- Normal molecules: these molecules, labeled with a number, will be part of the self-consistent procedure, and their voltage will be evaluated according to the charge distribution of each circuit molecule. The number in the variable 'circuit.structure' represents the clock region.
- Driver molecules: these molecules will have a voltage (V_D) that the user forces in each time step and will not be affected by the self-consistent procedure.
- Output molecules: the output of these molecules will be evaluated by the SCERPA tool, yet, the charge distribution of these molecules will always be zero, thus not influencing the circuit. These molecules can be thought of as voltage probes.

The position of the aggregated charges can be changed according to the molecules used for the simulation, which can be set with the variable *circuit.molecule*. The list of molecules is available in the SCERPA documentation [90]. Each molecule is described by an *info.txt* file. For instance, the bis-ferrocene info file is reported in the following lines. Fig. 4.5(a) shows the bis-ferrocene molecule represented by four charges.

```
CHARGES 4
-3.622       -5.062     -0.094
-3.588       +5.083     -0.094
+3.133515    -0.011731  -0.755
+11.776298   -0.053777  +0.409
```

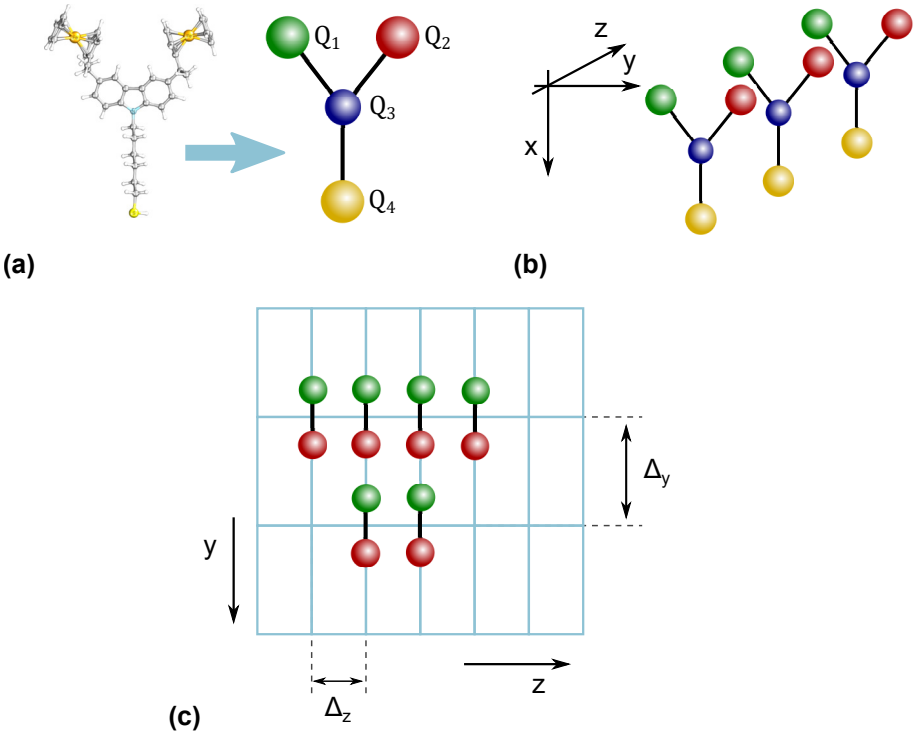

Fig. 4.5 SCERPA Layout: (a) Representation of the bis-ferrocene molecule into four aggregated charges. (b) SCERPA axis. (c) Positioning grid used for the placement of molecules in the SCERPA layout.

```
ASSOCIATION 3
1 3
2 3
3 4

CLOCKDATA 3
ck1.txt -2 V 39 values
ck2.txt 0 V 39 values
ck3.txt +2 V 37 values
```

The field *CHARGES* denotes the presence of four aggregated charges. In general, all the molecules in SCERPA are approximated using four Aggregated Charges. A future version of the SCERPA algorithm will generalize the number of aggregated charges, eventually considering N charges per molecule. Some efforts have already been reported in [91] where a bis-ferrocene molecule is modeled with 91 charges. Molecules with two or three aggregated charges are currently implemented as molecules with four dots where non-existing charges are considered null charges, thus not able to influence molecules electrostatically. The lines following the CHARGE keyword report the coordinates of the four charges on the x,y,z-axis. Fig. 4.5(b) reports the coordinate system used in the SCERPA layout to position molecules and charges. For the sake of completeness, the ASSOCIATION section reports the connection between charges, used for graphical reasons to show the lines connecting the aggregated charges, as depicted in Fig. 4.5(a). The CLOCKDATA section is used in the Algorithm section and reports the name of the files containing available transcharacteristics with specific clock values and the number of values in the file.

By acting on the input file, coordinates of each molecule can be shifted or rotated. In particular, by indicating with $(x,y,z)^T$ the position of a molecule aggregated charge, the coordinate in SCERPA are modified to $\boldsymbol{Z}_{PV}$ (PV: process variations) as:

$$\boldsymbol{Z}_{PV} = \begin{pmatrix} 1 & 0 & 0 \\ 0 & \cos\theta_x & -\sin\theta_x \\ 0 & \sin\theta_x & \cos\theta_x \end{pmatrix} \begin{pmatrix} \cos\theta_y & 0 & \sin\theta_y \\ 0 & 1 & 0 \\ -\sin\theta_y & 0 & \cos\theta_y \end{pmatrix} \cdot \begin{pmatrix} \cos\theta_z & -\sin\theta_z & 0 \\ \sin\theta_z & \cos\theta_z & 0 \\ 0 & 0 & 1 \end{pmatrix} \begin{pmatrix} x \\ y \\ z \end{pmatrix} + \begin{pmatrix} S_x \\ S_y \\ S_z \end{pmatrix}$$

Where Θ_x, Θ_y, and Θ_z are the rotation angles in the three directions, respectively, whereas S_x, S_y, and S_z are the shifts. The shift associated with the x-axis (S_x) can also be used to emulate the presence of a rough substrate. To conclude, the final coordinate of a single charge, $\boldsymbol{Z}$, also depends on the intermolecular distance. In SCERPA, the molecules are considered equally distributed on a grid with Δ_y and Δ_z lattice parameters, which are considered constant for the entire calculation and depending on the device fabrication [60], see Fig. 4.5(c).

$$\boldsymbol{Z} = \boldsymbol{Z}_{PV} + \begin{pmatrix} 0 \\ n \cdot \Delta_y \\ m \cdot \Delta_z \end{pmatrix}$$

Where n and m are two integer numbers denoting the molecule position in the circuit layout.

In addition to the molecular layout, the SCERPA layout section also permits the definition of testbench signals related to the clocking scheme and the input stimuli. Regarding the clocking field, SCERPA allows for the definition of two clock modes. The general procedure, named *phase mode*, consists in assigning a label to each molecule in the *circuit.structure* variable and to associate a clock value in each timestep using the variable *circuit.stack_phase*. The same clock value will guide all the molecules associated with a certain clock region.

A second possibility is the *map mode*, which is used to analyze non-ideal situations. With this mode, the clocking field is taken from a table containing x,y,z coordinates, and the field value. This mode permits SCERPA to consider clock fields eventually generated by external electrodes, which can be calculated using Finite Element Modelling (FEM). A third mode, which is still under development, consists

in using models that allow SCERPA to calculate the field by considering the practical structure of the electrodes without the need for external FEM tools.

Finally, SCERPA requires the definition of Driver molecule voltages. Indeed, these molecules have an input voltage that is not affected by the self-consistent procedure. Their voltage is defined with the variable *circuit.Values_Dr*.

Finally, the Layout section creates the layout SCERPA files, which can be read by the Algorithm section, which runs the simulation engine.

4.5.2 The algorithm

The algorithm section is responsible for the calculation of the circuit charge distribution. Code 2 reports the pseudocode of the SCERPA tool. The Algorithm section firstly imports the SCERPA settings. In particular, the settings are read from the input file, thus selected by the user. If some of the settings are not set by the user, default values are used. The SCERPA documentation lists all the default settings of the tool [90]. Therefore, it imports the file generated by the Layout Section regarding the circuit and the stimuli of the simulation. The Layout output files contain all the molecule circuit positions, the clock values, and the driver voltages in each timestep. The SCERPA algorithm, at this point, imports the transcharacteristics of the used molecules. To improve the calculation speed, SCERPA reshapes the data of the transcharacteristics on a uniform set of voltages to reduce the interpolation computation cost, thus following Equation (4.9).

Similarly, it also evaluates the *Distance Matrix*, thus the distances among all the charges of the circuit, so that it is not necessary to continuously evaluate constant distances in the evaluation of voltage contributions. Once the distance matrix is obtained, it is also used to define, for each molecule, the IR list. For each molecule, the molecules whose distance is smaller than a predefined value are inserted in the IR list of the molecule, as discussed in Section 4.4.1.

At this point, SCERPA evaluates the charge distribution in each time step of the simulation. At first, the voltage generated by driver molecules is obtained by associating a charge on each driver input voltage with the transcharacteristics, thus evaluating driver voltages V_D. Therefore, concerning the first time step, SCERPA initializes the input voltage of each molecule to zero and sets the charges of the molecules in the circuit according to the first step clock configuration. Moreover,

Algorithm 2 Pseudocode of the SCERPA algorithm.

```
Load settings;                                              ▷ Initialization
Import Layout;
Import and reshape transcharacteristics;
Create distance matrix;
Create IR lists;
for each timestep as τ do                                   ▷ Timestep definition
    Evaluate Driver contribution;
    if First timestep then
        Set initial voltage to zero;
        Initialize timestep clock values;
    else
        Update input voltages;
        Update clock values;
        Update AR lists;
    end if
    while Convergence is NOT reached do                     ▷ Self-Consistent Loop
        if Maximum number of steps reached then
            break;
        end if
        Define AR list;
        for each molecule in AR list as i do
            V_in,i = V_D,i;
            for each molecule in IR list of i as j do
                V_i,j = EvaluateMoleculeContribution(i,j);
                V_in,i = V_in,i + V_j,i
            end for
        end for
        Update Molecular input voltage;
        if Convergence is reached then
            if is refining mode requested then
                Disable AR mode;
            else
                Assert convergence flag;
            end if
        end if
    end while
    Evaluate output voltages;
    Evaluate step energy;
    Output QSS File;
    Dump simulation data in the table file;
end for
```

for the following timesteps, the SCERPA algorithm updates the input voltage by removing the previous driver effect and updating the new value of driver influences, according to Equation (4.7). Therefore, it also updates the clock values of each molecule to select the correct transcharacteristics.

It is necessary to highlight the update of the AR list. Indeed, all the molecules that vary the clock field or satisfy Equation (4.11) are considered active and inserted in the AR list, together with all the molecules in the active molecule IR lists.

After this initialization section and the timestep definition, SCERPA runs the core of the algorithm: the self-consistent procedure, which is terminated if the convergence is reached or when too many steps have been calculated. Therefore, apart from the first step of the timestep, which is already defined in terms of the AR list, SCERPA updates the AR list by inserting the molecules whose input voltage has been varied, concerning the previous step of the self-consistent procedure, by a quantity more significant than the AR threshold (V_{AR}).

The self-consistent procedure is then used to evaluate the voltages of each molecule in the AR list. In particular, SCERPA evaluates the voltage generated by each molecule in the IR list on the molecules of the AR list. Finally, the driver contribution is summed in the final result, and the transcharacteristics is applied to obtain the temporary charge distribution of the molecule.

Once all molecule input voltages are obtained, the difference concerning the previous step is estimated to evaluate the algorithm convergence. Therefore, if the convergence is reached, the loop is broken, and the SCERPA finalizes the timestep. Notice from Section 4.4.1, SCERPA permits a *refining mode*. If this mode is activated, the convergence flag is not asserted once the convergence is reached, yet SCERPA inserts all the molecules in the AR list and continues the self-consistent procedure. In these conditions, SCERPA evaluates a more precise solution while increasing the time for the evaluation.

Finally, the SCERPA algorithm evaluates the energy of the step by using the model proposed in Section 3.5 and manages the output files. In particular:

- It updates the QSS file by copying the information regarding each molecule for the timestep under consideration
- It updates the table file by inserting the information that the user has requested with dump settings in each timestep

- dumpClock: it dumps the clock of each molecule
- dumpVout: it dumps the voltage of each molecule
- dumpDriver: it dumps the voltage of each driver
- dumpOutput: it dumps the voltage of each output
- dumpComputationTime: it dumps the CPU time
- dumpEnergy: it dumps the energy values

A few other features are also implemented in the Algorithm section. Indeed, SCERPA allows the user to see the simulation result at runtime by enabling the intermediate plot function. This feature permits the visualization of the charge distribution and voltages during the calculation by permitting a fast analysis of circuits yet increasing the computational time. Also, together with the intermediate plot function, the execution may be paused at each time step so that the user can analyze the circuit at runtime. Finally, the verbosity of the log file may also be varied.

4.5.3 The Viewer

The Viewer Section is the last part integrated into the SCERPA algorithm. In this section, SCERPA imports the data from the Algorithm and the simulation results (QSS files), permitting the plot of some features. In particular, the Viewer Section currently implements five visualization modes that show information regarding the single time step:

- **1D Charge Plot**: it shows the charge of the molecules on a 1D plot. The x-axis writes the molecule index, whereas the y-axis shows the charge in atomic units of each molecule. This plot helps analyze molecular wires since the labels on the x-axis generally follow the molecule order. On the other side, this plot is difficult to be used when dealing with 2D circuits since the labels on the x-axis are not straightforward with the structure.
- **3D Charge Plot**: it shows the charge of the molecules on a 3D plot. In particular, all the molecules are depicted with dots representing the aggregated charges, whose size is proportional to the charge of the aggregated charge itself.

The aggregated charges are connected following the associations reported in the *info.txt* file. This plot is helpful for small circuits. However, when many molecules are present, it becomes difficult to understand since molecules are very close to each other and difficult to distinguish on a 3D plot.

- **Potential Viewer**: it shows the voltage generated by the molecular charge distribution evaluated on a surface above the circuit plane, using Equation (4.1). The user can set the distance from the molecules. The use of this plot is similar to the 3D Charge Plot. Indeed, it allows analyzing the charge distribution of entire circuits. It permits the visualization of larger circuits since molecules are not overlapped in the 3D space. Nevertheless, huge circuits may be difficult to analyze since the detail is on the single-molecule. This function permits the highest physical information with the most significant number of molecules.

- **Logic Viewer**: the logic viewer allows seeing the propagation and the elaboration of the information on the circuit. It evaluates the encoded information by using Equation (1.1), thus linking the charge of molecular cells to a high-level quantity (logic information). Then, it shows the logical information using red and blue colors. This plot removes some physical information, making it easy to understand large device logic behavior.

The presented plots permit the analysis of single-time steps and help design circuits. However, this level of detail may be exaggerated when dealing with logical functioning since input-output values would be enough for a first working principle analysis of devices. For this purpose, if input and output values are dumped in the table file, the **Waveform Plot** may be used. It plots the values of driver and output molecules in each timestep to view the device working principle.

Chapter 5

Molecular FCN circuits

In Chapter 4 the Self-Consistent ElectRostatic Potential Algorithm (SCERPA) algorithm has been deeply described. In this chapter, the SCERPA tool and theoretical discussion demonstrate the devices necessary to create complex digital circuits based on molecular Field-Coupled Nanocomputing (FCN) technology. First, the chapter analyses the propagation of the information in wires and routing connections, discussing bistability, crosstalk, and memory effects. In particular, bistability is studied by considering the bistable factor theory. Then, the main devices necessary for elaborating the information (inverters and majority voters) are analyzed by considering the effective nature of molecules and addressing the dependencies between molecular nature and circuit-level functioning. Analyzed devices are finally used to design more complex digital devices such as the XOR and a 1-bit full-adder to provide proof of physical-aware design, where the digital circuit is created by considering the effective physics of the molecules.

5.1 The molecular FCN wire

This section shows and analyses the characteristics of molecular FCN wires, thus the primary device permitting the information propagation. The device is created by aligning molecules on a line. To study the information propagation as a function of the wire characteristics, the intermolecular distance and the number of molecules in the wire are varied. In particular, the wires are first analyzed by considering 8, 16 molecules, whereas the intermolecular distance is varied as 1 nm, 0.8 nm, and 1.2 nm.

Considering the generality of the SCERPA algorithm, guaranteed by the Molecular Simulator Quantum-dot cellular automata Torino (MoSQuiTo) methodology, it is possible to analyze any molecule provided the proper Vin-Aggregated Charge Transcharacteristics (VACT). In the following analysis, the bis-ferrocene molecule is first used. Regarding the clocking scheme, a single clock region with a ramp clocking field (from $-2\,\mathrm{V\,nm^{-1}}$ to $+2\,\mathrm{V\,nm^{-1}}$) is used to guide the propagation in the entire wire. Clocked molecular devices will be studied in the following sections.

Fig. 5.1(a) reports the electrostatic potential obtained by SCERPA for a molecular wire composed of eight bis-ferrocene molecules with an intermolecular distance of 1 nm. The wire is analyzed by forcing the first and second molecules to encode logic values '0' and '1' to demonstrate the correct information propagation in all possible cases. The correct propagation of the information is confirmed by analyzing the two logic cases. Indeed, the alternating white spots report a correct propagation of the information for 1 nm intermolecular distance either with '0' and '1' logic values. It is interesting to notice a lower brightness of the potential map concerning the last molecules of the wire. This effect, known as the *border effect*, is related to the fact that the last molecules are not connected to any circuit; thus, they interact with a limited number of molecules. The border effect was also reported within the general Quantum-dot Cellular Automata (QCA) paradigm [4]. One may wonder whether this propagation reduction may be altered by the length of the molecular wire or the intermolecular distance.

Therefore, the analysis is repeated by reducing the intermolecular distance to 0.8 nm. Fig. 5.1(b) reports the obtained electrostatic potential. In this case, the electrostatic interaction among molecules is increased thanks to the lower distance, favoring the molecule polarization on the entire wire and reducing the border effect. A small intermolecular distance, in general, promotes the intermolecular interaction and facilitates the propagation of the information. On the contrary, the electrostatic interaction generally decreases by increasing the intermolecular distance. Thus propagation is expected to worsen for longer intermolecular distances. Fig. 5.1(c) reports the propagation of the information in the molecular wire by using 1.2 nm. In this case, the wire does not propagate the information. The alternating white spots are barely present in the first nanometers of the molecular wire, yet the information encoding is not evident and not propagated to the end of the molecular wire.

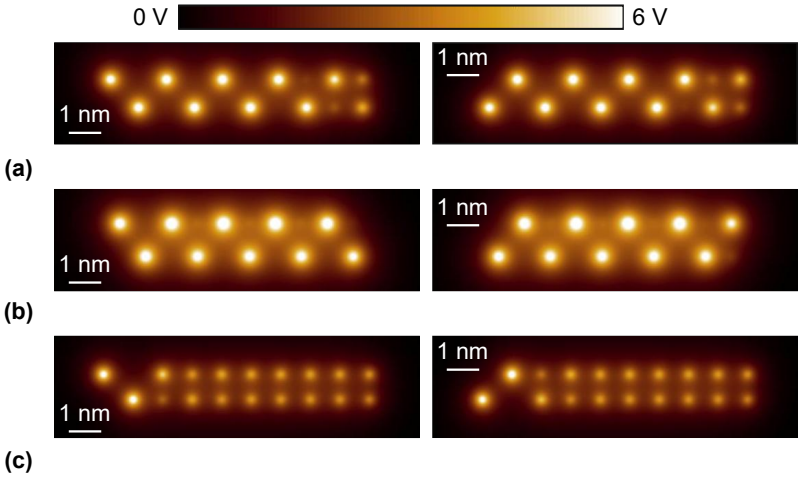

Fig. 5.1 SCERPA simulation of molecular FCN wires composed by 8 molecules with variable intermolecular distance. (a) 1 nm. (b) 0.8 nm. (c) 1.2 nm.

It is essential to mention that the intermolecular distance cannot be varied freely. Indeed, the interface between the self-assembled molecular monolayer and the substrate dictates the distance among molecules. For instance, for thiols, it is generally accepted that the intermolecular distance is multiple of 0.5 nm [60], which means the propagation of Fig. 5.1(b) may be feasible.

Therefore, the wire length is increased to 16 molecules to understand the dependence between information propagation and wire length. Fig. 5.2(a) reports the wire with 16 molecules and an intermolecular distance of 1 nm. The information propagation is correct both for the '0' and for '1' logic information. Comparing the analysis reported in the eight molecule wire, one could expect the border effect to appear in the central region of the wire, thus in a position consistent with the previous result. Nevertheless, this result confirms that the border effect is not related to the length of the wire. Instead, the border effect always shows up at the wire ends. The information propagation in the wire does not attenuate with wire length. The low intermolecular distance creates a bistability effect that permits the information to propagate also for large distances with no attenuation [5].

However, it is worth mentioning that long wires may be difficult to use due to possible noise that can force the molecules to polarize in the center of the wire. It is necessary to remind that the VACT used in SCERPA is evaluated by *ab initio* techniques and conceivably resemble the effective molecule nature, which can be not perfectly symmetric. Therefore, some molecules can be naturally biased with a

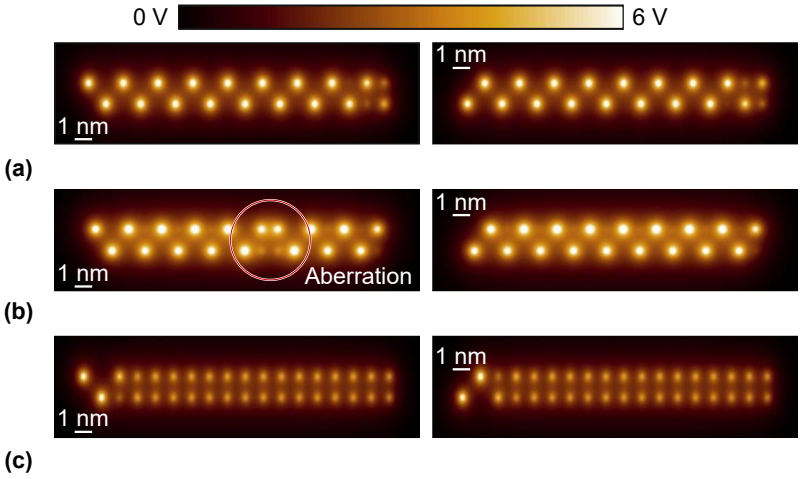

Fig. 5.2 SCERPA simulation of FCN wires composed by 16 molecules with variable intermolecular distance. (a) 1 nm. (b) 0.8 nm. (c) 1.2 nm.

specific charge distribution that may propagate concurrently with the driver. If the wire is too long, the effect of a possible error may propagate faster than the driver logic information.

Fig. 5.2(b) reports the analysis with reduced intermolecular distance (0.8 nm). In this case, the intermolecular interaction is favored with the shorter distance, and a logic aberration is present when propagating the logic '0'. In this case, the wire successfully propagates only one of the two logic values since the noise mentioned above makes it impossible to propagate the information correctly. The obtained results motivate clocking schemes and clocked molecular wires to guide the information propagation. Clocked molecular FCN wires will be analysed in Section 5.2.1.

Finally, Fig. 5.2(c) reports the analysis with 1.2 nm intermolecular distance. Again, the large intermolecular distance obstructs the information propagation and the correct functioning of the molecular FCN wire.

As the last analysis, the analysis published in [74] concerning a 40 molecule wire propagated logic '1' is here repeated. In particular, the analysis considers four different steps of the SCERPA Self-Consistent Field (SCF) procedure. This result is interesting to explain the application of approximation techniques described in Section 4.4.1. Fig. 5.3 shows the voltage map associated with the four steps: the first step considering only the driver contribution, two intermediate steps, and the convergent solution. This result demonstrates the phenomenon permitting the

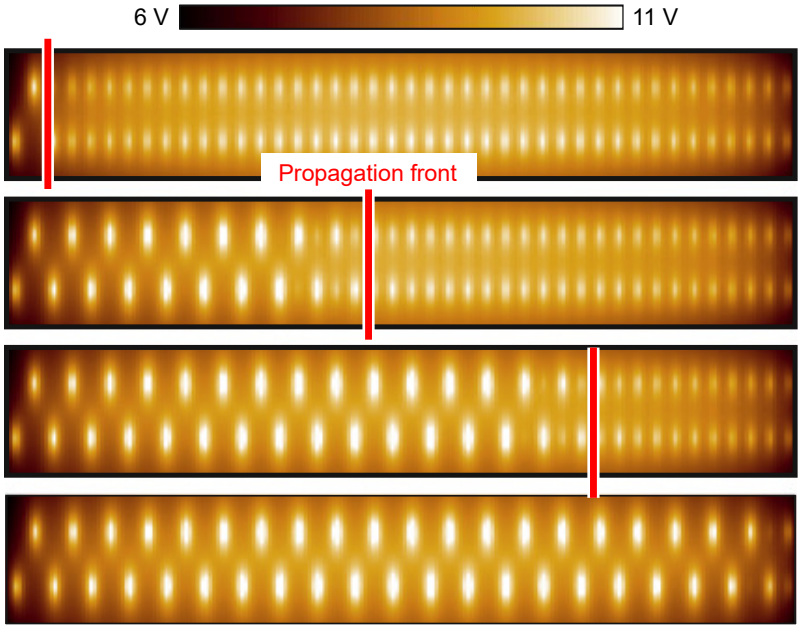

Fig. 5.3 SCERPA simulation of a molecular FCN wire composed by 40 molecules in four different time steps of the self-consistent SCERPA procedure: driver contribution only; step $k = 75$; step $k = 150$ and final charge distribution.

exploitation of the Active Region mode. Indeed, the propagation of the charge distribution on wires creates a propagation front, meaning that molecules generally impact neighbor molecules only (thus motivating the use of the IR mode). In addition, once molecules are well polarized, the charge distribution is generally kept constant: the first molecules of the wires do not change their polarization in the last three subplots. Similarly, the molecules do not propagate information when the propagation front has not reached molecules yet: the last molecules of the wires are not polarized in the first three subplots.

5.1.1 The stability of the information: bistable and the evanescent propagation

This section deepens the information propagation and encoding in molecular FCN devices by analyzing the interaction among molecules from a mathematical perspective. This analysis is also published in [5]. The molecule is modeled as an *ideal molecule* to analyze the interaction with the highest generality. As reported in Section 3.1, the ideal molecule is composed by two aggregated charges Q_1 and Q_2 at a

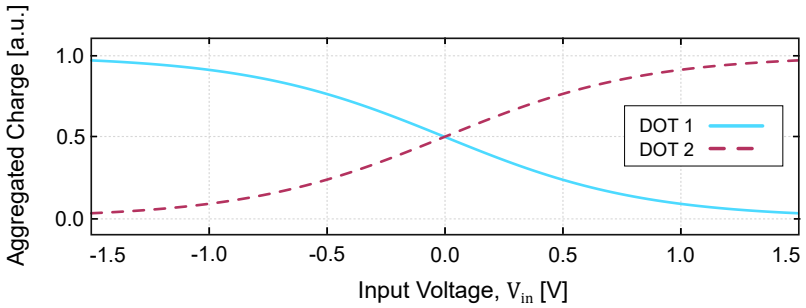

Fig. 5.4 VACT of the ideal molecules used to analyse the bistable properties of molecular FCN wire

distance w which can be linked to the input voltage according to Equation (3.6). The ideal molecule creates a dipole moment which can be written according to equation Equation (3.7) and the output voltage may be evaluated according to Equation (3.8).

This analysis focuses on studying the molecule polarization and the tendency of a molecule to react to the intermolecular interaction. The analysis may be intended for low input voltages, thus the linear dipole approximation can be applied by introducing the polarizability α as:

$$e(Q_2 - Q_1)\frac{w}{2} \approx \alpha\left(\frac{V_{in}}{w}\right) \quad \Longrightarrow \quad V_{out}(V_{in}) = -\frac{\alpha}{2\pi\varepsilon_0 w^2}\left(\frac{1}{d} - \frac{1}{\sqrt{d^2+w^2}}\right)V_{in} \tag{5.1}$$

Fig. 5.4 shows the charges Q_1 and Q_2 obtained with Equation (3.6) fixing: the polarizability to α=3000 a.u., the molecule width to w=0.7 nm, and the intermolecular distance to d=0.7 nm. *The ideal bistable propagation is defined as the propagation condition where the charge perfectly alternates on adjacent molecules*. In this condition, the input voltage oscillates between two values here named $\pm V_{sat}$. The input voltage of molecules may be written as:

$$V_{in,i} = -V_{in,i+1} = (-1)^{i+1}V_{sat} \tag{5.2}$$

In the simplest case of two molecules ($N = 2$), if the bistable propagation is ensured, it follows that:

$$V_{in,1} = V_{SAT} = -V_{in,2} = -V_{out,1} = -V_{sat} \tag{5.3}$$

Indeed, the input voltage of the second molecule must coincide with the output voltage of the first molecule $V_{out,1}$. In other words, when the first molecule is subjected to an input voltage equal to V_{sat}, the molecule must be reactive enough to supply V_{SAT} to the second molecule to satisfy the bistable condition. It is possible to define the so-called bistable coefficient to measure the capability of a molecule to generate bistable propagation [5]:

$$BF(d,w,\alpha) = \lim_{V_{in}\to 0}\left\{-\frac{V_{out}}{V_{in}}\right\}$$

When $BF > 1$, bistable propagation is possible. On the contrary, the propagation is *evanescent* if $BF < 1$. In the case of evanescent propagation, the information propagates for a limited number of molecules. For a two-molecule system:

$$BF0(d,w,\alpha) = \frac{\alpha}{2\pi\varepsilon_0 w^2}\left(\frac{1}{d} - \frac{1}{\sqrt{d^2+w^2}}\right) \tag{5.4}$$

The bistable propagation emerges favored by small intermolecular distances (d), small molecules (low w), or high polarizability molecules by analyzing the bistable factor. Among the three parameters, the width and the polarizability are molecular parameters, whereas the intermolecular distance can be engineered by correctly positioning the molecules on the substrate, considering eventual lattice limitations [60]. The bistable factor parameter also gives t chemists information for synthesizing future monostable molecules.

If more than two molecules are involved in the propagation mechanism, the input voltage of each molecule depends on the output voltage of all the circuit molecules. The condition $V_{in,i} = V_{sat}$ does not require the output voltage of adjacent molecules to be $V_{out,i\pm1} = V_{sat}$, since the input voltage of i-th molecule is obtained as the sum of output voltages. It comes out that the bistable condition can be reached more easily.

In a wire composed of N molecules, each molecule input voltage should satisfy the relation $|V_{in}| = V_{sat}$. The absolute value is used in this relationship. Indeed, it is necessary to distinguish between odd to even molecules because two types of interaction are possible between molecules. By taking as a reference the interaction between two generic i-th and j-th molecules:

- Molecule j, such that $|j-i|$ is even, has the same input voltage ($V_{in,i} = V_{in,j}$) and polarization of molecule j, thus produces an output voltage which has opposite sign with respect to $V_{in,i}$, decreasing $|V_{in,i}|$ and discouraging the bistability.

- Molecule j, such that $|j-i|$ is odd, has the opposite input voltage ($V_{in,i} = -V_{in,j}$) and polarization of molecule j, thus produces an output voltage which has the same sign with respect to $V_{in,i}$, increasing $|V_{in,i}|$ and favouring the bistability.

With N molecules, the bistable coefficient should consider the voltage generated by odd and even molecules.

$$BFN = \sum_{i=1}^{N} (-1)^{\left(\frac{d_j}{d}+1\right)} BF_0(d_i, w, \alpha)$$

Where N indicates the number of molecules involved in the calculation, e.g. BF10 refers to $N = 10$. Finally, it is necessary to distinguish two values of the bistable factor:

- When the molecule used to evaluate the input voltage is positioned in the center of a wire, the bistable factor is named "centered" (BFNc), and the input voltage of the molecule under test receives an equal number of odd and even molecules from the two sides.

- When the molecule used to evaluate the input voltage is positioned at the end of a wire, the bistable factor is named "ending" (BFNe), and the input voltage of the molecule under test is influenced only from one side of the wire, thus will show a lower input voltage.

Fig. 5.5(a) shows both $BFNc$ and $BFNe$ as a function of the number of molecules in the wire. This analysis confirms the expected relation $BFNc > BFNe$, thus demonstrating that bistability is favored in the center of wires. In addition, $BFNe < 1$, discouraging information encoding at the end of wires and producing the so-called border effects [5, 74]. At the same time, the curve also shows that the bistability effects are guaranteed after a certain number of molecules. Indeed, the BFN factors saturate after a certain number of molecules, which implies that increasing the

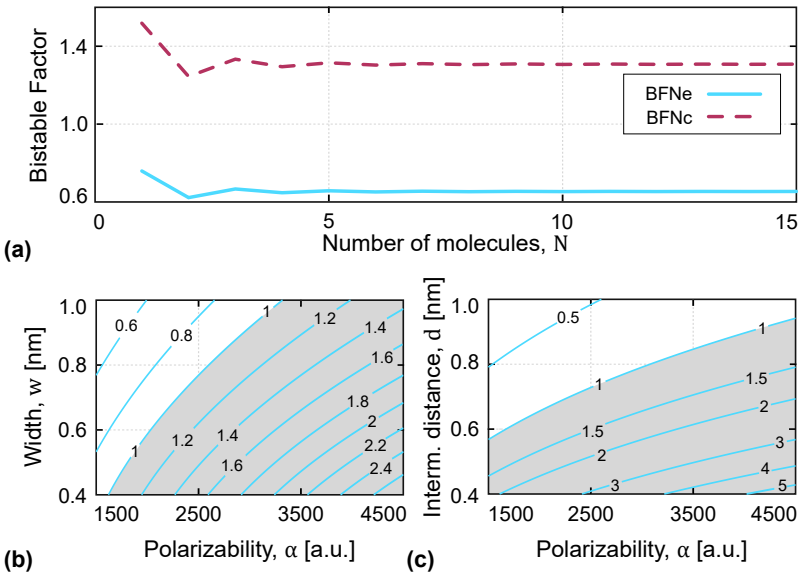

Fig. 5.5 Analysis of the bistable factor in molecular FCN wires: (a) Bistable factors (ending and centered) in molecular wires as a function of the wire length. (b) Molecular Safe-Operating Area. (c) Technological Safe-Operating Area.

number of molecules in the wire does not improve bistability after a certain quantity, yet the bistability is not guaranteed for a low number of molecules.

An interesting point regards the oscillating behavior of the bistable factor for a low number of molecules, which is a direct consequence of even and odd molecules. Odd molecules favor the bistability, thus increasing the bistable factor, whereas even molecules discourage it. The oscillation is dumped after a few molecules, reminding us that the electrostatic interaction among molecules vanishes after a few nanometers. The following empirical relation holds:

$$BF2 \leq \lim_{N \to \infty} BFN \leq BF1$$

Finally, the bistable factor can be studied by varying its main parameters. In particular, it is possible to define the so-called *(Molecular Safe-Operating Area (MSOA)* as the analysis of the BF coefficient for molecular parameters: width (w) and polarizability (α). At the same time, it is possible to define the *Technological Safe-Operating Area (TSOA)* as the analysis performed concerning intermolecular distance (d) and the polarizability (α). The two safe operating areas are reported in Fig. 5.5(b) shows the MSOA of the molecule under test. The reported lines show the BF10c isolines. In particular, the region $BF10c > 1$ indicates the possible combinations

Table 5.1 Bistable factor analyzed cases

Case label	α **[a.u.]**	w **[nm]**	d **[nm]**	**BF0**	**BF10c**	**BF10e**
A	3000	0.70	0.70	0.76	1.31	0.65
B	3000	0.70	0.40	2.29	3.73	1.86
C	2000	0.70	0.70	0.51	0.87	0.43
D	3000	0.90	0.70	0.57	0.96	0.48
E	3000	0.70	0.90	0.42	0.74	0.37

permitting the bistable propagation of the information. The intermolecular distance is fixed to d=0.7 nm.

Fig. 5.5(c) shows the TSOA of the molecule under test. The reported lines show the BF10c isolines. The intermolecular distance (d) is not fixed but is considered a variable parameter. The TSOA gives information on the required intermolecular distance a molecule should have to ensure propagation. The width of the molecule is fixed at 0.7 nm. Notice that the polarizability of the molecule is generally considered a fixed parameter for the molecule, even though molecules with variable polarizability are demonstrated to be very interesting in achieving particular elaboration. For instance, molecules with several polarizabilities have been used in [87] to accomplish neural computation.

At this point, several cases of molecule polarizabilities, width, and intermolecular distance are considered to demonstrate the validity of the bistable factor theory. Table 5.1 reports the essential parameters of the considered molecules and the evaluated bistable factors. A molecular FCN wire composed of 20 molecules is analyzed with all the combinations reported in Table 5.1. The first molecule of the wire is used as a driver to propagate the logic information.

Fig. 5.7(a) shows the propagation of the information obtained by the SCERPA algorithm concerning CASE A. The propagation is bistable for most of the molecules, yet there is some voltage attenuation on the last molecules of the wire. This behavior matches the values obtained for the bistable factors. Indeed, $BF10c > 1$, meaning that molecules in the center of the wire receive enough contributions to permit bistable propagation of the information. On the contrary, $BF10e < 1$, which means molecules at the end of the wire are not in the condition to guarantee bistable propagation. Fig. 5.7(b) shows the derivative of the molecule dipole moment concerning the input voltage, which motivates the use of the linear approximation concerning the

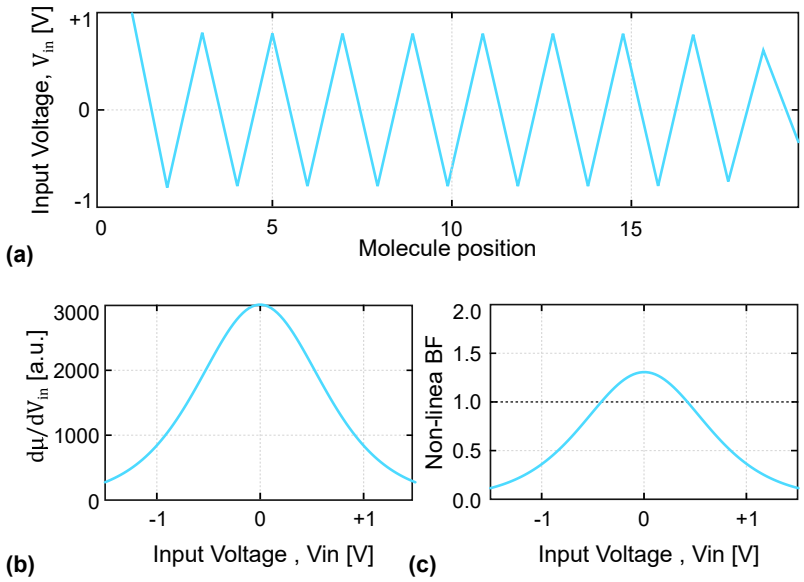

Fig. 5.6 Analysis of the bistable propagation: (a) Input voltage of molecules obtained by SCERPA for CASE A. (b) Derivative of the dipole moment with respect to the input voltage of the ideal molecules used for the analysis of CASE A. (c) Non-linear bistable factor related to CASE A.

study of the bistability. Indeed, the polarizability of the molecule represents the maximum dipole moment variation concerning the molecule input voltage, thus the most critical condition for the molecular interaction. Therefore, it is worth analyzing the bistable factor, intended as $\frac{dV_{out}}{V_{in}}$ variation without exploiting the linear approximation. Fig. 5.7(c) shows the obtained curve. It is interesting to notice again that the central point ($V_{out} \approx 0\,\mathrm{V}$) represents the most critical condition for the interaction, showing the maximum variation. In addition, it is worth noticing that the curve intersects with the unitary line for a voltage $|V_{in}| \approx 0.78\,\mathrm{V}$. This value coincides with the saturation voltage, then, the input voltage of molecules in bistable propagation, reported in Fig. 5.7(a). The obtained point can be justified by noting that for $BF = 1$ the propagation is neither bistable nor evanescent. Indeed, the molecules are not sufficiently reactive to increase the input voltage, yet they are sufficiently reactive to maintain their status. Therefore, the input voltage is kept fixed to the saturation voltage (V_{SAT}).

Fig. 5.7 shows the propagation of the information for cases B,C,D, and E. In particular, by decreasing the intermolecular distance from 0.7 nm to 0.4 nm(CASE B), both the ending and center bistable factors are increased and become larger than 1. In such conditions, the propagation is bistable both in the center of the wire and at

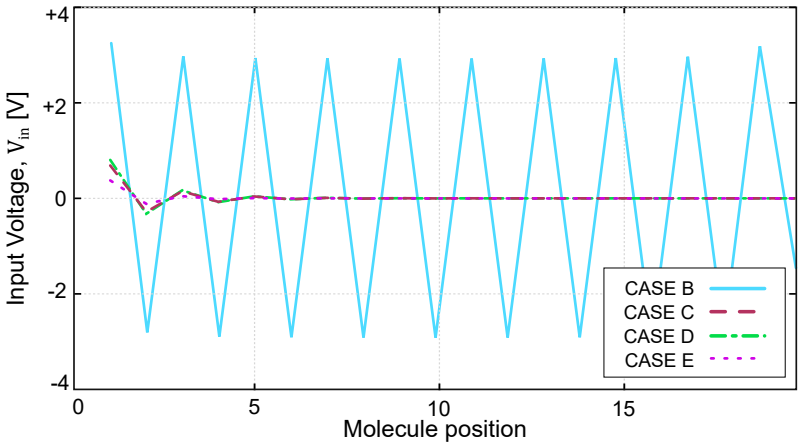

Fig. 5.7 Input voltage of molecules obtained by SCERPA for CASE B, C, D, and E.

Table 5.2 Bistable factor propagation scheme

	BFNc<1	**BFNc>1**
BFNe<1	No propagation	Propagation with border effect
BFNe>1	No propagation	Propagation

the end. Concerning cases C, D, and E, the information propagation, as expected, is evanescent since the bistable factors are always lower than one. In particular, it is interesting to notice the cross implication between the input voltage and the bistable factor, indeed:

$$|V_D| > |V_C| > |V_E| \Longleftrightarrow BF_D > BF_C > BF_E$$

The bistable factors are, in general, a good metric for quantifying the quality of the information propagation.

To sum up, Table 5.2 reports a summary of the obtained methodological results. The bistability of the wire can also be analyzed from an energy point of view using the model reported in Section 3.5. In particular, in the case of a bistable propagation (i.e., for $BF > 1$), one can expect the charge configuration to be stable in two possible configurations propagating zero and one at the saturation voltages. From an energy perspective, this configuration should present two minima. On the contrary, when the $BF < 1$, the propagation is supposed to be evanescent. Thus, the two configurations propagating the information are supposed to be energetically unstable, whereas an energy minimum is expected for a non-propagating configuration.

Following the procedure published in [31], the diallyl-butane data are used to analyse the bistability problem from an energy perspective:

- The width (w) of the molecule is set to 0.634 nm
- The molecular polarizability (α) is set to 2226.84 a.u..

In particular, the value of the polarizability is lower than the one mentioned in Section 3.5 to take into account the non-uniform field generated by molecules, which reduces the effectiveness of the field in polarizing molecules, thus reducing the capability of a molecule to be polarized as a response to an external electric field (i.e., the polarizability). Fig. 5.8(a) shows the $BF10c$ evaluated for the diallyl-butane wire as a function of the intermolecular distance (d). Therefore, two particular intermolecular distances, 0.65 nm and 0.75 nm, are chosen for the next analysis to cover both the evanescent and bistable cases. For the two configurations, the $BF10c$ equals 1.238 and 0.901, respectively. Therefore, the small intermolecular distance should propagate the information, whereas the other should provide evanescent propagation. The expectations are confirmed by the SCERPA tool, see Fig. 5.8(b), where the wire with the two intermolecular distances is analyzed.

Therefore, a wire composed of 21 diallyl-butane molecules is built and analyzed with the energy model to study the problem from an energy perspective. Two energy minima are expected for the small intermolecular distance since it should guarantee bistable propagation. The input voltage of the first molecule is fixed to emulate the presence of the driver molecule, whereas the input voltage of other molecules is alternated according to the following expression:

$$\boldsymbol{V}_{in,i} = \beta 2(-1)^i \quad [\mathrm{V}] \tag{5.5}$$

Where β is a linear coordinate denoting the information propagated by the wire: the wire propagates information for $\beta = \pm 1$, since the input voltage on the wire alternates on adjacent molecules, whereas it is completely unpolarized for $\beta = 0$. Therefore, the energy of the wire is studied by varying the linear coordinate (β). Fig. 5.8(c) shows the energy profile obtained for the 0.65 nm intermolecular distance. As expected, two energy minima are present in the energy trend, confirming the bistability of the molecular wire. A barrier separates the two energy minima. Notice that the minimum associated with $\beta = 1$ presents lower energy regarding the $\beta = -1$

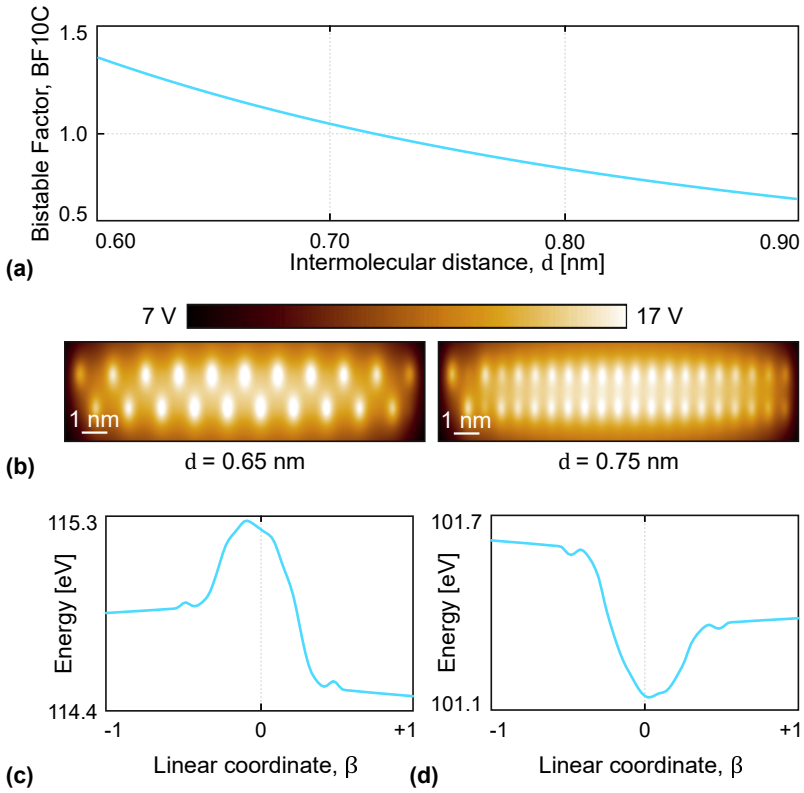

Fig. 5.8 Energy analysis of the information propagation: (a) BF10C factor evaluated as a function of the FCN wire intermolecular distance. (b) SCERPA simulation of two wires composed of 21 diallyl-butane molecules with 0.65 nm and 0.75 nm intermolecular distances (c) The energy of a wire as a function of the encoded information, β linear coordinate, for the 0.65 nm intermolecular distance. (d) The energy of a wire as a function of the encoded information, β linear coordinate, for the 0.75 nm intermolecular distance.

condition, which is favored by the $\beta = 1$ configuration. Indeed, the $\beta = 1$ condition propagates the correct information and provides consistency between the information encoded by the driver and the information propagated by the wire. The two separated minima also suggest a possible memory effect. Indeed, the $\beta = -1$ is an energy minimum, and, even though an energy barrier is present between the two states, the $\beta = -1$ state could be stable even though not a global minimum. Finally, Fig. 5.8(d) shows the energy trend for 0.75 nm. In this case, the propagation is evanescent, and there is only one energy minimum in $\beta \approx= 0$, which means the molecular wire is not stable when propagating information. The wire is stable with no encoded information, as expected for an evanescent propagation.

Concerning the bistable condition, the barrier between the two states may be reduced by diminishing the number of molecules involved in the molecular wire. Fig. 5.9(a) shows the energy trend for wires composed of 14, 10 and 4 molecules. In particular, when the length of the wire is reduced to 4 molecules, no barrier is present, suggesting there is no bistability of the molecular wire. On the contrary, for long wires, the analysis suggests possible memory effects may appear.

Molecular FCN wires with 3, 4, and 5 molecules have been analyzed in [31] by using the SCERPA tool to study the memory effect better. The linear coordinate β is evaluated by varying the driver input voltage in a cyclic manner between -1 V and +1 V. Fig. 5.9(b) shows the obtained linear coordinate. It is interesting to notice the appeared hysteresis. In a bistable condition ($BF > 1$), the wire may present hysteresis, thus memory effect. If a memory effect is present, a clocking system must delete the information if one wants to propagate new information, further motivating the need for clocked molecular devices. The obtained result also justifies the aberration shown in Fig. 5.2(b), since long non-clocked wires show bistable effects that may amplify possible noise on the wire, propagating erroneous logic information which can remain stable (i.e., in a memory condition). Notice that no hysteresis is shown for the wire composed of four molecules, consistently with the energy result presented in Fig. 5.9, which did not show any energy barrier with four molecules.

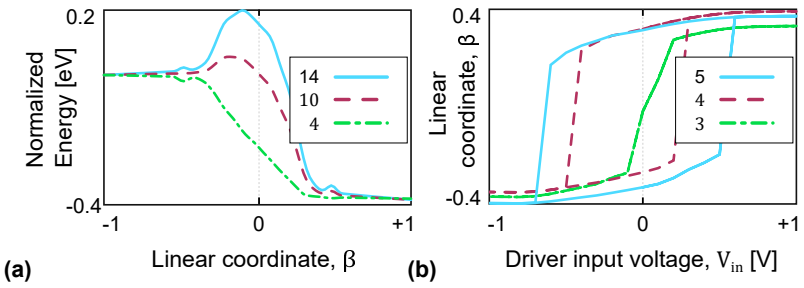

Fig. 5.9 Analysis of the memory effect: (a) Normalized energy of wires composed by 4, 10 and 14 molecules when varying the propagated logic information between '0' and '1'. (b) Hysteresis in the propagated logic information when varying the driver polarization in wires composed by 3, 4, and 5 molecules.

5.1.2 Device crosstalk

The crosstalk is the last problem analyzed in this thesis regarding the propagation of the information in molecular wires. Indeed, as already mentioned in [35], devices may influence each other when positioned at a close distance. In particular, [13] also demonstrated that the crosstalk depends on the molecular species. Therefore, it is necessary to study the crosstalk by changing the molecular specie of the molecule composing the FCN wire. The crosstalk is generally caused by the fact that molecules generate radial fields which may sum up in the input voltage of molecules in the vicinity of a specific device. In particular, following the procedure and the results published in [13], a wire composed of 20 molecules is analyzed, and the field generated by it is evaluated on a perpendicular line. Fig. 5.10(a) shows the system used for the analysis of the crosstalk. The distance from the wire (D) is the distance of an eventual wire probing the crosstalk effect.

The wire molecules are chosen as ideal molecules, and their voltage is fixed alternately according to Equation (5.5), with $\beta = 1$, to emulate the propagation of the information. Neutral, oxidized, and zwitterionic molecules are used to understand the impact of the molecular species on the device crosstalk.

According to Coulomb's law, the field generated by molecules at a far distance is null when the total charge of the molecule is globally neutral. Indeed, as it can be seen from Fig. 5.10(b), the neutral molecule is the one generating the lowest crosstalk effect since the field generated by neutral molecules is reduced. On the contrary, the oxidized molecules demonstrate a higher field, thus suggesting the worst condition for possible crosstalk effects. The situation is intermediate between

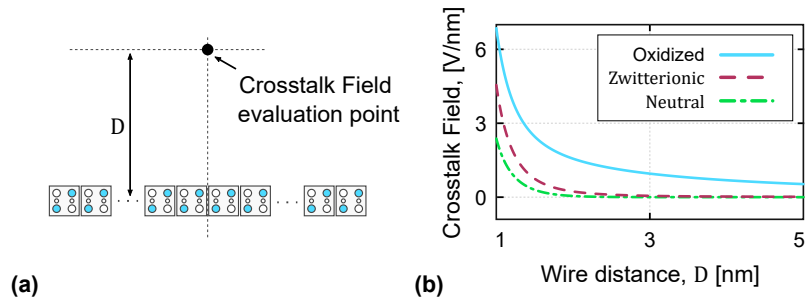

Fig. 5.10 Crosstalk effect in molecular FCN wires: (a) System used to evaluate the crosstalk. (b) Crosstalk field evaluated for the oxidized, neutral and zwitterionic ideal molecules.

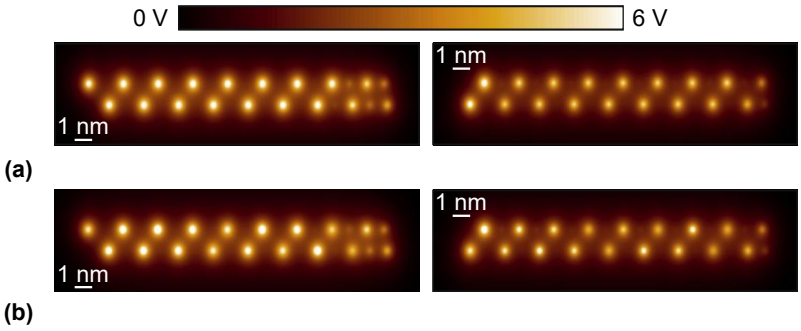

Fig. 5.11 Process variations in molecular FCN wires: (a) SCERPA simulation of a molecular FCN wire composed of 19 bis-ferrocene molecules with 1.00 nm intermolecular distance with molecules rotated by 10 °on the principal axis. (b) SCERPA simulation of a molecular FCN wire composed of 19 bis-ferrocene molecules with 1.00 nm intermolecular distance with molecules rotated by 10 ° on the principal axis; the molecules are also shifted on the x-axis to emulate substrate roughness.

the neutral and the oxidized nature regarding the zwitterionic molecules, which was somehow expected. Indeed, the zwitterionic molecule is neutral overall, yet the active dots are locally oxidized (i.e., $Q_1 + Q_2 = 1$), impacting the input voltage of other molecules in the vicinity, even though the presence of the counterion mitigates the effect.

5.1.3 Process variations

So far, all the cases for the information propagation were analysed on ideal wires, where the molecules aligned perfectly. In a more general case, precise manipulation of molecules is challenging, and molecule orientation is generally set by the deposition process and the molecule-substrate interface [60]. For this purpose, SCERPA permits considering molecule rotations and shifts, which may emulate the effects of

process variations and eventual post-deposition or environmental induced changes in the molecular layout. Details regarding the implementation of shifts and rotations are reported in Section 4.5.1.

Fig. 5.11(a) reports the SCERPA simulation of a molecular wire with all the molecules rotated on the axis orthogonal to the substrate by an angle Θ_x = 10 °. Secondly, Fig. 5.11(a) reports the simulation of a molecular wire where molecules have also been shifted on the x-axis. In particular, substrate roughness is obtained by shifting molecules according to a uniform distribution in the range [-0.5,0.5] nm. For the sake of repeatability, all the shifts are reported:

$$\begin{aligned} S_x = [&0.2411 - 0.2211 - 0.3026 - 0.2851 - 0.5098 - 0.1864 \\ &- 0.18280.30820.27170.0309 - 0.39420.2985 - 0.1475 \\ &- 0.43880.50240.4015 - 0.1197 - 0.0040] \text{ Å} \end{aligned}$$

In both cases, the algorithm convergence is guaranteed, and the two wires propagate the information correctly, demonstrating the robustness of the molecular FCN wire for such variations and the possibility of exploiting the SCERPA algorithm for studying accurate molecular layouts. Furthermore, other studies concerning process variations and substrate non-idealities have been reported in [60, 92].

5.2 The clocked molecular circuit connections

So far, the molecular wires have been intensely discussed to understand the propagation of the information, addressing specific problems related to the bistability of wires and crosstalk among devices. It is clear from the previous sections that a clocking scheme is necessary to guarantee the correct information propagation and, as demonstrated in the following sections, to accomplish logic operations. In the following sections, more complex devices used for the information propagation will be discussed: the clocked wires, the multi-line structures, and the L- and T-connections will permit the connection among molecular FCN devices required to accomplish complex digital operations.

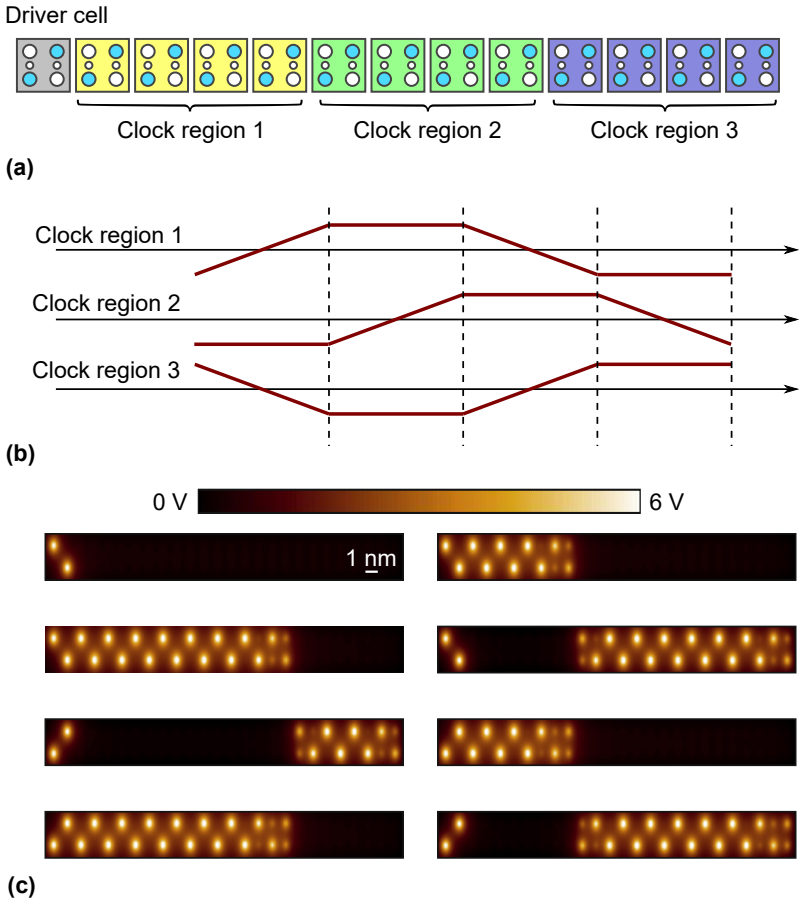

Fig. 5.12 Clocked molecular FCN wire: (a) Schematic of the molecular FCN wire composed by 24 molecules subdivided into three clock regions. (b) Clocking signals applied to the three clock regions of the clocked devices. (c) Propagation both of '0' and '1' logic values in a clocked molecular FCN wire.

5.2.1 The clocked propagation in wires and multi-line devices

As a first case studio of a clocked device, it is here reported the analysis of a molecular wire composed of 24 bis-ferrocene molecules and subdivided into three clock regions, see Fig. 5.12(a). The analysis is also reported in [35]. The first two molecules (driver cell) are used to force either the '0' or the '1' logic states. Fig. 5.12(b) shows the clock signals applied twice to the three clock regions to evaluate a complete propagation of the information in a pipeline mechanism. The signals are modeled in SCERPA as increasing staircase trapezoidal functions. Notice that the reported signals should be considered at the steady-state. Indeed, in the next simulations, all the clock regions start in the *Reset* phase, thus with a negative clock field inhibiting

the information propagation. Fig. 5.12(c) shows eight timesteps of the SCERPA simulation. In particular, all the steps related to the end of a clock phase (i.e., the lines reported in Fig. 5.12(b)) are reported in the picture to describe the propagation of the information well. Concerning each timestep:

T1 The driver is activated to propagate logic '0'. All the clock regions are in the *Reset* phase, therefore inhibiting all the molecules. The information is not propagated in the wire.

T2 The first clock region is in the *Switch* phase; therefore, the information is propagated in the first clock region. The second and third clock regions are in the *Reset* state. Notice that some border effect is present at the end of the first clock region, locally replicating the properties of a non-clocked molecular wire. The clock regions in the *Reset* phase do not participate in the information propagation, thus not favoring the bistability of the information encoding.

T3 The first clock region is in the *Hold* phase, whereas the second one is in the *Switch* phase. The information is propagated in the second clock region. Notice that the border effect is wholly canceled in the first clock region. Instead, the information is now present in the second clock region.

T4 The first clock region is in the *Release* phase, the second clock region is kept in the *Hold* phase, whereas the third clock region is in the *Switch* phase. The information is propagated in the third clock region. Notice that the border effect is again moved by one clock region, thus to the third clock region. In this timestep, the bistable condition permits storing the information in the second clock region while copying it into the third one. Indeed, the first clock region is in the *Release* phase, and it reaches the *Reset* phase when the timestep is evaluated. Thus the information is not maintained. Notice a new border effect at the beginning of the second clock region.

T5 The first clock region is in the *Reset* phase, the second one is in the *Release* phase, whereas the third one is now in the *Hold* state. The information is correctly propagated to the wire output and maintained thanks to the bistability created by a single clock region in the *Hold* phase. The driver logic can be switched to propagate logic '1' in the next clock cycle.

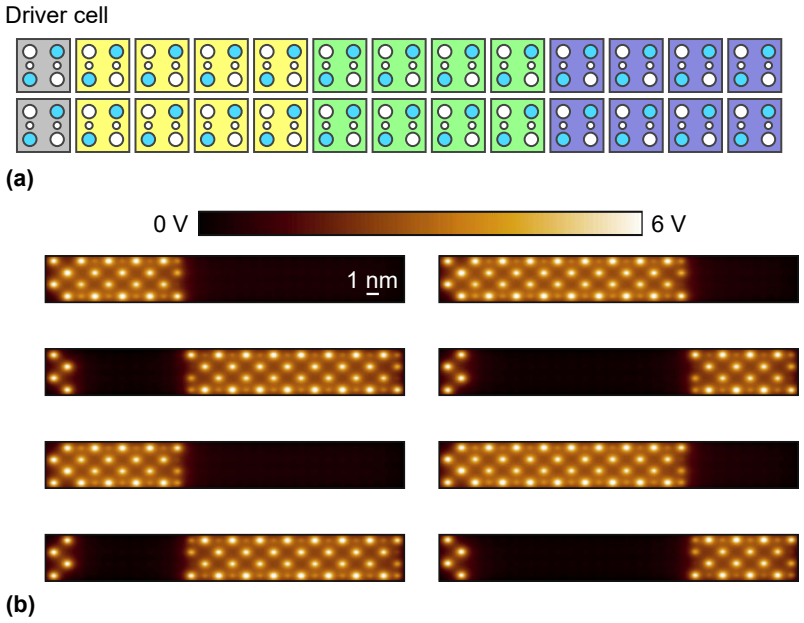

Fig. 5.13 Clocked 2-line molecular FCN wire: (a) Schematic of the clocked 2-line molecular FCN wire composed by two wires of 24 molecules subdivided into three clock regions. (b) Propagation both of '0' and '1' logic values in a clocked 2-line molecular FCN wire.

The following steps permit propagating the logic '1' in the same way. Notice that, in this case, the information propagation is perfectly guided, and no aberration is present for '0' or '1' logic values. If the single clock phase has a time duration T, the clocked wire introduces a $3T$ delay.

The reason why propagation is possible in molecular devices is related to bistability. Indeed, thanks to bistability, it is possible to maintain some information in a clock region, permitting the pipelining mechanism. For this purpose, the bistability of the information may be enhanced with the use of multi-line devices. Indeed, by juxtaposing two molecular wires, it is possible to create the so-called 2-line molecular FCN wire, also known as a molecular bus, which permits to enhance the bistability of the propagation and generally permits a better fault tolerance [93].

Fig. 5.13(a) shows the basic schematic of the 2-line molecular wire. Notice the larger structure of the device compared to the standard single-line molecular wire. Multi-line structures allow the realization of larger devices, eventually diminishing the required resolution for nanopatterning.

Fig. 5.13(b) shows the result of the SCERPA simulation demonstrating the propagation of the two logic values. The 2-line molecular wire correctly propagates both

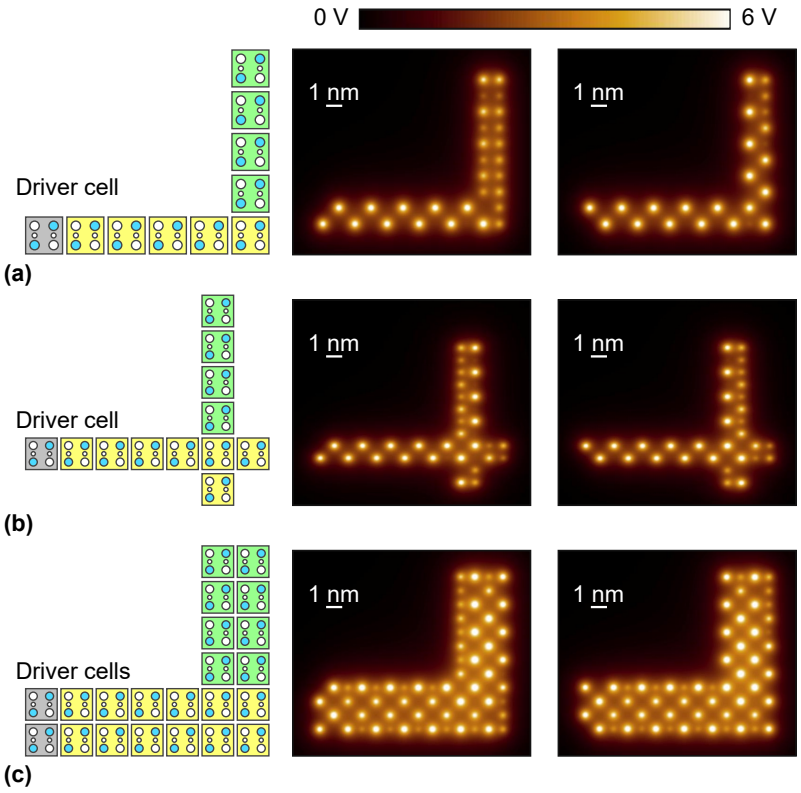

Fig. 5.14 SCERPA simulation of an L-connection: (a) Basic L-connection. (b) L-connection with stab correction. (c) 2-line L-connection.

the information. It is interesting to notice that the border effect is currently reduced thanks to the improvement of the intermolecular interaction, thus the bistability. A new effect, mentioned as *skin effect* and discussed in [35], appears in multi-line devices. Indeed, the two-wire crosstalk makes the molecules polarize on the "skin" of the 2-line device, even though its effect does not impinge on the propagation of the information. This effect demonstrates the advantages of using the SCERPA simulator, which allows for a great link between the circuit working principle and molecular physics.

5.2.2 The L-connection

Presented routing devices currently permit the propagation of the information horizontally. Nevertheless, the connection among devices requires realizing connections providing propagation capabilities in the vertical direction. For this purpose, the L-connection allows rotating the propagation direction by 90 degrees. The device

is simulated by the SCERPA tool to demonstrate the L-connection functionality following the same procedure employed for previous devices. Both ‘0’ and ‘1’ logic values are propagated to verify the correct behavior of the device.

Fig. 5.14(a) shows the schematic and propagation of the information of a standard L-connection realized with two orthogonal wires. While the device is supposed to work correctly in the general QCA paradigm, the molecular implementation fails in propagating the ‘0’ logic value, whereas it correctly propagates the ‘1’ logic value. The reason behind this result lies in the asymmetry of the device. Indeed, the functioning can be improved by introducing stabs intended to improve the symmetry of the device [92]. Also, the stab extends the length of the horizontal wire, thus diminishing the border effect at the rotation point and favoring the propagation of the information. Fig. 5.14(b) shows the schematic and propagation of the information of the L-connection realized with two orthogonal wires and two stubs extending the horizontal wire. In this case, the device correctly propagates the information, even though the vertical crosstalk makes the information encoding unclear, resembling the skin effect obtained for the multi-line molecular FCN wire. This effect is related to the electrostatic nature of the bis-ferrocene molecule, as demonstrated in [13], which is emulated in the SCERPA algorithm as a zwitterionic molecule. Indeed, even though the molecule is generally considered oxidized, the DOT4 of the bis-ferrocene molecule is diminished by a quantity of 1 a.u. to guarantee the molecule neutrality, thus imitating a zwitterionic nature.

Finally, Fig. 5.14(c) shows the schematic and propagation of the information of the 2-line L-connection. In this case, the bistability favors the information propagation, which is possible both for ‘0’ and ‘1’ logic values. No border effect is present in the molecules, thanks to the 2-line structure, yet some skin effects polarize molecules on the border of the device.

5.2.3 The T-connection

Secondly to the L-connection, the T-connection allows splitting the information into the two orthogonal directions to connect a specific signal to a few devices. This device is also simulated by the SCERPA tool following the same procedure as the previous devices, thus propagating both ‘0’ and ‘1’ logic values to demonstrate the T-connection functionality.

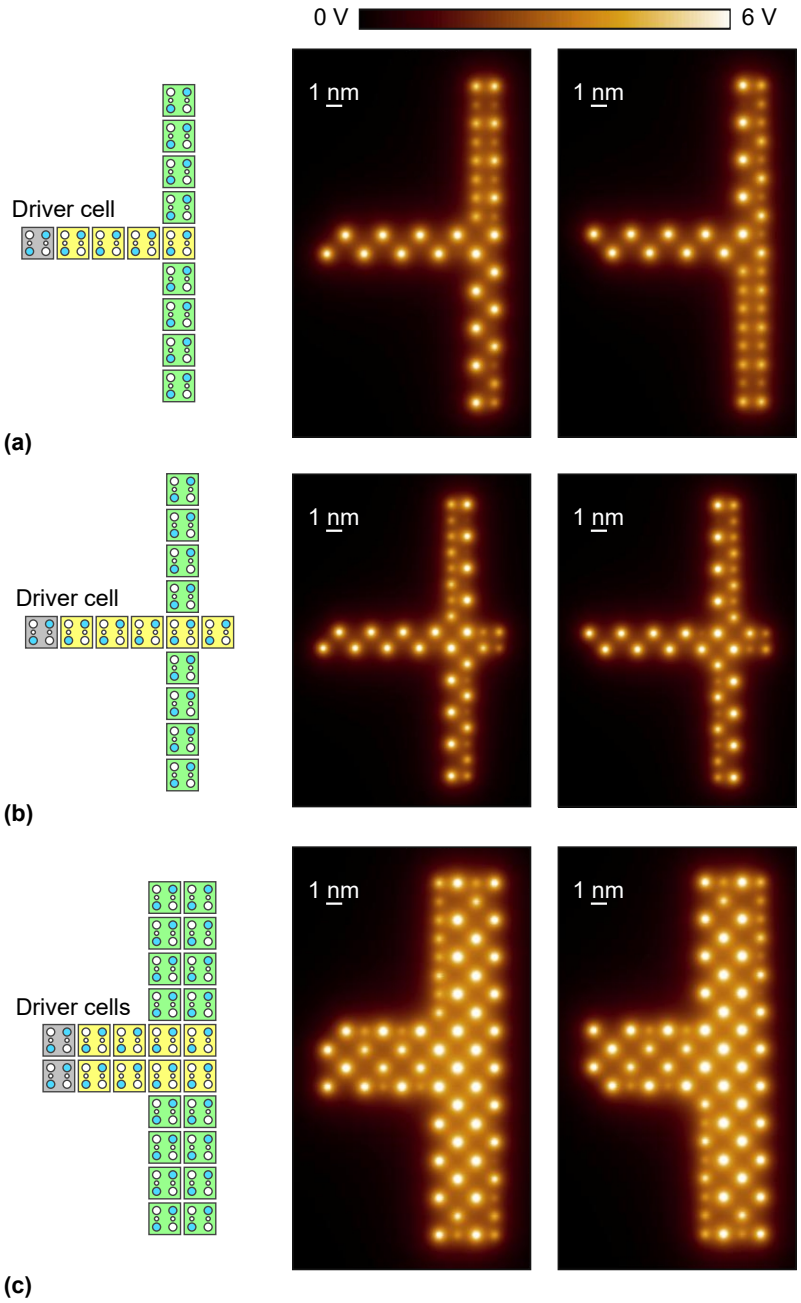

Fig. 5.15 SCERPA simulation of a T-connection: (a) Basic T-connection. (b) T-connection with stab correction. (c) 2-line T-connection.

Fig. 5.15(a) shows the schematic and propagation of the information of a standard T-connection. Again, the obtained results are not perfectly consistent with the QCA literature since the functioning is not straightforward, further motivating the necessity to use physics-aware simulators such as SCERPA. Similar to the L-connection, there is an asymmetry in the propagation of logic values '0' and '1', which propagates on one direction only. In particular, the bottom branch works correctly for the logic '1', whereas the '0' logic propagates well for the upper branch only. The other branch fails in propagating the correct information, which is again due to the asymmetry in the device. Again, the problem can be solved by using stabs. Fig. 5.15(b) shows the schematic and propagation of the information of the T-connection corrected with a stab extending the horizontal wire. In this case, the device correctly propagates the information. However, the vertical crosstalk caused by the electrostatic nature of the bis-ferrocene molecule ruins the encoding of the information in this case. Finally, Fig. 5.15(c) shows the schematic and propagation of the information of the 2-line T-connection. In this case, the bistability favors the information propagation in the T-connection. Therefore, the propagation is possible both for '0' and '1' logic values. Again, no border effect is present in the molecules, thanks to the 2-line structure, which is substituted with some skin effect.

5.3 The basic logic devices

So far, the thesis has discussed the devices and the associated characteristics related to information propagation in all directions. Designing and engineering basic digital logic gates is necessary to implement digital circuits. In particular, the inverter and the majority voter, which are the fundamental gates permitting the realization of digital architectures, will be deeply discussed in the following paragraphs. Notice that the molecular FCN technology bases the information encoding on molecules, minimizing the area occupation of digital architectures. In addition, the majority voter/inverter logic is also efficient regarding area occupation, further minimizing the area of molecular FCN devices and, generally, QCA paradigm-based technologies from a system perspective [9, 10].

Table 5.3 Inverter Truth table

A	Y
0	1
1	0

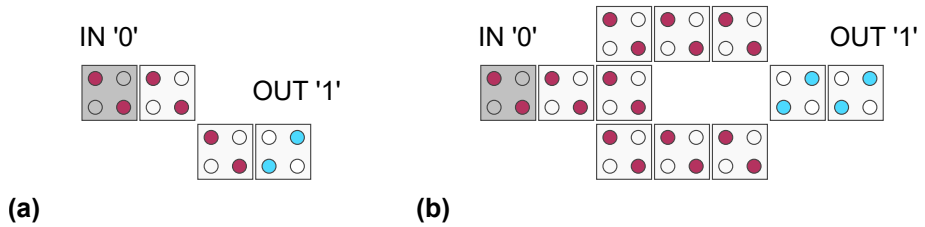

Fig. 5.16 Basics QCA inverters: (a) The single-branch QCA inverter. (b) The double-branch QCA inverter.

5.3.1 The inverter

The first device necessary to perform digital computation is the inverter, whose operation is evaluated as:

$$Y = \overline{A}$$

Where Y is the output, and A is the input. In particular, output Y provides the inversion of the input (A). Table 5.3 reports the truth table of the inverter.

Within the general QCA paradigm, two possible inverters have been proposed, denoted in [13] as *single-branch inverter*, shown in Fig. 5.16(a), and *double-branch inverter*, shown Fig. 5.16(b). The basic principle is the exploitation of the diagonal interaction to achieve inversion. The two inverters are generally used in the literature despite the technology used to realize the QCA. In [13], it has been demonstrated that the two circuits are not equivalent nor interchangeable in a digital layout. In particular, the functioning of the single-branch inverter strongly depends on the molecule electrostatics and may work only if implemented with neutral molecules or well-engineered zwitterions.

This section discusses the dependence of the inversion operation on the molecular structure. For this purpose, it is necessary to analyze the problem from an energy perspective by examining the fundamental interaction of the single-branch inverter

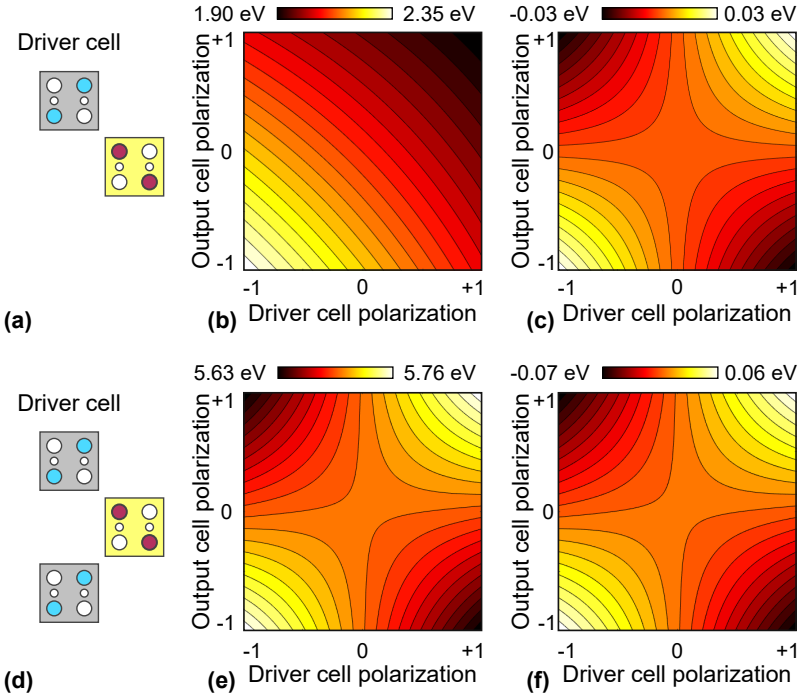

Fig. 5.17 Energy analysis of basic inverting interactions: (a) Single-branch inverter. (b) Energy map of an oxidised single-branch inverter. (c) Energy map of a neutral single-branch inverter. (d) Double-branch inverter. (e) Energy map of an oxidised double-branch inverter. (f) Energy map of a neutral double-branch inverter.

reported in Fig. 5.17(a). The two cells are built with ideal molecules, and the logic polarization, evaluated according to Equation (1.1), is varied both for the driver (P_D) and output (P_o) cells. Therefore, the intermolecular energy is evaluated using the model reported in 3.5.

Fig. 5.17(b) reports the energy of the two-cell system evaluated by considering oxidized molecules. By considering the driver cell polarization to be fixed to $P_D = -1$ or $P_D = +1$, it comes out that the energy minimum always lies on the line obtained for an output polarization equal to $P_o = +1$, which means the single-branch inverter always outputs $P_o = +1$, that is logic value '1'. This result suggests that the single-branch molecular inverter cannot work with oxidized molecules since the output is independent of the input.

Fig. 5.17(c) reports the energy of the two-cell system evaluated by considering neutral molecules. According to Gauss's theorem, the radial field generated by the neutral molecular cells is null. The energy minima lie on the points with opposite output polarizations ($P_o = -P_D$) when considering the driver cell polarization fixed to -1 or $+1$, denoting the inverting properties of the two-cell circuit. Indeed, for a driver cell polarization $P_D = -1$ (i.e., logic '0'), the energy minimum is obtained for $P_o = +1$ (i.e., logic '1'), and vice versa, that means the single-branch inverter perfectly matches the behaviour of an inverter, matching the truth table reported in Table 5.3. The single-branch inverter works when neutral molecules are used.

It is interesting to evaluate the Kink Energy (E_k) by evaluating the energy values in specific logic configurations. This quantity has been introduced in Equation (2.6) as the difference between the energy evaluated for a two-cell system with the same logic polarization, named E_{00} or E_{11}, and the one evaluated when encoding opposite polarization, E_{01} or E_{10}. Literature generally considers the kink energy independent of the driver cell polarization, which means it implicitly states that:

$$E_{00} - E_{01} = E_{11} - E_{10}$$

In this work, following the methodology adopted in [13], the kink energy is evaluated as driver dependent according to equations:

$$E_{k0} = E_{00} - E_{01} \qquad E_{k1} = E_{11} - E_{10}$$

Then, to highlight the difference with respect to the general QCA paradigm, it is possible to define the Kink Error (Δ) [13] as:

$$\Delta = E_{k0} - E_{k1}$$

Evaluating the two kink energies for the two molecular species shows that for oxidized molecules:

$$E_{00} = 2.376\,\text{eV} \qquad E_{01} = 2.087\,\text{eV} \qquad E_{11} = 1.929\,\text{eV} \qquad E_{10} = 2.087\,\text{eV}$$

That implies the kink energies to be:

$$E_{k0} = 0.289\,\text{eV} \qquad E_{k1} = -0.158\,\text{eV} \qquad \longrightarrow \qquad \Delta^{ox} = 0.447\,\text{eV}$$

The obtained Δ^{ox}, that is, the kink error evaluated for the oxidized species, highlights a driver-dependent characteristic of the intermolecular interaction. Indeed, the interaction energy between the two cells of the circuits varies by changing the logic encoded by the driver cell. In some sense, this value highlights a specific difference in the molecular FCN implementation concerning the general QCA paradigm, where the kink energy is always considered driver-independent. This difference motivates the use of simulators able to consider the effective electrostatic behavior of the molecule instead of using general QCA tools that take for granted the consistency of molecular FCN behavior with the general QCA paradigm.

Therefore, the Kink errors are also evaluated for the neutral species. In this case:

$$E_{00} = 0.033\,\text{eV} \qquad E_{01} = -0.033\,\text{eV} \qquad E_{11} = 0.033\,\text{eV} \qquad E_{10} = -0.033\,\text{eV}$$

In this case, the situation shows a higher symmetry. The kink energies are:

$$E_{k0} = 0.066\,\text{eV} \qquad E_{k1} = 0.066\,\text{eV} \qquad \longrightarrow \qquad \Delta^{n} = 0.000\,\text{eV}$$

With Δ^n the Kink Error of the neutral species. In this case, the inversion operation does not depend on the driver input logic, suggesting that the system-level behavior may be similar to the one expected from the general QCA paradigm. Notice that molecules are generally oxidized or zwitterionic at the current state-of-the-art. Thus, considering zwitterionic molecules, [13] demonstrates and deeply discusses the relation:

$$\Delta^n \leq \Delta^{zw} \leq \Delta^{ox} \tag{5.6}$$

In particular, the position of the zwitterionic behavior in the inequality depends on the position of the counterion. The larger the distance between active dots and counterion, the more oxidized and zwitterionic species are similar in electrostatic behavior. The opposite holds for molecules with a counterion close to active dots, which imitate the neutral molecule behavior. The single-branch inverter may work or may not work for zwitterionic molecules, depending on the molecule geometry. Further, this statement motivates using a physics-aware simulation to evaluate circuit behavior when single-branch inverters are present.

The analysis is now moved and repeated for the double-branch inverter, whose essential interaction is reported in Fig. 5.17(d). In this case, the higher symmetry of the two-branch inverter reflects in a higher symmetry of the energy map. For oxidized molecules, Fig. 5.17(e) shows a perfectly symmetric energy map similar to the one obtained for the neutral species in the single-branch inverter, thus suggesting a correct logic behavior. Notice that the energy obtained is strictly positive, which means that the system is highly repulsive.

Concerning the neutral species, reported in Fig. 5.17(f), the energy map is still symmetric, suggesting that the double-branch inverter may work both for neutral and oxidized species. Reminding Equation (5.6), the zwitterionic nature should also provide inversion using the double-branch structure.

Then, both single-branch and double-branch inverters are simulated to understand whether SCERPA can consider the electrostatic nature of the molecules in the inversion operation. In particular, the single-branch inverters are expected to work only for a neutral configuration.

Fig. 5.18(a) reports the result obtained with SCERPA for a single-branch inverter implemented with oxidised molecules. As predicted, the SCERPA simulation reports

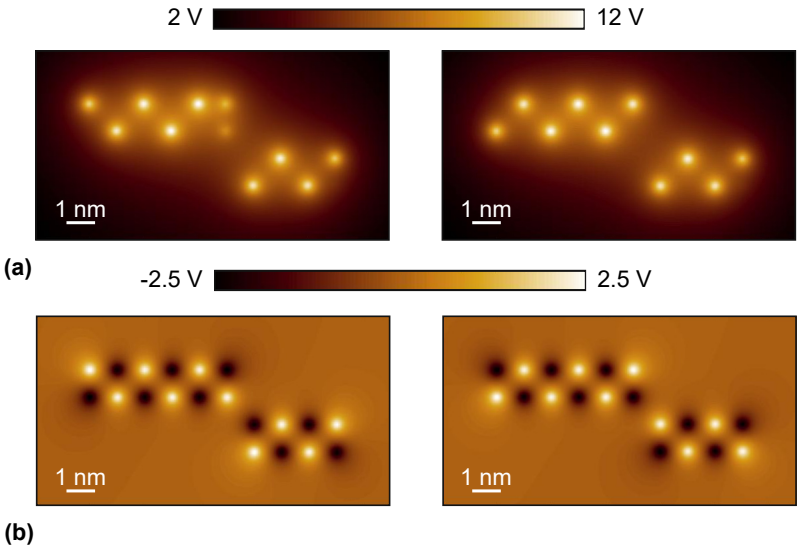

Fig. 5.18 SCERPA simulation of single-branch inverters: (a) Oxidised single-branch inverter. (b) Neutral single-branch inverter.

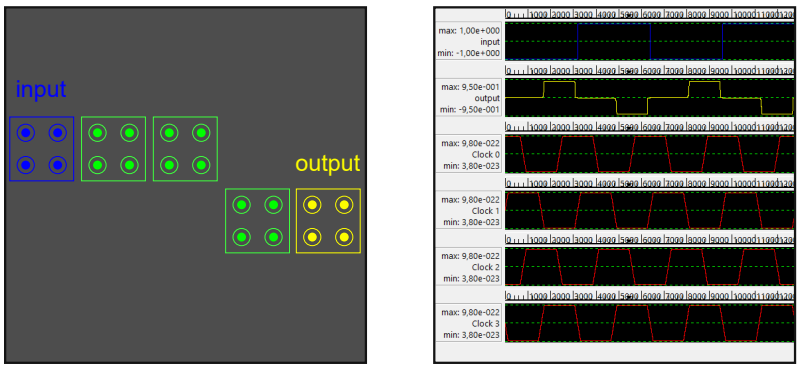

Fig. 5.19 QCADesigner simulation of a general QCA single-branch inverter.

that the single-branch inverter always outputs logic '1', confirming that the single-branch inverter cannot work with oxidized molecules. On the contrary, Fig. 5.18(b) shows the SCERPA simulation of the single-branch inverter implemented with neutral molecule. Also, in this case, SCERPA provides results consistent with theoretical discussions, confirming that the single-branch inverter works with neutral molecules.

Finally, for the sake of completeness, Fig. 5.19 reports the layout of a single-branch inverter, together with the obtained waveform, simulated in QCADesigner-E using the bistable approximation. This tool predicts the correct behavior of the single-branch inverter, perfectly inverting the input logic. QCADesigner-E is a

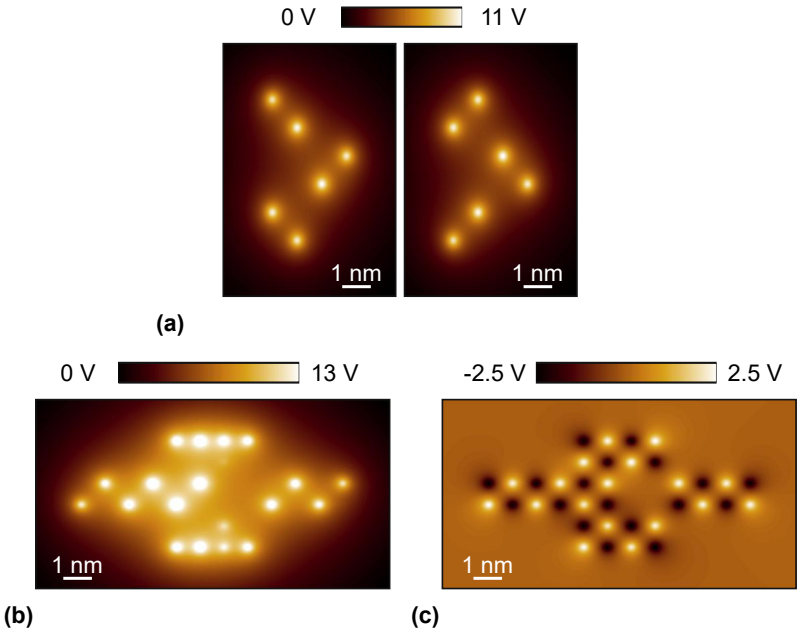

Fig. 5.20 SCERPA simulation of molecular FCN double-branch inverters: (a) Oxidised double-branch inverter basic interaction. (b) Oxidised double-branch inverter. (c) Neutral double-branch inverter.

general QCA tool that considers driver-independent kink energy, forecasting the result which may be obtained with neutral molecules.

Concerning the double-branch inverter, Fig. 5.20(a) shows the SCERPA simulation of the double-branch inversion basic interaction implemented with oxidized molecules, which works correctly, and consistently with theoretical discussion. Nevertheless, circuits based on oxidized molecules generally exhibit crosstalk problems, discussed in 5.1.2. Fig. 5.20(b) shows the double-branch inverter realized with oxidised molecules. In this simulation, the inverter does not work. The device is not working due to the crosstalk between the wires of the two branches. Indeed, it can be noticed that the molecules on the two branches polarize along with the outer directions orthogonal to the device due to the radial fields generated by oxidized molecules. This effect, described in [35], is similar to the skin effect shown for 2-lines devices.

The problem can be solved entirely with the use of neutral molecules. For example, Fig. 5.20(c) shows a double-branch inverter realized with neutral molecules, which perfectly propagate and invert the logic information from logic ‘1’ to logic ‘0’, further confirming the theoretical discussion.

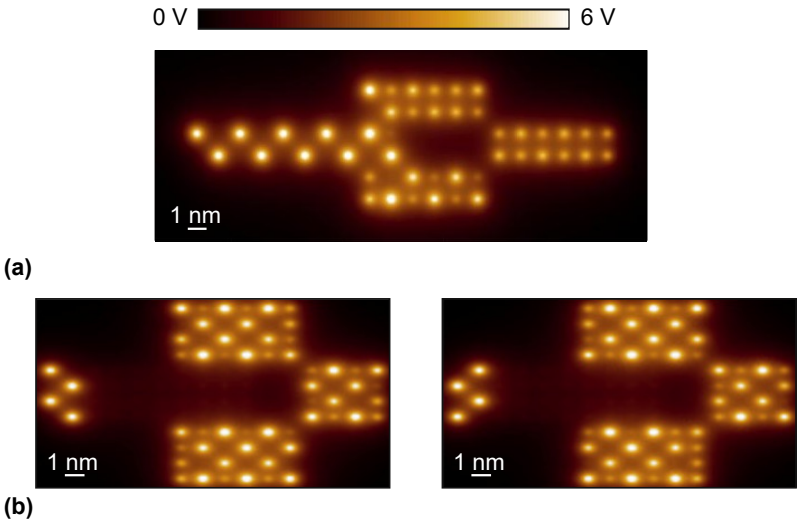

Fig. 5.21 SCERPA simulation of bis-ferrocene molecular FCN inverters: (a) Bis-ferrocene double-branch inverter. (b) 2-line bis-ferrocene double-branch inverter.

To sum up, the double branch inverter does not work with oxidized molecules, yet it can work with neutral molecules. [13] also discusses the double-branch inverter with zwitterionic molecules, which is here analyzed through the bis-ferrocene molecule.

Indeed, [35] clearly states that a counterion must be inserted to create devices beyond the standard wire to avoid crosstalk problems. For this purpose, the molecule is used in this work as a zwitterionic molecule by adding a quantity -1 a.u. to the total molecule aggregated charge Q_4 modeling the bis-ferrocene molecule in SCERPA, see Fig. 4.5(a). Notice that the presence of the counterion was already mentioned in the bis-ferrocene original work [20, 21]. Fig. 5.21(a) shows the simulation of a double-branch inverter realized with the bis-ferrocene molecule. The simulation predicts correct information propagation in the input branch of the device and one of the two branches. Nevertheless, the information is not propagated in the second branch, entrusting the inversion operation to a single diagonal and making the device not work properly. In this case, the problem is not related to crosstalk effects, strongly reduced by the zwitterionic nature of the molecule, nor to the input-dependent diagonal interaction, avoided by the double-branch configuration. In this case, the problem is related to poor stability, which makes the propagation of the information in both the inverter branches difficult. Multiline devices can be used to solve the problem. Finally, Fig. 5.21(b) shows a 2-line double-branch inverter. In this case, all the mentioned problems have been solved:

- The double-branch structure avoids driver-dependent behaviors.
- The zwitterionic molecules mitigate the crosstalk ruining the propagation on the two branches.
- The 2-line structure favors the bistable propagation and permits the correct propagation on the two branches.

Again, using the SCERPA tool appears necessary in linking molecular physics to the circuit-level behavior, permitting the physical-aware design of molecular FCN circuits.

To conclude, it is worth stressing an essential concept of the QCA literature. In general, the single QCA cell is defined as a cell composed of four quantum dots and two electrons. It should be stressed that the QCA is an ideal concept and that a real QCA composed of electrons only could not work since crosstalk would be exaggerated. This work highlights the need to have a neutral QCA cell. If the QCA cell is not perfectly neutral and ideal (i.e., in the case of a zwitterionic QCA), the effective electrostatic behavior must be considered in the design and the simulation of the logic device.

5.3.2 The majority voter

The second device necessary to accomplish digital computation is the majority voter, whose operation is evaluated as:

$$Y = \mathrm{MV}(A,B,C) = AB + BC + AC$$

Where Y is the output, and A, B, and C are the inputs. In particular, output Y provides the most recurrent logic value among inputs A, B, and C. This function should be, in principle, obtained with the combination of four logic gates (i.e., three AND gates and an OR gate). In molecular FCN, the logic is based on inverters and majority voters. Thus the majority voter can be created directly with a single gate. Table 5.4 reports the truth table of the majority voter. It is here reminded that, by fixing input $A = 0$, the majority voter operation generates the AND gate, whereas the OR gate is generated with $A = 1$ fixed input.

Table 5.4 Majority voter Truth table

A	B	C	Y
0	0	0	0
0	0	1	0
0	1	0	0
0	1	1	1
1	0	0	0
1	0	1	1
1	1	0	1
1	1	1	1

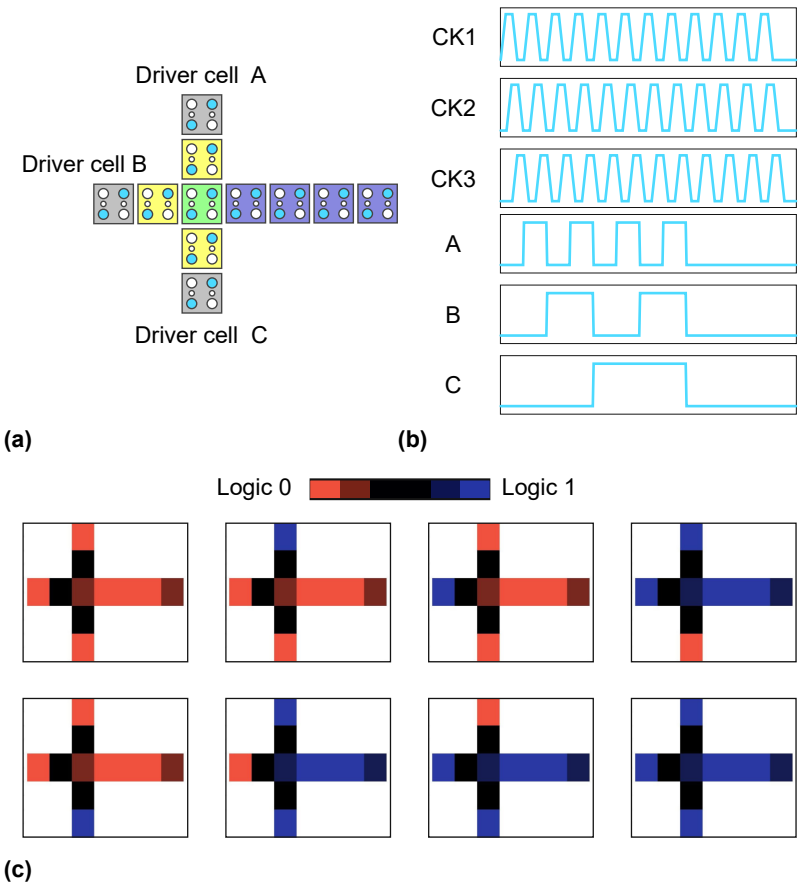

Fig. 5.22 SCERPA simulation of a molecular FCN majority voter: (a) Schematic of a majority voter. (b) Signals used for the simulation. (c) Logic plot obtained by SCERPA.

The majority voter is analyzed directly with the bis-ferrocene molecule in this section. Fig. 5.22(a) reports the layout of a majority voter implemented with three clock regions, highlighted in the figure with three different colors. The SCERPA tool simulates the circuit by stimulating it with the signals depicted in Fig. 5.22(b). All the input combinations are tested to verify the logic operation correctness formally.

Fig. 5.22(c) shows the result obtained with the SCERPA tool concerning the simulation. In particular, to facilitate the reader in understanding the working principle, the Logic Viewer is used. The color red represents logic '0', whereas the color blue represents '1'. The logic is obtained by evaluating, for each molecular cell, equation Equation (1.1). The figures report the time steps showing the logic on the majority voter gate when the second and third clock regions are in the HOLD state, whereas the first clock region is in the RESET state, inhibiting the molecules. The RESET state can be found in the figure with the black regions. Concerning the obtained simulation, it can be noticed that all the combinations are consistent with expectations since the output is always equal to the most recurrent input logic. In other terms, the color of the output branch is equal to the most recurrent color in the input driver cells.

It is worth noting that the central, thus the one permitting the realization of the majority logic, has been clocked independently in the device layout. The independent clock permits a good synchronization of the operation with input branches, which may reach the central cell in different time instants. Unbalanced majority voters are now analyzed to explain this layout requirement. Fig. 5.23(a) shows an unbalanced majority voter with no independent central cell. The information related to input A, i.e., *Driver cell A*, is close to the central cell, whereas B and C are far. Consequently, A is expected to reach the evaluation point before the inputs B and C. Fig. 5.23(b) shows the same layout with the evaluation cell clocked independently.

Being the A input faster than the other two, one may wonder what happens in a case where the logic encoded by the inputs is such that $A \neq B = C$. In these conditions, the logic forced by A may reach the evaluation point before the other two and propagate toward the inputs B and C, which are slower. Fig. 5.23(c) reports the SCERPA simulation obtained for the combination $A = 1$, $B = C = 0$. The result confirms the expectations. Indeed, input A propagates on the two other input branches, hampering the correct functioning of the device, which outputs the logic value '1' instead of '0'.

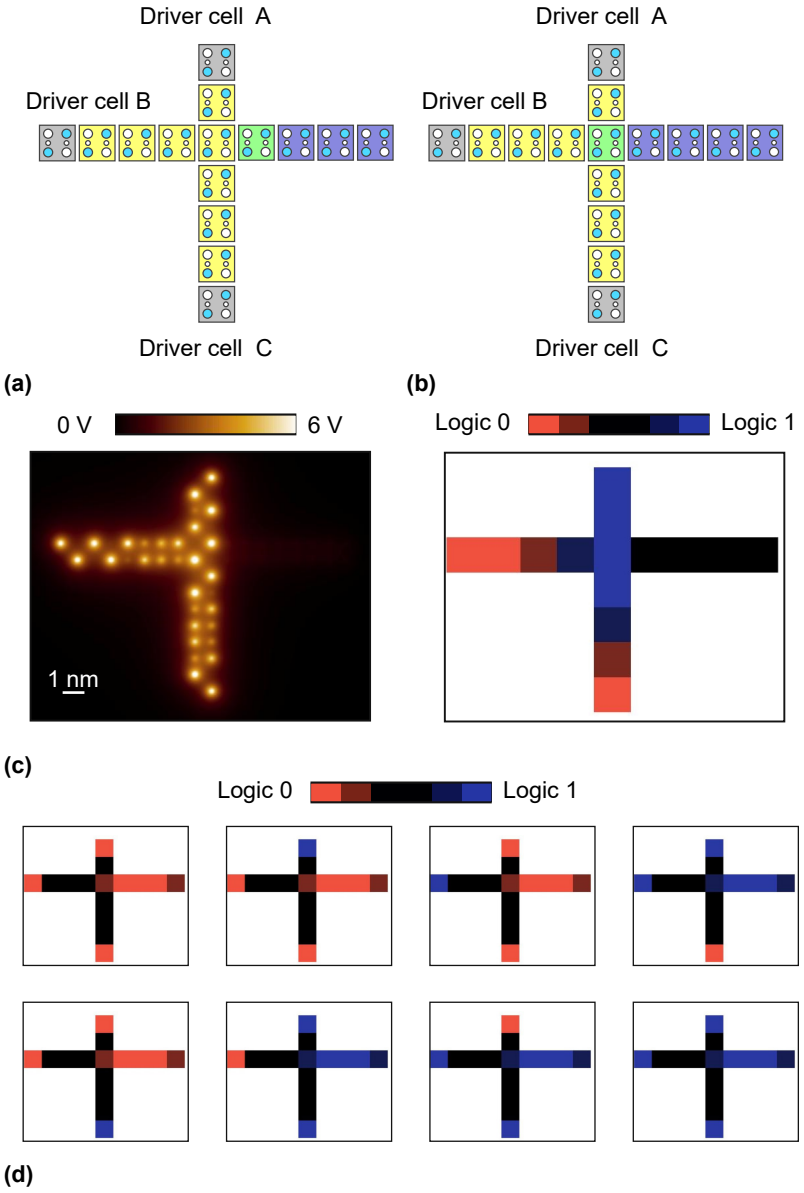

Fig. 5.23 SCERPA simulation of unbalanced molecular FCN majority voters: (a) Schematic of an unbalanced majority voter with no independent clock in the central region. (b) Schematic of an unbalanced majority voter with an independent clock in the central region. (c) SCERPA simulation of an unbalanced majority voter with no independent clock in the central region shows a logical error. (d) SCERPA simulation of an unbalanced majority voter with an independent clock in the central region.

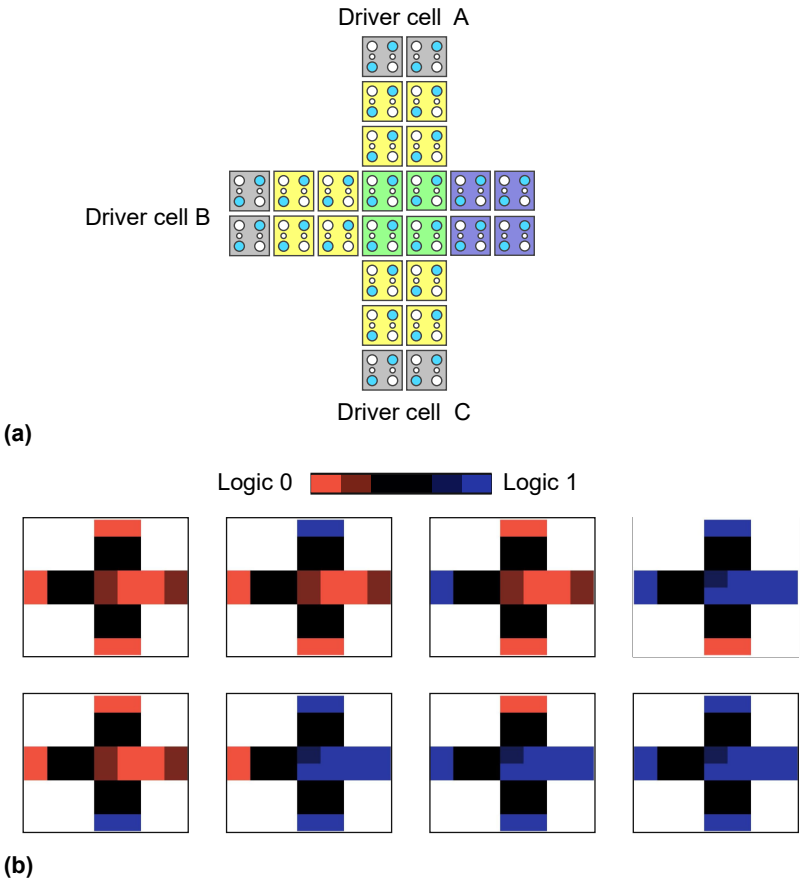

Fig. 5.24 SCERPA simulation of a 2-line molecular FCN majority vote: (a) Schematic of a 2-line molecular majority voter. (b) SCERPA simulation of a 2-line molecular majority voter.

Finally, Fig. 5.23(c) shows the simulation of the unbalanced majority voter with an independent clocking region in the central cell. In this case, the clock region synchronizes the input evaluation, permitting the correct behavior of the majority voter device.

The obtained result highlights the synchronizing function of the clocking mechanism and shows the use of SCERPA to discover and analyze layout constraints in digital circuits.

For the sake of completeness and consistency with other devices presented in this thesis, Fig. 5.24(a) also shows the layout of a 2-line majority voter. In this case, the multiline structure should improve the device bistability, favoring the logic correctness. Fig. 5.24(b) shows the results obtained by the SCERPA tool, that, again,

Table 5.5 Exclusive-OR Truth table

A	B	Y
0	0	0
0	1	1
1	0	1
1	1	0

shows results consistent with expectations since the output always encodes the most recurrent logic present at the input branches.

5.4 The design of digital circuits

The design of more complex digital devices can be performed by assembling majority voters and inverters with interconnection. Furthermore, the use of majority voter logic, in general, to accomplish logic operations permits the realization of area-optimized devices [10]. In the following sections, two molecular FCN devices are designed and discussed: a molecular FCN XOR, also reported in [35], and a 1-bit molecular FCN full-adder, also reported in [92].

5.4.1 The Exclusive OR

The Exclusive OR (XOR) is the digital gate realizing the operation associated with the truth table reported in Table 5.5. The XOR operation sets the output (Y) to '1' when the two device inputs (here named A and B) are different. The XOR device can be implemented in majority-voter logic as:

$$Y = A \oplus B = \mathrm{MV}\left(\mathrm{MV}\left(A, \overline{B}, 0\right), 1, \mathrm{MV}\left(\overline{A}, B, 0\right)\right)$$

Where $\mathrm{MV}()$ denotes the operation of a majority voter, whereas $\overline{A}$ and $\overline{B}$ are the two inverter inputs. The device is realized in the molecular FCN paradigm by exploiting 2-line majority voters, 2-line inverters, and 2-line interconnection to improve the device bistable properties.

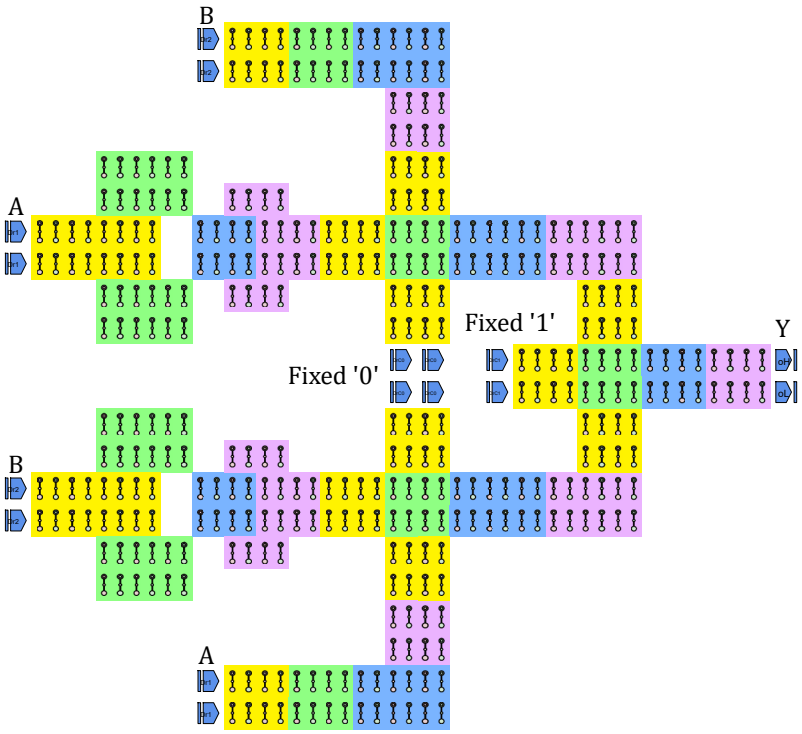

Fig. 5.25 Layout of a molecular FCN XOR drawn in MagCAD. The device is partitioned in four clock regions, indicated with colours yellow, green, blue and purple.

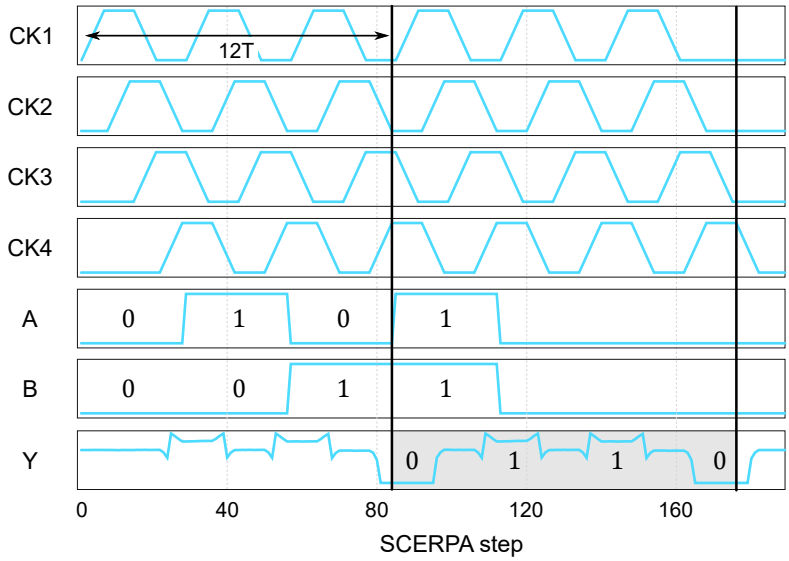

Fig. 5.26 Waveforms of a molecular FCN XOR obtained with SCERPA

Fig. 5.25 shows the layout drawn in MagCAD, subdivided by a clock system composed of four clock regions. For the analysis of complex devices, the SCERPA tool is indeed used with the MagCAD Integrated Development Environment (IDE), providing a graphical interface facilitating the realization of the layout. For example, Code A.2.1 provides the input file of the SCERPA simulation. Notice that the input A and B are replicated in the XOR layout. This operation permits to avoid the use of wire-crossing. The design of digital devices using wire-crossing in molecular FCN technology is left as future work, even though some introductory work has been already performed in [92] and some discussion is reported in this work in Section 1.2.

The drawn layout occupies an area of $0.0007\,\mu m^2$. Considering T the delay introduced by a single clock region, $4T$ is the delay introduced by the four clock regions composing a single gate. The total delay of the device is obtained by considering the path connecting inputs to outputs, which crosses a total number of three clocking systems, thus introducing a $12T$ delay. Notice the XOR device is pipelined, which means the inputs can be changed every clock cycle with a frequency $\frac{1}{4T}$.

Fig. 5.26 reports the signals obtained by SCERPA concerning the molecular FCN XOR. In particular, signals CK1, CK2, CK3, and CK4 are the clocking signals applied to the four clock regions intended to guide the information propagation and

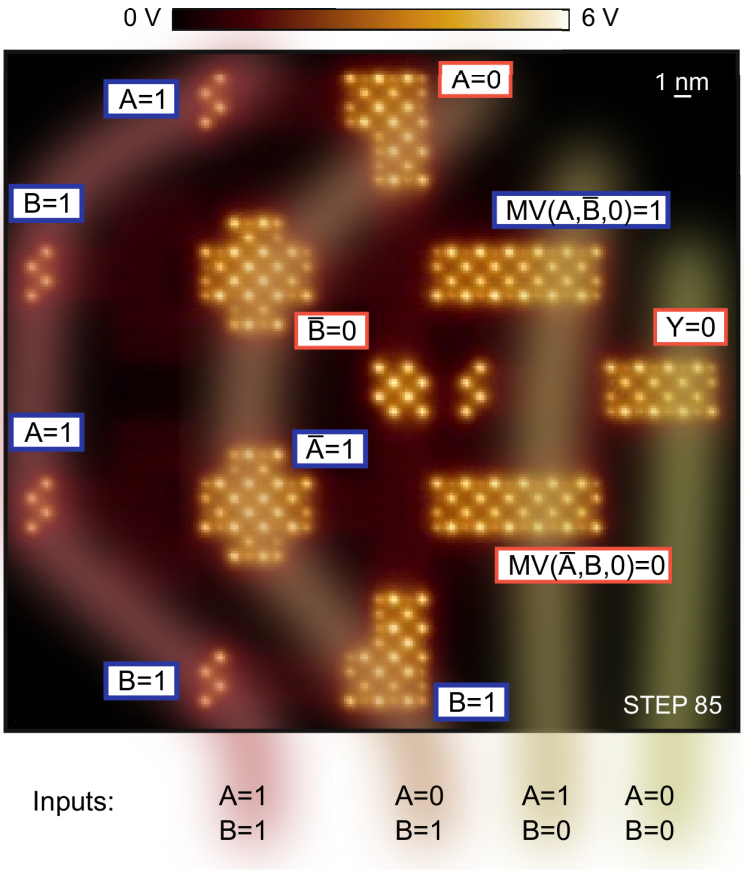

Fig. 5.27 Potential generated by a molecular FCN XOR in a precise timestep ($k = 85$) obtained with SCERPA

elaboration to enable pipelining. Signals A and B are the input stimuli, which span all the possible cases to verify the correct functioning of the device. Finally, signal Y is the output of the device. As expected, a delay of $12T$ separates the first input combination from the first correct output value, consequently to the delay introduced by the clocking mechanism. Notice that the output is not as clear as the inputs. Indeed, the simulation is physical, and the information degradation due to border and non-ideal intermolecular interaction effects are considered. Nevertheless, the signal Y matches the expected behavior of an XOR device, thus fitting the functional behavior reported in Table 5.5. In total, SCERPA computed 189 timesteps in 10 min and 21.67 s on Intel(R) Core(TM) i7-7700 CPU @ 3.60 GHz used in single-core calculation. The circuit is composed of 374 bis-ferrocene molecules.

In particular, Fig. 5.27 shows the result of the SCERPA simulation in a precise time step ($k = 85$). By comparing this figure with the layout reported in Fig. 5.25,

the consistency with the waveforms reported in Fig. 5.27 can be verified. Indeed, at step $k = 85$, the clock regions '1' and '2' are in the RESET state (CK1 and CK2 signals are low). Thus, since molecules are inhibited, no potential is generated in clock regions '1' and '2' (close to drivers). On the contrary, clock regions '3' and '4' are activated since CK3 and CK4 signals are high. By analyzing the pipelining mechanism, sections can be identified in the snapshot highlighted with shadows in the figure.

- In the section ($A = 0$, $B = 0$), it is possible to see the XOR device propagating the output signal $Y = 0$ as a consequence of the operation $0 \oplus 0$.
- In the section ($A = 1$, $B = 0$), it is possible to see the propagation of the operation $1 \oplus 0$. In particular, the operations MV $\left(\overline{A}, B, 0\right) = 0$ and MV $\left(A, \overline{B}, 0\right) = 1$ obtained with $A = 1$ and $B = 0$, which are supposed to be evaluated by the final majority voter, that will $Y = 1$ as output in the next clock cycle.
- In the section ($A = 0$, $B = 1$), the input logic has been propagated both as they are and inverted to reach the first level of majority voters. The inversion operation can be noticed.
- In the section ($A = 1$, $B = 1$), the device has not analyzed the inputs yet, which are ready to be evaluated when the first clock region is activated.

It is worth noticing that the information is well encoded on the XOR device. Indeed, multi-line devices strengthen the intermolecular interaction and permit the encoding of logic information on the device.

The result shows the possibility of using SCERPA as a simulator for more complex digital devices. Furthermore, it demonstrates for the first time the simulation of an XOR device with physical precision and shows the potentiality of the SCERPA tool to show both functional and physical results, showing on one side the physical characteristics of devices. The circuit-level quantities are requested for the design of complex architectures, thus fulfilling the gap between the physical perspective and the circuit level.

Table 5.6 1-bit Full-Adder Truth table

A	B	C	S	C_{out}
0	0	0	0	0
0	0	1	1	0
0	1	0	1	0
0	1	1	0	1
1	0	0	1	0
1	0	1	0	1
1	1	0	0	1
1	1	1	1	1

5.4.2 The 1-bit Full Adder

The 1-bit full adder is the basic element permitting the sum operation on 1-bit operands. Table 5.6 reports the truth table of the considered devices. In particular, the device performs the sum between two input values, denoted as A and B, eventually considering the presence of a carry-in (C_{in}), which can be taken from another full-adder in a Ripple-Carry Adder configuration. The 1-bit full-adder outputs the sum of the three operands (S) and the eventual output carry (C_{out}). The output can be formally obtained with majority-voter logic as:

$$\begin{cases} C_{out} = \mathrm{MV}(A,B,C_{in}) \\ S = \mathrm{MV}\left(\overline{C_{out}}, C_{in}, \mathrm{MV}\left(A,B,\overline{C_{out}}\right)\right) \end{cases}$$

Fig. 5.28 reports the 1-bit molecular FCN full adder implemented with 2-line connections and devices drawn in MagCAD. Also, in this case, wire-crossing is avoided, and input signals are replicated. The circuit is composed of 810 bis-ferrocene molecules. The area occupied by the molecules is 0.00162 μm^2, whereas the full-adder, also considering substrate regions not occupied by molecules, occupies an area of approximately 0.004 μm^2. This result shows the advantages of implementing logic devices with molecular FCN technology. Indeed, the area occupied is far lower concerning conductive Complementary Metal-Oxide Semiconductor (CMOS) technologies and other QCA technologies [92].

Fig. 5.29 reports the waveform plot obtained with the SCERPA tool. Listing A.2.2 provides the input file of the SCERPA simulation. Also, in this case, the output is delayed by time $17T$ caused by the clocking mechanism. Indeed, from inputs

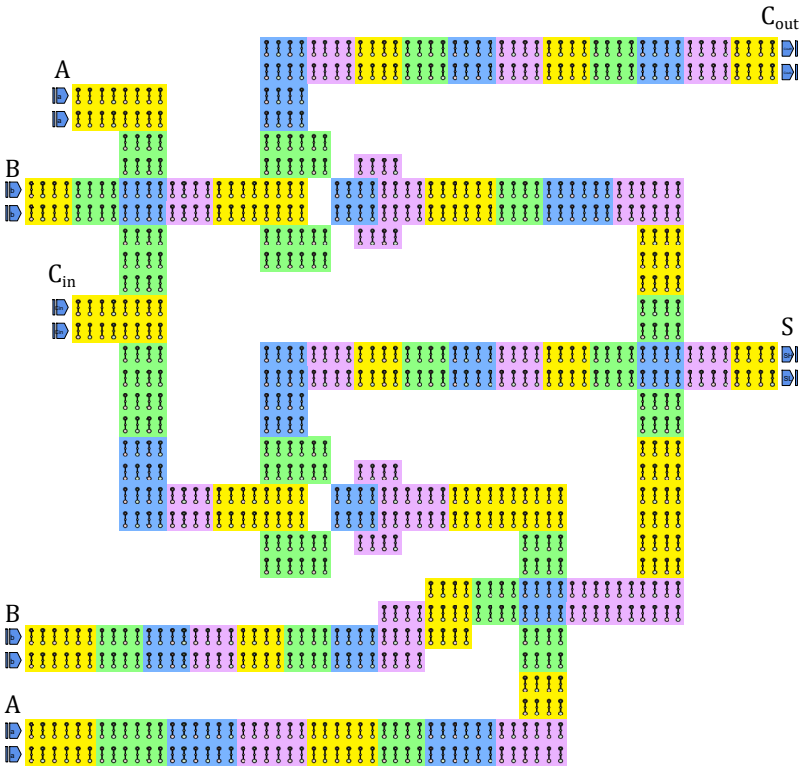

Fig. 5.28 Layout of a 1-bit molecular FCN full-adder drawn in MagCAD.

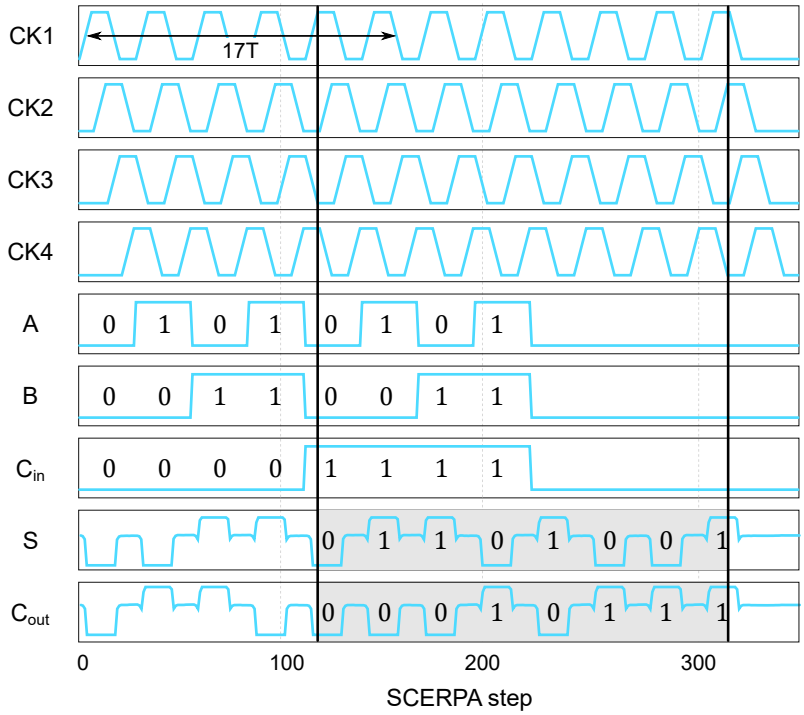

Fig. 5.29 Waveforms of a molecular FCN 1-bit full-adder obtained with SCERPA

to outputs, the information crosses 17 clock regions. Nevertheless, the sum and carry-out outputs are consistent with expectations, thus with the truth table reported in Table 5.6.

In total, SCERPA computed 357 timesteps in 38 min and 58.65 s on Intel(R) Core(TM) i7-7700 CPU @ 3.60 GHz used in single-core calculation. This result demonstrates the use of the SCERPA tool on a sophisticated circuit, permitting the simulation of molecular devices by considering the effective physics of molecules. The SCERPA simulator paves the way for the physical-aware design of molecular FCN architectures.

Conclusion and future perspectives

This work demonstrates a methodological approach to bridging the gap between the physical molecular perspective and the circuit level. First, it analyzes molecules using *ab initio* in the static and dynamic domains. In particular, this work demonstrates that molecules can be well-characterized using the so-called Vin-Aggregated Charge Transcharacteristics (VACT), providing an electronics perspective of the molecule, which can be seen as an electronics device with proper input (the electric field) and output (the charge distribution). Indeed, this function links the molecular charge to the electric field generated by other molecules, which can be evaluated with electrostatic equations from the molecular charge, or external electrodes.

Ab Initio Molecular Dynamics (AIMD) calculation demonstrates that the effect of molecular vibrations makes the molecule charge distribution fluctuate. Regardless, the average charge on the molecule remains consistent with the value predicted with the VACT at the equilibrium evaluated through static *ab initio* calculation, confirming the validity of the VACT in modeling the molecule. Moreover, the effect of the molecular vibrations and the consistency of the average molecular charge distribution with the VACT have been confirmed for different temperatures, demonstrating that the molecule can encode the information at ambient temperature. This thesis confirms with a simulative approach the molecular FCN as a technology permitting nanoscale information encoding at ambient temperature, hence addressing the technology as one of those not requiring cryogenic temperature. Notice that dynamic results presented in this work have been carried out using *ab initio* molecular dynamics, permitting the study of the nuclear movement. A second study, performed with Real-Time Time-Dependent Density Functional Theory (RT-TDDFT), left as future work, would allow the study of electron movement, eventually permitting the evaluation of switching speed, which is a second expected advantage of the molecular FCN technology.

The results of the VACT confirm the possibility of modeling molecules as electronic devices by maintaining a good link with the physical and technological levels. This thesis, therefore, develops the Self-Consistent Electrostatic Potential Algorithm (SCERPA): an optimized tool for rapidly simulating molecular FCN circuits while maintaining a solid connection to molecular physics and providing solutions based on *ab initio* characterized molecules. In particular, SCERPA evaluates the field generated by all the molecules of the circuit. In turn, it associates the charge on each molecule by linking the evaluated field to the molecule charge with the VACT.

The SCERPA tool has been mathematically analyzed in this thesis deeply, providing information regarding the convergence of the iterative procedure and discussing possible approximation techniques. In particular, algorithm convergence is favored by large intermolecular distances or low-polarizability molecules. A damping technique can eventually be utilized to diminish variations between steps of the iterative procedure, eventually favoring the convergence. The damping technique is enough to simulate the molecular devices proposed in the thesis.

Regarding approximation techniques, two modes have been discussed. The Active Region (AR) approximation permits evaluating the charge distribution of molecules that are effectively supposed to change their charge distribution, removing the need to evaluate the charge distribution of all the molecules of the circuit. The Interaction Radius (IR) approximation limits the number of intermolecular interactions evaluated for each molecule. The electrostatic nature of the interaction justifies the IR mode. Indeed, the electrostatic interaction diminishes with a large intermolecular distance.

The use of approximation techniques permits strongly reducing the calculation time. For example, the thesis reported the evaluation of the charge distribution of a wire composed of 500 molecules in 128 s, whereas 17 h were necessary for the evaluation with no approximation techniques. The obtained time is minimal compared to *ab initio* calculation techniques, which generally require hours for a single molecule.

At the current state of the algorithm, the SCERPA algorithm considers the circuit behavior adiabatic, meaning the electrons always lie in the ground state. However, using RT-TDDFT techniques would permit the modeling of the dynamic electron behavior, which can be eventually integrated into the tool to permit the dynamic simulation of devices. In addition, dynamic molecular mechanics models can also be

considered in the future to predict the effects of molecular vibrations, and eventual environmental-induced geometry variations, in the intermolecular interaction.

The SCERPA tool permits investigating and identifying the encoding and propagation characteristics of molecular FCN technology. Indeed, the bistability of the information encoding has been intensely discussed in this thesis by introducing and validating the bistable factor theory, which defines the so-called Bistable Factor (BF), indicating the possibility of a molecule to provide bistable propagation of the information. The bistability study provides essential feedback to chemists regarding the requirement the molecule should satisfy to be usable for the encoding and propagation digital information. Indeed, bistability is favored by small molecules with very high polarizability and low intermolecular distances. It is worth highlighting that polarizability and size are molecular parameters, whereas the intermolecular distance is related to the molecule-substrate interface and the technological process.

In general, the bistability of the molecular encoding also creates a possible memory effect that permits storing the information in molecular wires. First, the memory effect strengthens the need for a clocking mechanism. Indeed, it demands the use of a clock system that deletes the information when the wire is supposed to propagate a different logic. Also, the wires and the devices can be partitioned into regions that can be activated/deactivated to guide the information propagation, avoiding the propagation of logic errors and permitting pipelining. This work also analyzes the memory effect from an energy perspective by showing a hysteresis effect on the logic propagated on a molecular wire amplified by the length (i.e., by the number of molecules composing the wire).

Crosstalk effects on the propagation of the information have also been discussed. Indeed, molecular wires exhibit crosstalk due to the radial field generated by oxidized molecules. For this purpose, it is evident from this work that molecules should be neutral to limit the crosstalk effects and permit wires to propagate information without influencing each other. Moreover, specific and well-engineered zwitterionic (or oxidized molecules with counterions) can also be exploited to create neutral molecules and limit the crosstalk among molecular devices and wires.

The bistable properties have been successfully exploited in this work to implement the essential connections permitting the propagation of the information in the molecular circuit and the connection among logic gates. Furthermore, multi-line devices have been demonstrated to provide efficient information encoding and

propagation in wires, connections, and devices. In particular, this thesis has deeply discussed two devices: the inverter and the majority voter.

Regarding the inverter gate, the thesis discussed the two essential devices proposed in the literature connected to the Quantum-dot Cellular Automata: the single-branch inverter and the double-branch inverter. This study makes evident the need to use a tool strongly linked to molecular physics for simulating devices. Indeed, the single-branch, often used in the literature as a molecular device, may work only with neutral molecules. On the contrary, the 2-line double branch inverter has been demonstrated to work well for neutral molecules and well-engineered zwitterionic molecules.

Concerning the majority voter, the thesis highlights the necessity to clock the central cell of a majority voter independently to synchronize the device and avoid errors caused by different delays on the input branches. Furthermore, SCERPA demonstrates its efficiency in highlighting possible physical constraints that may be necessary to consider at the design level. Notice that the SCERPA results have been validated on a few molecules with *ab initio* techniques in [74]. Indeed, the computational difficulties make challenging the simulation of many-molecule circuits. Some efforts should also be performed to validate the SCERPA results on more complex circuits composed of many molecules. This study can be performed with a simulative approach, eventually exploiting periodic boundary conditions which facilitate the *ab initio* calculation or experimentally.

However, a working molecular FCN circuit prototype has not been realized yet, even though some efforts have been performed in this direction. One of the main difficulties in realizing experimental prototypes to validate SCERPA and, in general, to demonstrate the molecular FCN functioning is the necessity of realizing nanopatterned devices with sub-nm precision. For this purpose, some simulative work has already been started in [94] to permit the realization of devices without the need for nanopatterning, eventually creating logic encoding, propagation, and elaboration on Self-Assembled Monolayers (SAM). Charge measurement on the SAM can eventually be exploited in the SCERPA assessment procedure by comparing the results obtained with the tool and the experimental technique.

A second problem making the realization of a working prototype difficult is the readout. A possibility to facilitate the readout of molecular charge can be to transform the charge distribution in a geometrical conformation or position of a

molecule, eventually favoring the readout of the charge. The study of position-based information encoding is left as future work of this thesis.

To conclude, the SCERPA tool is used to analyze molecular FCN circuits and to establish physically aware designs of digital devices by considering the effective physical properties of the molecules. The majority voters and inverters have been used to design and demonstrate the realization of a $0.0007\,\mu m^2$ XOR and a $0.0016\,\mu m^2$ 1-bit full adder, which have been fully simulated with about 10 min and 38 min, respectively. Currently, devices have been realized by replicating the inputs to avoid information crossing. Some efforts have also been carried out to demonstrate the possibility of realizing wire crossing, showing promising results, making molecular FCN a candidate for realizing digital architectures.

The low computational time and the demonstrated link with the physics motivate further research in developing the SCERPA algorithm, introducing dynamic calculation and power consumption evaluation and providing techniques to characterize molecular devices as electronic devices, eventually constituting a library of standard devices to provide design capabilities of complex architectures. Finally, some efforts have already been carried out in [92] to integrate the SCERPA tool into the ToPoliNano suite. The introduction of CAD tools in the molecular FCN framework would permit discovering the advantages of the molecular FCN technology in complex digital architectures, eventually motivating efforts to realize a working prototype.

References

[1] IRDS experts. International roadmap for devices and systems 2021 edition, 2021.

[2] ITRS experts. International technology roadmap for semiconductors 2.0, 2015.

[3] C. S. Lent, P. D. Tougaw, W. Porod, and G. H. Bernstein. Quantum cellular automata. *Nanotechnology*, 4(1):49, 1993.

[4] C. S. Lent and P. D. Tougaw. Lines of interacting quantum-dot cells: A binary wire. *Journal of Applied Physics*, 74(10):6227–6233, 1993.

[5] Y. Ardesi, L. Gnoli, M. Graziano, and G. Piccinini. Bistable propagation of monostable molecules in molecular field-coupled nanocomputing. In *2019 15th Conference on Ph.D Research in Microelectronics and Electronics (PRIME)*, pages 225–228, 2019.

[6] J. Timler and C. S. Lent. Power gain and dissipation in quantum-dot cellular automata. *Journal of Applied Physics*, 91(2):823–831, 2002.

[7] P. D. Tougaw and C. S. Lent. Logical devices implemented using quantum cellular automata. *Journal of Applied Physics*, 75(3):1818–1825, 1994.

[8] V. S. Kalogeiton, D. P. Papadopoulos, O. Liolis, V. A. Mardiris, G. Ch. Sirakoulis, and I. G. Karafyllidis. Programmable crossbar quantum-dot cellular automata circuits. *IEEE Transactions on Computer-Aided Design of Integrated Circuits and Systems*, 36(8):1367–1380, 2017.

[9] L. Amarú, P. E. Gaillardon, and G. De Micheli. Majority-inverter graph: A novel data-structure and algorithms for efficient logic optimization. In *2014 51st ACM/EDAC/IEEE Design Automation Conference (DAC)*, pages 1–6, San Francisco, CA, USA, 2014. IEEE.

[10] L. Amarú, P. E. Gaillardon, S. Mitra, and G. De Micheli. New logic synthesis as nanotechnology enabler. *Proceedings of the IEEE*, 103(11):2168–2195, 2015.

[11] A. Gin, P. D. Tougaw, and S. Williams. An alternative geometry for quantum-dot cellular automata. *Journal of Applied Physics*, 85(12):8281–8286, 1999.

[12] A. Majeed and E. Alkaldy. A new approach to bypass wire crossing problem in QCA nanotechnology. *Circuit world*, ahead-of-print(ahead-of-print), July 2021.

[13] Y. Ardesi, G. Beretta, M. Vacca, G. Piccinini, and M. Graziano. Impact of molecular electrostatics on field-coupled nanocomputing and quantum-dot cellular automata circuits. *Electronics*, 11(2), 2022.

[14] M. Mitic, M. C. Cassidy, K. D. Petersson, R. P. Starrett, E. Gauja, R. Brenner, R. G. Clark, A. S. Dzurak, C. Yang, and D. N. Jamieson. Demonstration of a silicon-based quantum cellular automata cell. *Applied Physics Letters*, 89(1):013503, 2006.

[15] F. Perez-Martinez, I. Farrer, D. Anderson, G. A. C. Jones, D. A. Ritchie, S. J. Chorley, and C. G. Smith. Demonstration of a quantum cellular automata cell in a gaas/algaas heterostructure. *Applied Physics Letters*, 91(3):032102, 2007.

[16] C. S. Lent and P. D. Tougaw. Bistable saturation due to single electron charging in rings of tunnel junctions. *Journal of Applied Physics*, 75(8):4077–4080, 1994.

[17] C. S. Lent, B. Isaksen, and M. Lieberman. Molecular quantum-dot cellular automata. *J. Am. Chem. Soc.*, 125(4):1056–1063, January 2003.

[18] A. Pulimeno, M. Graziano, A. Antidormi, R. Wang, A. Zahir, and G. Piccinini. *Understanding a Bisferrocene Molecular QCA Wire*, pages 307–338. Springer Berlin Heidelberg, Berlin, Heidelberg, 2014.

[19] A. Pulimeno, M. Graziano, C. Abrardi, D. Demarchi, and G. Piccinini. Molecular qca: A write-in system based on electric fields. In *The 4th IEEE International NanoElectronics Conference*, pages 1–2, 2011.

[20] L. Zoli. *Active bis-ferrocene molecules as unit for molecular computation*. PhD thesis, Università di Bologna, Bologna, Italy, 2010.

[21] V. Arima, M. Iurlo, L. Zoli, S. Kumar, M. Piacenza, F. Della Sala, F. Matino, G. Maruccio, R. Rinaldi, F. Paolucci, M. Marcaccio, P. G. Cozzi, and A. P. Bramanti. Toward quantum-dot cellular automata units: thiolated-carbazole linked bisferrocenes. *Nanoscale*, 4(3):813–823, 2012.

[22] Y. Lu and C. S Lent. A metric for characterizing the bistability of molecular quantum-dot cellular automata. *Nanotechnology*, 19(15):155703, mar 2008.

[23] C.S. Lent and B. Isaksen. Clocked molecular quantum-dot cellular automata. *IEEE Transactions on Electron Devices*, 50(9):1890–1896, 2003.

[24] R. Wang, A. Pulimeno, M. Ruo Roch, G. Turvani, G. Piccinini, and M. Graziano. Effect of a clock system on bis-ferrocene molecular qca. *IEEE Transactions on Nanotechnology*, 15(4):574–582, 2016.

[25] Y. Ardesi, A. Pulimeno, M. Graziano, F. Riente, and G. Piccinini. Effectiveness of molecules for quantum cellular automata as computing devices. *Journal of Low Power Electronics and Applications*, 8(3), 2018.

[26] C. S. Lent. Bypassing the transistor paradigm. *Science*, 288(5471):1597–1599, 2000.

[27] F. Mohn, L. Gross, N. Moll, and G. Meyer. Imaging the charge distribution within a single molecule. *Nature nanotechnology*, 7:227–31, feb 2012.

[28] J. Peng, S. Sokolov, D. Hernangómez-Pérez, F. Evers, L. Gross, J. M. Lupton, and J. Repp. Atomically resolved single-molecule triplet quenching. *Science*, 373(6553):452–456, 2021.

[29] E. Barkai, Y. Jung, and R. Silbey. Theory of single-molecule spectroscopy: beyond the ensemble average. *Annu. Rev. Phys. Chem.*, 55(1):457–507, 2004.

[30] E. Rahimi and J. R. Reimers. Molecular quantum cellular automata cell design trade-offs: latching vs. power dissipation. *Phys. Chem. Chem. Phys.*, 20:17881–17888, 2018.

[31] Y. Ardesi, M. Graziano, and G. Piccinini. A model for the evaluation of monostable molecule signal energy in molecular field-coupled nanocomputing. *Journal of Low Power Electronics and Applications*, 12(1), 2022.

[32] Y. Lu and C. S. Lent. Self-doping of molecular quantum-dot cellular automata: mixed valence zwitterions. *Phys. Chem. Chem. Phys.*, 13:14928–14936, 2011.

[33] T. Groizard, S. Kahlal, and J. F. Halet. Zwitterionic mixed-valence species for the design of neutral clocked molecular quantum-dot cellular automata. *Inorg. Chem.*, 59(21):15772–15779, November 2020.

[34] H. Qi, S. Sharma, Z. Li, G. L. Snider, A. O. Orlov, C. S. Lent, and T. P. Fehlner. Molecular quantum cellular automata cells. electric field driven switching of a silicon surface bound array of vertically oriented two-dot molecular quantum cellular automata. *Journal of the American Chemical Society*, 125(49):15250–15259, 2003. PMID: 14653760.

[35] Y. Ardesi, G. Turvani, M. Graziano, and G. Piccinini. Scerpa simulation of clocked molecular field-coupling nanocomputing. *IEEE Transactions on Very Large Scale Integration (VLSI) Systems*, 29(3):558–567, 2021.

[36] Y. Lu, M. Liu, and C. S. Lent. Molecular quantum-dot cellular automata: From molecular structure to circuit dynamics. *Journal of Applied Physics*, 102(3):034311, 2007.

[37] J. A. Christie, R. P. Forrest, S. A. Corcelli, N. A. Wasio, R. C. Quardokus, R. Brown, S. A. Kandel, Y. Lu, C. S. Lent, and K. W. Henderson. Synthesis of a neutral mixed-valence diferrocenyl carborane for molecular quantum-dot cellular automata applications. *Angewandte Chemie International Edition*, 54(51):15448–15451, 2015.

[38] T. Sadhu, B. Das, D. De, and J. C. Das. Design of binary subtractor using actin quantum cellular automata. *IET Nanobiotechnol.*, 12(1):32–39, February 2018.

[39] S. Siccardi and A. Adamatzky. Actin quantum automata: Communication and computation in molecular networks. *Nano Communication Networks*, 6(1):15–27, 2015.

[40] X. Wang, L. Yu, V. S. S. Inakollu, X. Pan, J. Ma, and H. Yu. Molecular quantum dot cellular automata based on diboryl monoradical anions. *J. Phys. Chem. C Nanomater. Interfaces*, 122(4):2454–2460, February 2018.

[41] A. Pulimeno, M. Graziano, D. Demarchi, and G. Piccinini. Towards a molecular qca wire: simulation of write-in and read-out systems. *Solid-State Electronics*, 77:101–107, 2012. Special Issue of IEEE INEC 2011(IEEE International Nano Electronics Conference).

[42] R. Wang. *Analysis and modulation of molecular quantum-dot cellular automata (QCA) devices*. PhD thesis, Politecnico di Torino, Department of Electronics and Telecommunications, 2017.

[43] N. Liza, D. Murphey, P. Cong, D. W. Beggs, Y. Lu, and E. P. Blair. Asymmetric, mixed-valence molecules for spectroscopic readout of quantum-dot cellular automata. *Nanotechnology*, 33(11), December 2021.

[44] L. Wang, G. Cao, T. Tu, H.O. Li, C. Zhou, X.J. Hao, Z. Su, G.C. Guo, H. W. Jiang, and G. P. Guo. A graphene quantum dot with a single electron transistor as an integrated charge sensor. *Applied Physics Letters*, 97(26):262113, 2010.

[45] A. O. Orlov, I. Amlani, G. H. Bernstein, C. S. Lent, and G. L. Snider. Realization of a functional cell for quantum-dot cellular automata. *Science*, 277(5328):928–930, 1997.

[46] A. Orlov, A. Imre, G. Csaba, L. Ji, W. Porod, and G. H. Bernstein. Magnetic quantum-dot cellular automata: Recent developments and prospects. *Journal of Nanoelectronics and Optoelectronics*, 3(1):55–68, 2008.

[47] L. Verstraete, P. Szabelski, A. M. Bragança, B. E. Hirsch, and S. De Feyter. Adaptive self-assembly in 2d nanoconfined spaces: Dealing with geometric frustration. *Chemistry of Materials*, 31(17):6779–6786, 2019.

[48] J. N. Randall, J. W. Lyding, S. Schmucker, J. R. Von Ehr, J. Ballard, R. Saini, H. Xu, and Y. Ding. Atomic precision lithography on si. *Journal of Vacuum Science & Technology B: Microelectronics and Nanometer Structures Processing, Measurement, and Phenomena*, 27(6):2764–2768, 2009.

[49] Wenchuang Hu, K. Sarveswaran, M. Lieberman, and G.H. Bernstein. High-resolution electron beam lithography and dna nano-patterning for molecular qca. *IEEE Transactions on Nanotechnology*, 4(3):312–316, 2005.

[50] A. Halder and N. Ravishankar. Ultrafine single-crystalline gold nanowire arrays by oriented attachment. *Advanced Materials*, 19(14):1854–1858, 2007.

[51] N. Pazos-Pérez, D. Baranov, S. Irsen, M. Hilgendorff, L. M. Liz-Marzán, and M. Giersig. Synthesis of flexible, ultrathin gold nanowires in organic media. *Langmuir*, 24(17):9855–9860, 2008. PMID: 18652498.

[52] T. Xiao, J. Huang, D. Wang, T. Meng, and X. Yang. Au and au-based nanomaterials: Synthesis and recent progress in electrochemical sensor applications. *Talanta*, 206:120210, 2020.

[53] F. Schreiber. Structure and growth of self-assembling monolayers. *Progress in Surface Science*, 65(5):151–257, 2000.

[54] J. C. Love, L. A. Estroff, J. K. Kriebel, R. G. Nuzzo, and G. M. Whitesides. Self-assembled monolayers of thiolates on metals as a form of nanotechnology. *Chem. Rev.*, 105(4):1103–1169, April 2005.

[55] S. M. Barlow and R. Raval. Complex organic molecules at metal surfaces: bonding, organisation and chirality. *Surf. Sci. Rep.*, 50(6-8):201–341, August 2003.

[56] S. Kowarik, A. Gerlach, and F. Schreiber. Organic molecular beam deposition: fundamentals, growth dynamics, andin situstudies. *J. Phys. Condens. Matter*, 20(18):184005, May 2008.

[57] A. M. Pintus, A. Gabrieli, F. G. Pazzona, G. Pireddu, and P. Demontis. Molecular qca embedding in microporous materials. *Phys. Chem. Chem. Phys.*, pages –, 2019.

[58] A. Pulimeno, M. Graziano, R. Wang, D. Demarchi, and G. Piccinini. Charge distribution in a molecular qca wire based on bis-ferrocene molecules. In *2013 IEEE/ACM International Symposium on Nanoscale Architectures (NANOARCH)*, pages 42–43, jul 2013.

[59] R. Wang, M. Chilla, A. Palucci, M. Graziano, and G. Piccinini. An effective algorithm for clocked field-coupled nanocomputing paradigm. In *2016 IEEE Nanotechnology Materials and Devices Conference (NMDC)*, pages 1–2, 2016.

[60] M. Graziano, R. Wang, M. Ruo Roch, Y. Ardesi, F. Riente, and G. Piccinini. Characterisation of a bis-ferrocene molecular QCA wire on a non-ideal gold surface. *Micro Nano Lett.*, 14(1):22–27, January 2019.

[61] K. Walus, T. J. Dysart, G. A. Jullien, and R. A. Budiman. Qcadesigner: a rapid design and simulation tool for quantum-dot cellular automata. *IEEE Transactions on Nanotechnology*, 3(1):26–31, mar 2004.

[62] G. Toth. *Correlation and Coherence in Quantum-Dot Cellular Automata*. PhD thesis, Univ. Notre Dame, Notre Dame, IN, USA, 2000.

[63] F. Sill Torres, R. Wille, P. Niemann, and R. Drechsler. An energy-aware model for the logic synthesis of quantum-dot cellular automata. *IEEE Transactions on Computer-Aided Design of Integrated Circuits and Systems*, 37(12):3031–3041, dec 2018.

[64] S. Srivastava, A. Asthana, S. Bhanja, and S. Sarkar. Qcapro - an error-power estimation tool for qca circuit design. In *2011 IEEE International Symposium of Circuits and Systems (ISCAS)*, pages 2377–2380, may 2011.

[65] S. S. H. Ng, J. Retallick, H. N. Chiu, R. Lupoiu, L. Livadaru, T. Huff, M. Rashidi, W. Vine, T. Dienel, R. A. Wolkow, and K. Walus. Siqad: A design and simulation tool for atomic silicon quantum dot circuits. *IEEE Transactions on Nanotechnology*, 19:137–146, 2020.

[66] T. R. B. S. Soares, J. G. Nizer Rahmeier, V. C. de Lima, L. Lascasas, L. G. Costa Melo, and O. P. Vilela Neto. NMLSim: a nanomagnetic logic (NML) circuit designer and simulation tool. *J. Comput. Electron.*, 17(3):1370–1381, September 2018.

[67] U. Garlando. *Enabling Field-Coupled Nanocomputing Multi-Technological Circuits: Design, Simulation and Validation*. PhD thesis, Politecnico di Torino, Department of Electronics and Telecommunications, 2020.

[68] F. Riente, G. Turvani, M. Vacca, M. R. Roch, M. Zamboni, and M. Graziano. Topolinano: A cad tool for nano magnetic logic. *IEEE Transactions on Computer-Aided Design of Integrated Circuits and Systems*, 36(7):1061–1074, jul 2017.

[69] U. Garlando, M. Walter, R. Wille, F. Riente, F. Sill Torres, and R. Drechsler. Topolinano and fiction: Design tools for field-coupled nanocomputing. In *2020 23rd Euromicro Conference on Digital System Design (DSD)*, pages 408–415, 2020.

[70] U. Garlando, F. Riente, and M. Graziano. Funcode: Effective device-to-system analysis of field coupled nanocomputing circuit designs. *IEEE Transactions on Computer-Aided Design of Integrated Circuits and Systems*, pages 1–1, 2020.

[71] F. Riente, U. Garlando, G. Turvani, M. Vacca, M. Ruo Roch, and M. Graziano. Magcad: Tool for the design of 3-d magnetic circuits. *IEEE Journal on Exploratory Solid-State Computational Devices and Circuits*, 3:65–73, dec 2017.

[72] F. Neese. The orca program system. *Wiley Interdisciplinary Reviews: Computational Molecular Science*, 2(1):73–78, 2012.

[73] F. Neese. Software update: the orca program system, version 4.0. *Wiley Interdisciplinary Reviews: Computational Molecular Science*, 8(1):e1327, 2018.

[74] Y. Ardesi, R. Wang, G. Turvani, G. Piccinini, and M. Graziano. Scerpa: A self-consistent algorithm for the evaluation of the information propagation in molecular field-coupled nanocomputing. *IEEE Transactions on Computer-Aided Design of Integrated Circuits and Systems*, 39(10):2749–2760, 2020.

[75] C. M. Breneman and K. B. Wiberg. Determining atom-centered monopoles from molecular electrostatic potentials. the need for high sampling density in formamide conformational analysis. *J. Comput. Chem.*, 11(3):361–373, April 1990.

[76] P. W. Atkins and J. De Paula. *Physical Chemistry*. Oxford University Press, 8 edition, 2206.

[77] M. R. Provorse and C. M. Isborn. Electron dynamics with real-time time-dependent density functional theory. *Int. J. Quantum Chem.*, 116(10):739–749, May 2016.

[78] K. Lopata and N. Govind. Modeling fast electron dynamics with real-time time-dependent density functional theory: Application to small molecules and chromophores. *J. Chem. Theory Comput.*, 7(5):1344–1355, May 2011.

[79] J. Timler and C. S. Lent. Maxwell's demon and quantum-dot cellular automata. *J. Appl. Phys.*, 94(2):1050–1060, July 2003.

[80] Y. Ardesi, A. Gaeta, G. Beretta, G. Piccinini, and M. Graziano. Ab initio molecular dynamics simulations of Field-Coupled nanocomputing molecules. *JICS. J. integr. circuits syst.*, 16(1):1–8, April 2021.

[81] S. Grimme, J. Antony, S. Ehrlich, and H. Krieg. A consistent and accurate ab initio parametrization of density functional dispersion correction (dft-d) for the 94 elements h-pu. *The Journal of Chemical Physics*, 132(15):154104, 2010.

[82] S. Grimme, S. Ehrlich, and L. Goerigk. Effect of the damping function in dispersion corrected density functional theory. *Journal of Computational Chemistry*, 32(7):1456–1465, 2011.

[83] F. Weigend and R. Ahlrichs. Balanced basis sets of split valence, triple zeta valence and quadruple zeta valence quality for h to rn: Design and assessment of accuracy. *Physical Chemistry Chemical Physics*, 7(18):3297, 2005.

[84] P. Tamarat, A. Maali, B. Lounis, and M. Orrit. Ten years of single-molecule spectroscopy. *J. Phys. Chem. A*, 104(1):1–16, January 2000.

[85] G. Sanclemente. Analysis and simulation of the sinusoidal clocking field in molecular fcn. Master's thesis, Politecnico di Torino, Department of Electronics and Telecommunications, 2019.

[86] B. T. Sutcliffe and R. G. Woolley. On the quantum theory of molecules. *The Journal of Chemical Physics*, 137(22):22A544, 2012.

[87] G. Beretta, Y. Ardesi, M. Graziano, and G. Piccinini. Multi-molecule field-coupled nanocomputing for the implementation of a neuron. *IEEE Transactions on Nanotechnology*, 21:52–59, 2022.

[88] M.J. Frisch et al. Gaussian09 revision a.1, 2009. Gaussian Inc.Wallingford CT.

[89] A. Quarteroni, R. Sacco, and F. Saleri. *Numerical Mathematics (Texts in Applied Mathematics)*. Springer-Verlag, Berlin, Heidelberg, 2006.

[90] G. Beretta, Y. Ardesi, M. Graziano, and G. Piccinini. Scerpa documentation. Internal document; accessed 22 April 2022.

[91] Y. Ardesi. Energy analysis and bistability study of molecular fcn. Master's thesis, Politecnico di Torino, Department of Electronics and Telecommunications, 2017.

[92] Y. Ardesi, U. Garlando, F. Riente, G. Beretta, G. Piccinini, and M. Graziano. Taming molecular field-coupling for nanocomputing design. *J. Emerg. Technol. Comput. Syst.*, jul 2022. Just Accepted.

[93] Y. Mahmoodi and M. A. Tehrani. Novel fault tolerant qca circuits. In *2014 22nd Iranian Conference on Electrical Engineering (ICEE)*, pages 959–964, 2014.

[94] Y. Ardesi, G. Beretta, C. Fabiano, M. Graziano, and G. Piccinini. A reconfigurable field-coupled nanocomputing paradigm on uniform molecular monolayers. In *2021 International Conference on Rebooting Computing (ICRC)*, pages 124–128, 2021.

Appendix A

Supplementary information

A.1 Diallyl-butane geometries

Appendix A.1 reports the coordinate used in the analyses reported in this thesis for the diallyl-butane molecule.

A.1.1 Diallyl-butane obtained with bistable method (M1)

The reported geometry was obtained by an *ab initio* optimization performed with Hartree-Fock (HF) method using STO-3G basis set, known in the thesis as bistable method M1. Total charge was fixed to 1 a.u..

```
26
Optimized with UHF/STO-3G - Charge = 1
    C    0.696571      0.000377     -0.357610
    C   -0.683678     -0.000682      0.338217
    C    1.848623     -0.001581      0.691085
    C   -1.842071      0.001333     -0.690431
    H    1.777544     -0.887047      1.320368
    H    1.777523      0.881593      1.323556
```

```
    H   -1.750863      -0.875468      -1.328326
    H   -1.750705       0.880470      -1.325182
    H    0.791621       0.880977      -0.991124
    H    0.791357      -0.878006      -0.994216
    H   -0.761689       0.875845       0.978687
    H   -0.762001      -0.879611       0.975370
    C   -3.212703      -0.000000       0.000000
    C   -3.815479       1.229878       0.333350
    C   -3.823224      -1.231294       0.313316
    H   -3.349142       2.173592       0.087080
    H   -4.773249       1.263815       0.833427
    H   -3.363310      -2.173751       0.050780
    H   -4.781218      -1.267543       0.812858
    C    3.212703       0.000000      -0.000000
    C    3.861319       1.209218      -0.351173
    C    3.864961      -1.207454      -0.350297
    H    3.416105       2.177900      -0.106220
    H    4.823134       1.209589      -0.871557
    H    3.421012      -2.177335      -0.107690
    H    4.829232      -1.205198      -0.866153
```

A.1.2 Diallyl-butane obtained with monostable method (M2)

The reported geometry was obtained by an *ab initio* optimization performed with Density Functional Theory (DFT) using CAM-B3LYP functional, def2-TZVPP basis set and D3 correction, known in the thesis as monostable method M2. Total charge was fixed to 1 a.u..

```
26
Optimized with CAM-B3LYP/def2-TZVPP/D3 - Charge = 1
    C   0.70294970983571 -0.00000489358221 -0.31887793170390
    C  -0.70294974044079 -0.00000491857897  0.31887797269943
    C   1.81890995062196 -0.00000924872975  0.75554592734450
    C  -1.81890997733100 -0.00000887869091 -0.75554590051489
    H   1.71363124084263  0.87797047321607  1.38952279852832
    H   1.71363459775213 -0.87799707230309  1.38951139031474
    H  -1.71363119196510  0.87797101845925 -1.38952246994649
    H  -1.71363463050826 -0.87799648998094 -1.38951161894648
    H   0.81338167196722 -0.87717439607798 -0.95421769299749
    H   0.81338336301203  0.87716767447802 -0.95421317528975
    H  -0.81338176469701 -0.87717457400564  0.95421749068748
    H  -0.81338330333110  0.87716747371512  0.95421345332738
    C  -3.21725921843826 -0.00000285148008 -0.12648228439618
    C  -3.86191076130233 -1.19862929892102  0.17764280036107
    C  -3.86182167915575  1.19863200149564  0.17780597280240
    H  -3.40901392204591 -2.16333519352707 -0.04386446264578
    H  -4.84742867269362 -1.21222911231499  0.63980299501027
    H  -3.40885294057491  2.16333379261098 -0.04357193584884
    H  -4.84733811543762  1.21224321689513  0.63996880009732
```

```
    C   3.21725915983508  -0.00000309965199   0.12648224147677
    C   3.86191096952594  -1.19862944478818  -0.17764242069182
    C   3.86182125186301   1.19863175983503  -0.17780643266172
    H   3.40901426723733  -2.16333534740838   0.04386527017359
    H   4.84742889007747  -1.21222915147339  -0.63980268726985
    H   3.40885214387188   2.16333348165494   0.04357122351230
    H   4.84733770147928   1.21224307915438  -0.63996932342236
```

A.1.3 Diallyl-butane mirrored geometry

The reported geometry was obtained from Appendix A.1.1 by applying the transformation described by Equation (3.9).

```
26
Optimized with UHF/STO-3G - Charge = 1 - Then mirrored
    C    0.683678     -0.000682     -0.338217
    C   -0.696571      0.000377      0.357610
    C    1.842071      0.001333      0.690431
    C   -1.848623     -0.001581     -0.691085
    H    1.750863     -0.875468      1.328326
    H    1.750705      0.880470      1.325182
    H   -1.777544     -0.887047     -1.320368
    H   -1.777523      0.881593     -1.323556
    H    0.761689      0.875845     -0.978687
    H    0.762001     -0.879611     -0.975370
    H   -0.791621      0.880977      0.991124
    H   -0.791357     -0.878006      0.994216
    C   -3.212703      0.000000      0.000000
    C   -3.861319      1.209218      0.351173
    C   -3.864961     -1.207454      0.350297
    H   -3.416105      2.177900      0.106220
    H   -4.823134      1.209589      0.871557
    H   -3.421012     -2.177335      0.107690
    H   -4.829232     -1.205198      0.866153
    C    3.212703     -0.000000     -0.000000
    C    3.815479      1.229878     -0.333350
    C    3.823224     -1.231294     -0.313316
    H    3.349142      2.173592     -0.087080
    H    4.773249      1.263815     -0.833427
    H    3.363310     -2.173751     -0.050780
    H    4.781218     -1.267543     -0.812858
```

A.1.4 Diallyl-butane averaged geometry

The reported geometry was obtained by combining geometries reported in Appendix A.1.1 and Appendix A.1.3 according to the transformation described by Equation (3.10).

```
26
Optimized with UHF/STO-3G - Charge = 1 - Then mirrored and averaged w.r.t.
    optimized geometry
    C     0.690125      -0.000153      -0.347914
    C    -0.690125      -0.000153       0.347914
    C     1.845347      -0.000124       0.690758
    C    -1.845347      -0.000124      -0.690758
    H     1.764204      -0.881258       1.324347
    H     1.764114       0.881032       1.324369
    H    -1.764204      -0.881258      -1.324347
    H    -1.764114       0.881032      -1.324369
    H     0.776655       0.878411      -0.984906
    H     0.776679      -0.878809      -0.984793
    H    -0.776655       0.878411       0.984906
    H    -0.776679      -0.878809       0.984793
    C    -3.212703       0.000000       0.000000
    C    -3.838399       1.219548       0.342262
    C    -3.844093      -1.219374       0.331807
    H    -3.382624       2.175746       0.096650
    H    -4.798192       1.236702       0.852492
    H    -3.392161      -2.175543       0.079235
    H    -4.805225      -1.236371       0.839506
    C     3.212703       0.000000       0.000000
    C     3.838399       1.219548      -0.342262
    C     3.844093      -1.219374      -0.331807
    H     3.382624       2.175746      -0.096650
    H     4.798192       1.236702      -0.852492
    H     3.392161      -2.175543      -0.079235
    H     4.805225      -1.236371      -0.839506
```

A.2 SCERPA input files

Appendix A.2 reports the input files used for simulating molecular Field-Coupled Nanocomputing (FCN) circuits in this thesis using Self-Consistent ElectRostatic Potential Algorithm (SCERPA) implemented as a MATLAB tool.

A.2.1 Exclusive-OR SCERPA input

A.2.2 1-bit full-adder SCERPA input

A.2.1 Exclusive-OR SCERPA input

The reported input file was used to simulate the Exclusive-OR (XOR) which is analysed in Section 5.4.1. The layout of the device is drawn with MagCAD and shown in Fig. 5.25.

```
clear variables
close all

%clock definitions
clock_low    = -2; % [V/nm] RESET field
clock_high   = +2; % [V/nm] HOLD field
clock_step   = 7;  % number of points in the phase ramp

%normal clock phases
pSwitch  = linspace(clock_low,clock_high,clock_step);   % SWITCH phase
pHold    = linspace(clock_high,clock_high,clock_step);  % HOLD phase
pRelease = linspace(clock_high,clock_low,clock_step);   % RELEASE phase
pReset   = linspace(clock_low,clock_low,clock_step);    % RESET phase

%complete clock cycle definition
pCycle   = [pSwitch pHold pRelease pReset];

%logic values
D0 = num2cell(+4.5*ones(1,clock_step*4)); % Logic '0'
D1 = num2cell(-4.5*ones(1,clock_step*4)); % Logic '1'

%layout (MagCAD)
file = 'xor.qll';
circuit.magcadImporter = 1;
circuit.qllFile = fullfile(pwd,file);

%output path
settings.out_path = fullfile(pwd,'xor');

%layout configuration
circuit.dist_z = 10;                    % intermolecular distance 1 nm
circuit.doubleMolDriverMode = 1;        % use two molecules per driver

%driver definition
circuit.Values_Dr = {
    'Dr1'       D0{:} D1{:} D0{:} D1{:} D0{:} D0{:} D0{:} D0{:} 'end' % Driver
     1
    'Dr1_c'     D1{:} D0{:} D1{:} D0{:} D1{:} D1{:} D1{:} D1{:} 'end' % Driver
     1 second molecule (opposite polarization)
    'Dr2'       D0{:} D0{:} D1{:} D1{:} D0{:} D0{:} D0{:} D0{:} 'end'
    'Dr2_c'     D1{:} D1{:} D0{:} D0{:} D1{:} D1{:} D1{:} D1{:} 'end'
    'DrC1'      D1{:} D1{:} D1{:} D1{:} D1{:} D1{:} D1{:} D1{:} 'end'
    'DrC1_c'    D0{:} D0{:} D0{:} D0{:} D0{:} D0{:} D0{:} D0{:} 'end'
    'DrC0'      D0{:} D0{:} D0{:} D0{:} D0{:} D0{:} D0{:} D0{:} 'end'
    'DrC0_c'    D1{:} D1{:} D1{:} D1{:} D1{:} D1{:} D1{:} D1{:} 'end'
};
```

```
45
46 %clock phases
47 circuit.stack_phase(1,:) = [pCycle pCycle pCycle pCycle pCycle pCycle pReset
       pReset pReset];
48 circuit.stack_phase(2,:) = [pReset pCycle pCycle pCycle pCycle pCycle pCycle
       pReset pReset];
49 circuit.stack_phase(3,:) = [pReset pReset pCycle pCycle pCycle pCycle pCycle
       pCycle pReset];
50 circuit.stack_phase(4,:) = [pReset pReset pReset pCycle pCycle pCycle pCycle
       pCycle pCycle];
51
52 %SCERPA settings
53 settings.doubleMolDriverMode = 1;
54 settings.damping = 0.6;
55 settings.activeRegionThreshold=0.005;
56 settings.verbosity = 1;
57 settings.conv_threshold_HP = 0.005;
58 settings.enableRefining = 0;
59 settings.enableActiveRegion = 1;
60 settings.dumpDriver = 1;
61 settings.dumpOutput = 1;
62 settings.dumpClock = 1;
63 settings.dumpComputationTime = 1;
64
65 %PLOT settings
66 plotSettings.plot_3dfig = 0;
67 plotSettings.plot_waveform = 1;
68 plotSettings.plot_logic = 1;
69 plotSettings.plot_potential = 1;
70 plotSettings.plotSpan = 7;
71 plotSettings.fig_saver = 1;
72 plotSettings.plotList = 0;
73
74 %copy output path from algorithm settings if specified by the user
75 if isfield(settings,'out_path')
76     plotSettings.out_path = settings.out_path;
77 end
78
79 %%%%
80 this_path = pwd;
81 scerpa_path = fullfile('SCERPA');
82 cd(scerpa_path)
83 generation_status = SCERPA('generateLaunch', circuit, settings);
84                     SCERPA('plotSteps', plotSettings);
85 cd(this_path)
```

A.2.2 1-bit full-adder SCERPA input

The reported input file was used to simulate the 1-bit full adder which is analysed in Section 5.4.2. The layout of the device is drawn with MagCAD and shown in Fig. 5.28.

```
clear variables
close all

%clock definitions
clock_low    = -2; % [V/nm] RESET field
clock_high   = +2; % [V/nm] HOLD field
clock_step   = 7;  % number of points in the phase ramp

%normal clock phases
pSwitch  = linspace(clock_low,clock_high,clock_step);   % SWITCH phase
pHold    = linspace(clock_high,clock_high,clock_step);  % HOLD phase
pRelease = linspace(clock_high,clock_low,clock_step);   % RELEASE phase
pReset   = linspace(clock_low,clock_low,clock_step);    % RESET phase

%complete clock cycle definition
pCycle   = [pSwitch pHold pRelease pReset];

%logic values
D0 = num2cell(+4.5*ones(1,clock_step*4)); % Logic '0'
D1 = num2cell(-4.5*ones(1,clock_step*4)); % Logic '1'

%layout (MagCAD)
file = 'fulladder.qll';
circuit.magcadImporter = 1;
circuit.qllFile = fullfile(pwd,file);

%output path
settings.out_path = fullfile(pwd,'fulladder');

%layout configuration
circuit.dist_z = 10;                    % intermolecular distance 1 nm
circuit.doubleMolDriverMode = 1;        % use two molecules per driver

%driver definition
circuit.Values_Dr = {
    'a'     D0{:} D1{:} D0{:} D1{:} D0{:} D1{:} D0{:} D1{:} D0{:} D0{:} D0{:}
    D0{:} D0{:} D0{:} D0{:} D0{:} 'end' % Driver a
    'a_c'   D1{:} D0{:} D1{:} D0{:} D1{:} D0{:} D1{:} D0{:} D1{:} D1{:} D1{:}
    D1{:} D1{:} D1{:} D1{:} 'end' % Driver a second molecule (opposite
    polarization)
    'b'     D0{:} D0{:} D1{:} D1{:} D0{:} D0{:} D1{:} D1{:} D0{:} D0{:} D0{:}
    D0{:} D0{:} D0{:} D0{:} D0{:} 'end'
    'b_c'   D1{:} D1{:} D0{:} D0{:} D1{:} D1{:} D0{:} D0{:} D1{:} D1{:} D1{:}
    D1{:} D1{:} D1{:} D1{:} D1{:} 'end'
    'Cin'   D0{:} D0{:} D0{:} D0{:} D1{:} D1{:} D1{:} D1{:} D0{:} D0{:} D0{:}
    D0{:} D0{:} D0{:} D0{:} D0{:} 'end'
```

```
    'Cin_c' D1{:} D1{:} D1{:} D1{:} D0{:} D0{:} D0{:} D0{:} D1{:} D1{:} D1{:}
    D1{:} D1{:} D1{:} D1{:} D1{:} 'end'
};

%clock phase
circuit.stack_phase(1,:) = [pCycle pCycle pCycle pCycle pCycle pCycle pCycle
    pCycle pCycle pCycle pCycle pCycle pReset pReset pReset];
circuit.stack_phase(2,:) = [pReset pCycle pCycle pCycle pCycle pCycle pCycle
    pCycle pCycle pCycle pCycle pCycle pCycle pReset pReset];
circuit.stack_phase(3,:) = [pReset pReset pCycle pCycle pCycle pCycle pCycle
    pCycle pCycle pCycle pCycle pCycle pCycle pCycle pReset];
circuit.stack_phase(4,:) = [pReset pReset pReset pCycle pCycle pCycle pCycle
    pCycle pCycle pCycle pCycle pCycle pCycle pCycle pCycle];

%SCERPA settings
settings.doubleMolDriverMode = 1;
settings.damping = 0.6;
settings.activeRegionThreshold=0.005;
settings.verbosity = 1;
settings.conv_threshold_HP = 0.005;
settings.enableRefining = 0;
settings.enableActiveRegion = 1;
settings.dumpDriver = 1;
settings.dumpOutput = 1;
settings.dumpClock = 1;
settings.dumpComputationTime = 1;

%PLOT settings
plotSettings.plot_3dfig = 0;
plotSettings.plot_logic = 1;
plotSettings.plot_potential = 1;
plotSettings.plotSpan = 7;
plotSettings.plotList = [309:330];
plotSettings.plot_waveform = 1;
plotSettings.fig_saver = 1;

%copy output path from algorithm settings if specified by the user
if isfield(settings,'out_path')
    plotSettings.out_path = settings.out_path;
end

%%%%
this_path = pwd;
scerpa_path = fullfile('SCERPA');
cd(scerpa_path)
generation_status = SCERPA('generateLaunch', circuit, settings);
                    SCERPA('plotSteps', plotSettings);
cd(this_path)
```